KU LEUVEN

FACULTEIT GENEESKUNDE

BIOMEDISCHE WETENSCHAPPEN

Evolutionary genetics of human cold adaptation using *Drosophila melanogaster*

Masterproef voorgedragen tot het behalen van de graad Master in de Biomedische Wetenschappen door

Febe CAPPELAERE

Promotor: Prof. Dr. Patrick CALLAERTS

Begeleiders: Daan MOONS en Dr. Sofie DE GROEF

Centrum Menselijke Erfelijkheid

Laboratorium voor Gedrags- en Ontwikkelingsgenetica

Leuven, 2025-2026

KU LEUVEN

FACULTEIT GENEESKUNDE

BIOMEDISCHE WETENSCHAPPEN

Evolutionary genetics of human cold adaptation using *Drosophila melanogaster*

Masterproef voorgedragen tot het behalen van de graad Master in de Biomedische Wetenschappen door

Febe CAPPELAERE

Promotor: Prof. Dr. Patrick CALLAERTS

Begeleiders: Daan MOONS en Dr. Sofie DE GROEF

Centrum Menselijke Erfelijkheid

Laboratorium voor Gedrags- en Ontwikkelingsgenetica

Leuven, 2025-2026

1 PREFACE

First, I would like to thank my promotor, Prof. Callaerts, for giving me the opportunity to work on this project and for the guidance throughout.

I am especially grateful for my supervisors, Daan Moons and Dr. Sofie De Groef. To Daan, thank you for the consistent support and feedback, while enduring my many questions and doubts, often leading to yap sessions, and the fly room music intermezzos of One Direction, Taylor Swift and K3. To Sofie, thank you for unexpectantly and without hesitation stepping into the role of co-supervisor. Your truck factor in this project was immense, your expertise invaluable and your humour my favourite. Feeling like mad scientists trying to design a larval behavioural assay is one of my fondest memories of this thesis. To both, thank you for providing me structure when I desperately needed it, for your patience and support during the lows, while also celebrating the highs of this whirlwind journey.

Alongside my supervisors, I would also like to thank the rest of the lab, Veerle, Lien, Elien and Jayati, for their warm welcome into the team and supporting me through the many (sometimes failed) experiments.

Outside the lab, I want to thank Robin, Imane, Anna and Amber for the many laughs, the constant support, and for making the trial and tribulations of this thesis feel less lonely. Our friendship began with *Wicked*, and because I knew you, my time at university has been changed for good.

Last but not least, to my parents, thank you for providing me a safe haven that always welcomed me with open arms and for always listening with open hearts.

2 TABLE OF CONTENTS

3 LIST OF ABBREVIATIONS

AP	Action potential
ATGL	Adipose Triglyceride Lipase
BAT	Brown Adipose Tissue
Bp	Basepairs
BL	Bloomington Drosophila Stock Center
dFOXO	*Drosophila* Forkhead box O transcription factor
DG	Diacylglycerol
DGRP	*Drosophila* Genetic Reference Panel
DOG	Dorsal organ ganglion
dsRNA	Double stranded RNA
FA	Fatty acids
FCI	Freezing Cold Injury
FPKM	Fragments Per Kilobase of transcript per Million mapped reads
GFP	Green Fluorescent Protein
GWAS	Genome-wide Association Study
iHS	Integrated Haplotype Score
LD	Lipid droplet
NFCI	Non-Freezing Cold Injury
nSL	Number of Segregating Sites by Length
RING	Rapid Iterative Negative Geotaxis
RISC	RNA-induced Silencing Complex
RNAi	RNA interference
SDS	Sodium dodecyl sulphate
SNP	Single Nucleotide Polymorphism
TG	Triglycerides
TH	Thyroid hormones
TOG	Terminal organ ganglion
TRP	Transient Receptor Potential
UAS	Upstream Activating Sequence
UCP1	Uncoupling Protein 1
VDRC	Vienna Drosophila Resource Center

4 ABSTRACT

Throughout evolution, humans have adapted to extreme environments, including the harsh climate of the Arctic region. During chronic cold exposure, activation of brown adipose tissue is essential to elevate the metabolic rate and sustain heat production. Moreover, observational studies report significantly reduced serum lipid levels in indigenous populations of the Arctic region, suggesting a hepatic contribution to chronic cold adaptation. Animal research supports this association, revealing substantial cold-induced shifts in hepatic lipid metabolism.

Whole genome sequencing of Siberian individuals previously identified 756 protein coding genes in regions presenting evolutionary selection. This project investigated the functional role of a prioritized subset of these genes in cold adaptation by studying their homologues in an *in vivo Drosophila melanogaster* model. Candidate genes were selected using the criteria of most significant p-value in Siberian populations, non-significance in reference populations, elevated liver expression, and a representative *Drosophila melanogaster* homologue. The top 20 candidate genes were chosen, supplemented by the known cold responsive TRP channel *inactive*.

A targeted knockdown of the genes of interest was induced in the fat body with the GAL4/UAS system and validated by RT-qPCR. Most gene of interest knockdowns proved to be associated to cold stress responses via two behavioural assays targeting chill coma induction and recovery. The vast majority of gene knockdowns induced a chill coma recovery delay, while several RNAi genotypes had modified chill coma susceptibility. Moreover, lipid quantification of the abdominal fat body revealed an increased lipid storage in numerous knockdown genotypes. In addition to the novel chill coma susceptibility assay in adult flies, a novel behavioural assay in third instar wandering larvae was designed to assess locomotion recovery following cold exposure. Both assays enable more in-depth research regarding potential cold stress response alterations. Overall, we have shown that several genes of interest, first identified in cold adapted human populations, influence cold stress responses and lipid storage when silenced in the *Drosophila melanogaster* fat body, indicating potential conserved mechanisms of metabolic cold adaptation across species.

5 INTRODUCTION

5.1. Human evolution and adaptation

According to the Out of Africa theory, modern humans have originated in Africa, predominantly characterized by tropical climate conditions. Archaeological and genetic evidence implies that all present-day human populations descended from a relatively small group that departed Africa roughly 60.000 years ago. As these populations expanded into Eurasia, environmental conditions differed markedly from the initial warm climates. This shift towards higher latitudes coincided with colder temperatures and reduced sunlight, forcing human adaptation to the new environment (1). Among the most extreme climates where human inhabitation occurred is the Arctic, a region encircling the North Pole and reaching into Siberia, Alaska, Canada and other high-latitude areas (2). The oldest archaeological evidence suggesting human activity in the Siberian Arctic is represented by remains associated with a mammoth kill site, dated approximately 45.000 years ago. This finding marks an important milestone and provides a timeframe for the first human inhabitation of the Arctic region (3). Climatic conditions of each polar region depend on factors such as latitude, proximity to the sea, elevation, and topography. For example, winter in the central Siberian Arctic is characterized by mean temperatures of -37°C, while North American winters range from -34 to -29°C. The most extreme winter temperatures recorded in these regions fall between -54 and -46°C. Therefore, survival in such drastically colder ambient temperatures, and overall extreme environment, for many thousands of years would have required profound physiological, behavioural, and cultural adaptations. Understanding how humans adapted to these extreme conditions provides important insight into human evolutionary flexibility and the mechanisms by which populations respond to environmental pressures.

5.1 Cold perception in humans

The importance of adaptive responses in extreme environmental conditions and of cold perception is illustrated by the severe physiological consequences that occur when the body fails to maintain adequate thermal balance.

The human body is divided in two compartments, namely the external shell and the internal core. The external shell corresponds to the skin, which experiences temperature fluctuations depending on the environment. The internal core includes the central nervous system and viscera, and to function adequately, a controlled temperature range of circa 37°C is required (4).

Two important disruptions of thermal balance are hypothermia and cold-induced injury. Hypothermia is generally defined as a reduction of core temperature below 35°C, typically classified into different stages based on the severity of the temperature decline (5). Decrease of body temperature below this threshold will gradually impact functionality of various organs with e.g. loss of consciousness when the core temperature is around 33°C. In addition to systemic effects, cold exposure can also cause localized tissue damage known as cold-induced injury. These injuries are generally categorized into freezing cold injury (FCI), commonly referred to as frostbite, and non-freezing cold injury (NFCI). Cutaneous sensation is lost at skin temperatures at or below 10°C, and as cooling progresses, FCI may develop (6). FCI is defined as tissue damage caused by exposure to temperatures below tissue freezing point, which is approximately -0,55°C (7,8). Non-freezing cold injury (NFCI) represents a distinct category of cold-related tissue damage. Unlike frostbite, NFCI occurs when tissues are exposed for prolonged periods

to cold temperatures between approximately 0 °C and 15 °C without freezing (6,8). These injuries cause persistent sensory symptoms, such as pain and long-lasting cold hypersensitivity. Therefore, NFCI is more frequently regarded as a form of sensory neuropathy (6,8). Prevention of these cold-induced adverse events are critical for the survival of the human body and therefore requires cold perception and thermoregulatory responses to prevent tissue damage and maintain physiological stability.

Human cold sensation can be subdivided into innocuous and noxious cold, reflecting whether the cold stimulus is perceived as harmless or painful. Innocuous cold sensation is defined as “the perception of cold temperature deviating from thermoneutral temperature without pain”, and in general lacks the affective component to reinstate thermoregulation. In contrast, noxious cold is defined as “the sensation of cold with pain” (9). Research indicates that the initial cold sensation typically occurs at a skin temperature of ± 28,2°C, intensifies to cold ache at ± 16,4°C, and becomes painful below ± 14,9°C (10).

The human body possesses a diverse set of peripheral sensory neurons, of which approximately 10% are specialized in detection of cool and cold temperatures (11). Initially, thermal perception begins at the skin, where sensory receptors detect slight temperature changes resulting from direct contact with objects, ambient environmental conditions or internal body temperature (12). At the molecular level, cold stimuli are transduced into electric signals through activation of temperature-sensitive Transient Receptor Potential (TRP) channels, such as TRPM8, TRPA1 and TRPC5, and mechanothermal voltage-gated ion channels (13)(14). The signal generated by the activation of the TRP channels is transmitted to the central nervous system eventually leading to activation of peripheral sympathetic and parasympathetic circuits to induce an adequate physiological response (4).

5.2 Human response to acute cold exposure

Human responses to cold exposure can broadly be classified into physiological and behavioural adaptations (15). Behavioural thermoregulation can be defined as “any conscious decisions taken with the aim of maintaining thermal balance” (12). Examples of behavioural mechanisms are upregulation of physical activity to produce more heat, altered body posture, wearing high-insulation clothing and building shelter (15,16). When behavioral adjustments are insufficient to maintain thermal homeostasis, physiological mechanisms are activated to compensate. These autonomic responses function to preserve core body temperature and sustain normal physiological processes during cold exposure (16).

At the physiological level, thermal homeostasis in response to decreased environmental temperature is maintained through thermoregulatory or thermo-effector responses (16). One major response involves the adjustment of blood flow to peripheral tissues. The initial response to cold exposure is cutaneous vasoconstriction, thereby reducing heat transfer of the core to the shell, resulting in increased insulation (16,17). Prolonged cold-induced vasoconstriction makes distal skin regions, such as fingers and toes, susceptible to cold injury as the blood decreases in velocity and therefore can reach lower temperatures. In these areas, a vasomotor response in the form of cold-induced vasodilation will occur, temporarily increasing blood flow and restoring tissue temperature (16).

The second major physiological response is cold induced thermogenesis, which can be further divided in shivering- and non-shivering-thermogenesis (15). Shivering thermogenesis consists of involuntary repeated contractions of skeletal muscles to convert metabolic energy into heat. During intense cold exposure, shivering can increase heat production up to five times the resting metabolic rate (15,16,18).

The shivering response is triggered when core and skin temperature drop below a certain thermoregulatory threshold, in which the severity of the cold stress drives the muscle contraction intensity. Despite the heat production efficiency, shivering thermogenesis is limited in time according to the available glycogen and water resources, and may compromise overall muscle function (15–17,19). In addition to shivering thermogenesis, humans are capable of increasing metabolic heat production through non-shivering-thermogenesis (17). At thermoneutral conditions, the basal and resting metabolic rate are sufficient to maintain body temperature and normal body function, defining them as obligatory non-shivering thermogenesis (18). During prolonged cold exposure, brown adipose tissue (BAT) becomes activated and sustains enhanced heat production (19,20). Non-shivering thermogenesis also occurs in skeletal muscle and internal organs, but in a much lower capacity compared to BAT (17,18). BAT has the ability to generate heat due to the enrichment of mitochondria containing uncoupling protein 1 (UCP1) (21). UCP1 causes a depletion of the generated proton gradient across the inner mitochondrial membrane during oxidative phosphorylation (20). This results in ATP production inefficiency, yet enabling energy conversion to heat, leading to thermogenesis without inducing muscular activity (20,21).

As previously mentioned, cold exposure elicits activation of TRP channels in sensory neurons that subsequently send a signal to the central nervous system and increase the activity of sympathetic neurons (22). The subsequent release of noradrenaline stimulates BAT via the β-adrenergic receptor and triggers intracellular pathways, including hydrolysis of triglycerides, β-oxidation of the resulting fatty acids, and activation of UCP1 (20,22). In addition, cold induced noradrenergic signalling activates type 2 iodothyronine deiodinase (Dio2) in brown adipocytes, catalysing the local conversion of thyroxine (T4) to the more metabolically potent triiodothyronine (T3) (22). Both thyroid hormones (TH) are essential in regulating energy expenditure as they promote oxidative metabolism in most cells (23). High TH levels induce a hypermetabolic state, characterized by increased resting energy metabolism, weight loss, reduced cholesterol levels, increased lipolysis, and gluconeogenesis (19). The cold induced increment of intracellular T_3 levels in BAT enhances UCP1 expression, thereby amplifying the thermogenic capability (20). Studies show that BAT activation by cold exposure can also increase systemic T_3 levels (20).

5.3 Human adaptation to chronic cold exposure

Chronic cold exposure in humans induces adaptations in physiological responses compared to those appearing during acute or initial cold exposure (16). This phenomenon is called cold adaptation, in which adaptation is defined as “the changes that reduce the physiological strain produced by stressful components of the total environment” (24).

Clarification of related terms is essential to explain cold adaptation, namely “acclimatization”, “acclimation”, and “habituation” (18). Acclimatization describes the set of physiological and/or behavioural changes that occur within the lifetime of an organism to minimize the strain of stressful changes in the natural climate, including geographical differences or seasonal changes (18,24). Acclimation refers to adaptive changes induced under controlled experimental conditions, such as temperature manipulation. (18). Lastly, habituation denotes a reduction in physiological responses to or perception of repeated stimuli (18,24). Whole body exposure is not necessary to trigger habituation as it is able to develop in relatively small regions, such as the hands of fishermen who work with one or both hands immersed in cold water (16). Indigenous populations of circumpolar regions exhibit cold responses similar to individuals from temperate climates (16). However, in comparison to people living

in warmer climates, the increase in metabolic heat production and the vasoconstriction to reduce peripheral heat loss appear to be less pronounced, consistent with habituation (16).

People living in the circumpolar region have a higher resting metabolic rate than individuals from more temperate climates, enabling them to maintain warmer skin temperatures with less shivering during cold exposure (16). Observational studies indicate that human populations frequently exposed to chronic environmental cold stress show increased metabolic activity of brown adipose tissue (BAT), through maximization of β-oxidation, electron transport activity and UCP1 expression (20,25). Moreover, evidence shows that long term cold exposure and hormonal stimulation not only remodel BAT, but can also induce the "browning" of competent white adipose tissue, characterized by increased mitochondrial content and subsequent UCP1 expression, in addition to other BAT-associated genes (20).This so-called browning of white adipose tissue increases thermogenic potential, resulting in an increased non-shivering thermogenesis capacity (22,25). In addition, studies in Greenlandic populations have reported elevated circulating T_3 levels and an overall modulation of thyroid hormones in response to cold exposure, supporting the previously mentioned link between thyroid hormones and the activation of BAT (25).

Chronic cold adaptation also manifests in lipid metabolism. Despite a diet predominantly composed of animal products, indigenous Arctic populations exhibit relatively low serum lipid concentrations (25). The study of Vlasova et al. (2025) demonstrates that the indigenous populations of the Russian Arctic have lower LDL and higher HDL levels compared to the population of Caucasian ethnicity (26). At the level of triglycerides, significant differences were observed exclusively in females, with the highest prevalence of hypertriglyceridemia reported in the Caucasian control group (28).

While BAT is primarily responsible for thermoregulation, the liver plays a central role in systemic nutrient metabolism (27). Therefore, the serum lipid decrease during chronic cold exposure might be due to a potential hepatic contribution. Currently, only animal studies investigating the effect of the liver in chronic cold adaptation are available. In neonatal goats, 24-hour exposure to 6°C significantly elevated serum glucose while reducing circulating non-esterified fatty acids and triglycerides, without affecting cholesterol fractions. Consistent with these systemic changes, a significant reduction in triglyceride content was observed after cold treatment, indicating decreased lipid deposition (27). Similar alterations in glucose and triglyceride levels were reported in dairy goats subjected to chronic cold exposure for 21 days (28). Altogether, these findings suggest that both acute and prolonged cold exposure cause a comparable shift in hepatic lipid metabolism. Research using non-hibernating rodents further supports this pattern. Rats exposed to 4°C and a 1h light/23h dark cycle for 4 weeks displayed significantly reduced plasma triglycerides, while glucose and cholesterol remained unchanged (29). Ex vivo hepatic perfusion at 37°C showed a 23.0% increase in fatty acid uptake for β-oxidation, pointing to enhanced lipid catabolism (29). While this summary mainly focused on mammalian lipid metabolism, significant changes in hepatic carbohydrate and protein metabolism were also reported (27). Together, these studies demonstrate a consistent pattern across various mammalian species. Specifically, cold exposure induces increased lipid utilization and altered metabolic homeostasis in the liver, supporting the liver as an active contributor to mammalian cold adaptation.

When considering the effects of each organ system in humans, it is reasonable to assume that the physiological adaptations observed in cold-acclimatized populations have also been subject to genetic selection.

5.4 Genetic basis of human cold adaptation

Although the out of Africa theory has considerable support, the specifics regarding the expansion of the human population remain a subject of debate (30). The Estonian Biocentre Human Genome Diversity Panel (EGDP) established a relevant study cohort by assembling a dataset of 483 high-coverage human genomes from 148 populations worldwide. To ensure broad representation, each continent was represented by one or more distinct populations. For instance, Asia was stratified in West Asia, South Asia, Island Southeast Asia, East Asia, Central Asia and Siberia. Siberia was further regionally divided in West, Central, South and North-East (30). The genomes were sequenced using 'Complete Genomics' sequencing technology, which specifically includes rolling circle amplification and sequencing by ligation (31). This methodology offers several advantages, such as adequate detection rate of SNPs and small indels, dense sequencing coverage of the whole genome, while simultaneously providing high throughput results, making this technique ideal for large-scale whole-genome sequencing projects (31). The primary focus of the EGDP are the genetic signatures of selection in populations that have lived hundreds of generations in environments markedly different to their ancestors.

In the current project, we focus on the selection signatures in human populations that have lived in extreme cold environments such as the harsh Arctic climate of Siberia. To investigate these patterns, three complementary selection tests, iHS, nSL and Tajima's D, were applied on the data of each global population. The Integrated Haplotype Score (iHS) is designed to detect strong, recent positive selection acting on alleles that have not yet reached fixation (32). Similarly, nSL (Number of Segregating sites by Length) identifies signatures of elevated haplotype homozygosity, but differs from iHS in its calculation: while iHS evaluates the area under the haplotype homozygosity decay curve, nSL directly measures the length of homozygous haplotype segments between pairs of haplotypes (33). In contrast, Tajima's D is a population genetics statistic that assesses whether a set of DNA sequences deviates from the expectations under neutral evolution using DNA polymorphisms, thereby identifying potential regions shaped by selection rather than drift (34).

Of the approximately 13.000 windows of 200 kilo basepairs (kb) spanning the human genome, 418 windows of the Siberian genomes exhibited a selection signal of $p < 0.01$ in at least one of the three previously mentioned tests. To ensure that these signals were specific to cold adapted populations, candidate regions were required to display non-significant selection signals ($p > 0.05$) in reference populations from Africa, the Middle East, Island Southeast Asia, and South Asia, which are not historically exposed to extreme cold. Applying these combined criteria, 756 protein-coding genes were identified within the 418 candidate regions (unpublished results, Anna Kolesnikova & Toomas Kivisild). Many of these protein-coding genes have not previously been functionally characterized or their relationship to cold adaptation established. I have used *Drosophila melanogaster* as a genetic model organism for the functional characterization of human genes with positive cold selection signatures.

5.5 *Drosophila melanogaster* as model organism

Since *Drosophila melanogaster*, hereafter referred to as *Drosophila* or fruit fly, was first used to elucidate the chromosome theory of inheritance. It has since become a leading genetic model

organism for a number of reasons, ranging from practical advantages over strong similarities at cellular, tissue and organ level to conserved genetic mechanisms.

First, *Drosophila* research is highly cost-effective. Flies can be maintained and bred in a limited space using simple media (35,36). Moreover, they can be handled safely and efficiently, using carbon dioxide, ether or cooling as anaesthesia (35)

Another major advantage of *Drosophila* is its short and well-characterized life cycle. Females can lay up to 100 eggs per day, enabling rapid generation of large numbers of progeny. At 25°C, development from a fertilized egg to an adult takes approximately 9-10 days (37). Embryos hatch after approximately 24 hours and spend circa four days as larvae. The larval stage consists of three distinct phases, namely first, second and third instar larvae, with the third-instar larvae leaving the food to pupate. Metamorphosis takes four days, during which pupae progress to adults before eclosing around days 9-10 (37). Adult flies undergo a brief maturation period following eclosion, during which the cuticle hardens, pigmentation stabilizes, and neuromuscular and metabolic systems complete development. Five to seven day old flies are generally considered the optimal age for experimental use. With an average life span of about two months, *Drosophila* also provides opportunities for studying aging phenomena in a relatively short timeframe (35).

A final practical advantage is that there are very few legal restrictions regarding their use and (genetic) manipulation in research, and ethical approval is typically not required (35,36).

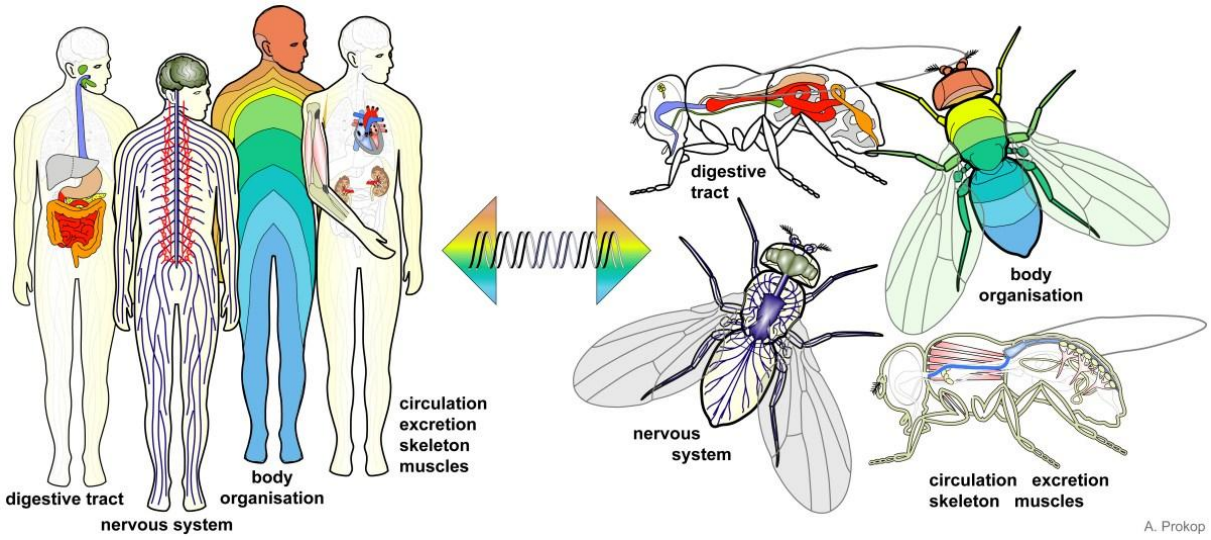

Figure 1. Anatomical comparison between humans and Drosophila melanogaster. Figure adapted from https://droso4schools.wordpress.com/, website made by Andres Prokop (36).

Despite obvious differences in terms of anatomy, work of the past decades has revealed that due to our shared evolutionary history, many molecular mechanisms that regulate development and drive cellular and physiological processes are conserved (38). In addition, organs in both species perform analogous functions and rely on homologous genes to coordinate their development, organisation and function (36). A prominent example is the *Drosophila* nervous system, which mediates the perception and processing of sensory information, including vision, hearing, olfaction, proprioception, and gustation (38). Analogous to humans, these sensory signals are transmitted to the central nervous system, where they are integrated and processed to generate appropriate motor outputs. Despite substantial anatomical differences between the human and *Drosophila* brain, numerous genetic, cellular, electrophysiological and chemical properties are conserved (38). Motor outputs in both

species are executed by muscle tissue, which is similarly categorized into smooth, cardiac and skeletal muscle (36). Skeletal muscle is the only type characterized by voluntary control and is striated in both species. In *Drosophila*, a single muscle fibre constitutes an entire muscle, whereas human muscle is composed of many muscle fibres. Yet the fundamental mechanisms of contraction are identical. However, the structural context differs as in humans the skeletal muscle tissue is indirectly attached to the skeleton via tendons, while flies possess an exoskeleton to which muscles are attached via the tendon matrix (36).

These examples illustrate the evolutionary conservation of organ systems and their underlying molecular and cellular mechanisms. The primary tissue of interest in this project is the fat body, which serves as the central organ for energy metabolism and storage in *Drosophila*.

5.5.1 Comparative physiology of the fat body

The *Drosophila* fat body is composed of adipocytes and distributed throughout the body in a sheet-like configuration, with the majority residing in the cavity between the gut and cuticle wall (39,40). During its lifecycle, *Drosophila* develops two distinct types of fat body, namely the larval and adult fat body, both of mesodermal origin but arising from separate progenitor lineages (40,41). The larval fat body is primarily optimized in accumulating biomass and nutrient storage during development, whereas the adult fat body specializes in energy metabolism, with differential features such as multinucleated cells and distinct storage granules (40).

The larval fat body originates during embryogenesis as two contiguous sheets that persist throughout the larval instar stages (40,41). The larval fat body undergoes extensive remodelling during metamorphosis, driven by autophagy, resulting in cell dissociation, progressive cell death, and an approximate three-fold reduction in tissue mass (40,42). This remodelling facilitates the mobilization of stored nutrients to support the growth and differentiation of newly formed adult structures (41). However, a subset of larval adipocytes persists 2-3 days post eclosion, continuing their function as major energy and nutrient reservoir (40).

While the larval fat body remodels during metamorphosis, the adult fat body progenitor cells establish the adult monolayer. In addition to their distinct progenitor origins, the metabolic profiles of the larval and adult fat body are specialized to support different physiological functions (40).

In the context of chronic cold exposure in humans, mammalian white- and brown adipose tissues play a key role in metabolic adaptation. The insect fat body shares several functional similarities to white adipose tissue, serving as the primary site for lipid, glycogen and protein storage. Furthermore, the fat body is capable of mobilizing energy stores during high energy needs, such as fasting, similar to mammalian adipose tissue (43)

In addition to being the organ equivalent to mammalian adipose tissue, the *Drosophila* fat body is also the functional counterpart of the mammalian liver. When considering the important hepatic contributions to mammalian lipid metabolism, particularly lipogenesis and lipolysis, the fly fat body exerts a similar function (see Section 5.8 Lipid metabolism in the fat body) (44). While the fat body remobilizes stored lipids to meet energy needs, oenocytes are responsible for ketone body synthesis during fasting (44).

5.6 Lipid metabolism in the fat body

Although adult and larval fat bodies are optimized for their designated developmental stages, core metabolic pathways are conserved, reflecting the essential role in energy storage and utilization (39). The primary cell type of the fat body, the adipocyte, is characterized by abundant lipid droplets occupying most of the intracellular space, along with glycogen and protein granules. Each lipid droplet (LD) consists of a hydrophobic core of neutral lipids, mainly triglycerides (TG), surrounded by a hydrophilic monolayer of phospholipids and cholesterol, with which regulatory proteins are associated (39).

Triglyceride (TG) metabolism begins when the fly ingests dietary TG, a natural component of standard laboratory diets (45). In the midgut lumen, digestive lipases hydrolyse these TG into free fatty acids (FA) and glycerol, or other acylglycerol intermediates. Enterocytes absorb the released metabolites and synthesize diacylglycerol (DG), the major transport form of neutral lipids in the haemolymph. Furthermore, excess dietary FA can also be converted into TG and stored transiently as intracellular LDs in the enterocytes. While DGs are distributed to various tissues, including the brain, oocytes, oenocytes and other tissues, most midgut-derived DGs are directed towards the fat body, with its uniquely high capacity for TG storage. In addition to dietary sources, many tissues, including the fat body, are able to synthesize TG de novo from acetyl-CoA. These TG and other lipid esters are subsequently stored into the hydrophobic core of the LDs (45).

LDs are central regulators of lipolysis, as their surface represents a barrier to access TG that is regulated by lipid droplet storage proteins, also known as Perilipins, which are conserved across many species (39,46). Once TGs become accessible, lipolysis proceeds through the sequential cleavage of the three fatty acids from the glycerol backbone (42,45). A key enzyme in both processes is *brummer*, the *Drosophila* homologue of human adipose triglyceride lipase (ATGL), as its gene encodes a LD-associated TG lipase that directly regulates systemic TG levels of the adult fly (42,46).

Downstream pathways, including DG to FA conversion and subsequent mitochondrial or peroxisomal β-oxidation, have not yet been elaborately characterized in the fly concerning the involved genes and their regulatory mechanisms (45).

5.7 Cold-evoked reactions in *Drosophila*

Drosophila melanogaster is an ectothermic organism, meaning its body temperature is determined by heat exchange with the external environment. Unlike endotherms such as humans, *Drosophil*a do not generate or retain enough metabolic heat to maintain a body temperature above ambient levels. Consequently, they rely on behavioral thermoregulation to remain within favorable temperature ranges (52,53). One major consequence of the ectothermic physiology is the strong temperature-dependence of their life cycle which is extended at lower temperatures. The extended developmental process can be explained by the temperature-induced reductions in metabolic rate. Despite the fact that the overall duration increases, the relative proportion of time spent in each developmental stage remains unaffected (47).

Similar to the evolutionary migration of humans described earlier, *Drosophila melanogaster* originated in a warm sub-Saharan climate and became associated with human settlements, enabling their global dispersal (48). As a result, contemporary populations now inhabit environments considerably colder than their ancestral range. Such within species variation in thermal tolerance seems to be driven by several physiological adjustments, including modifications in haemolymph ion and metabolite

composition, shifts in membrane lipid composition to preserve fluidity at lower temperatures, and enhanced capacity to maintain metabolic homeostasis during cold stress (49).

5.7.1 Cold perception and sensation

Cold perception in *Drosophila* starts with the primary thermosensory neurons of the peripheral nervous system, which contain distinct sensors for external and internal temperature. Cold-sensing neurons are located in the antenna and express the cold-activated transient receptor potential (TRP) channel named *brivido-1* (brv1) (50). In addition to brv1, genes brv2 and brv3 also encode cold sensing channels that have homology to mammalian TRP channels. Loss of any of these Brv proteins impairs behavioural discrimination of 25°C from cool temperatures (51). Interestingly, cold-sensing neurons are inhibited by heat, whereas heat-sensing neurons are inhibited by cold. Consequently, the removal of a thermal stimulus can produce a disinhibitory effect, thereby eliciting the perception of the opposite thermal sensation (59). Both categories of temperature-sensing neurons project to the central nervous system (proximal antennal protocerebrum) to form synapses with downstream neurons for further processing (50). Although the mechanisms underlying cold perception in the antenna have been extensively characterized, considerably less is known about temperature detection by peripheral sensory structures located in the body.

Drosophila wild type adults show a strong temperature preference of ±24°C, unaffected by prior acclimatization of five days at either 18°C or 29°C (52). In contrast to larvae, no clear distinction has been made in what is considered innocuous or noxious cold in adult flies. Instead, exposure to temperatures below 10°C is commonly associated with the onset of chill coma, a phenomenon reported across numerous insect species. During gradual cooling, insect activity progressively declines until individuals lose their ability to perform coordinated movements at a certain critical temperature. A state of complete neuromuscular paralysis, also known as chill coma, is observed when fruit flies are further cooled until the chill coma onset temperature (53,54).

5.7.2 Chill-coma as a state of complete neuromuscular paralysis

The exact mechanism underlying cold-induced neuromuscular paralysis is still under debate, as it is not certain if this state is primarily triggered by neuronal, synaptic or muscular failure (54). Not all insect species exhibit muscle depolarization at coma-inducing temperatures, suggesting that chill coma may arise through different mechanisms across species (53,54).

Depending on the severity of the cold exposure, cold-induced neuromuscular paralysis is completely reversible when the insect is returned to warmer temperatures. Recovery is typically defined as the return of an upright position, and the time required to recover is commonly referred to as the chill coma recovery time, which is influenced by duration and intensity of the cold stress (53,54).

5.7.3 Behavioural assays to measure cold sensation or tolerance

Both the onset and recovery of chill coma have been widely used to determine differences regarding cold tolerance in insects. The onset can be measured in variables regarding the temperature at which coordinated movements are lost or the time interval to induce the paralysis during a controlled temperature decrease. Chill coma recovery time is usually measured by exposing flies to temperatures of 0-4°C during multiple hours (2-6 hours) and determine the time needed to resume an upright position (55).

Moreover, assays have been developed that do not use chill coma. Instead, some studies use locomotor tracking during a temperature decrease that does not induce paralysis. The readouts used are walking speed, turning frequency and activity bouts. An example of such a set-up is the Rapid Iterative Negative Geotaxis (RING) assay used to study the effect of cold stress in locomotor performance and behaviour by Garcia & Teets (2019) (56). The assay starts by transferring flies into clean falcon tubes, which are then tapped against a hard surface three times using an apparatus. The flies were allowed to recover their position on the walls during four seconds before their progress was photographed. Following this initial climbing assessment, the experimental flies were exposed to cold treatment, and after recovery, this assay was performed again (56).

Another assay measures cold-flight performance, as cold affects the ability to fly earlier than walking. The flight assay of Frazier et al. (2008) measured flight performance by first cooling individual flies in a covered water-jacketed beaker to a certain test temperature (57). After one minute of recovery, flight performance was measured by chasing each fly with a paintbrush, thereby encouraging them to escape by flying (57).

This project is aimed at identifying genes that enable greater cold resistance and/or tolerance in *Drosophila*. For that reason, I selected chill coma onset and recovery as behavioural assays.

5.7.4 Cold perception in larvae

In contrast to adults, the temperature ranges that evoke cold-induced behaviour in third instar larvae have been experimentally defined. Larvae prefer ambient temperatures between 18-22°C, perceive innocuous cold at 11-17°C, and experience noxious cold at ≤ 10°C (58,59).

Larval thermosensation is mediated by specialized thermosensory neurons that reside in the dorsal organ ganglion (DOG) and the terminal organ ganglion (TOG). DOG neurons express cool-responsive ionotropic receptors, allowing rapid activation upon temperature decrease, while their activity is inhibited when temperature rises (50).

Larvae also possess peripheral sensory neurons in the lateral body wall that respond to temperature changes (50). These multiple dendritic (md) sensory neurons have complex dendritic structures that cover the epidermis (50,58). This type of sensory neurons is typically present in each larval body segment and project to the ventral nerve cord (58). Based on dendritic morphology, a further classification can be made into four different classes (I-IV) (50,58). Class III md neurons become activated upon cold as well as gentle touch stimuli (58).

Larval cold-evoked behaviours arise from coordinated muscle activation patterns. During cold-evoked contraction responses, the anterior and posterior segments reach peak activation before central segments. Within each segment, dorsal and ventral muscles reach peak responses before lateral muscles (60). These spatial and temporal activation patterns generate the characteristic cold-evoked behaviours observed in larvae, summarized in Figure 2 (61).

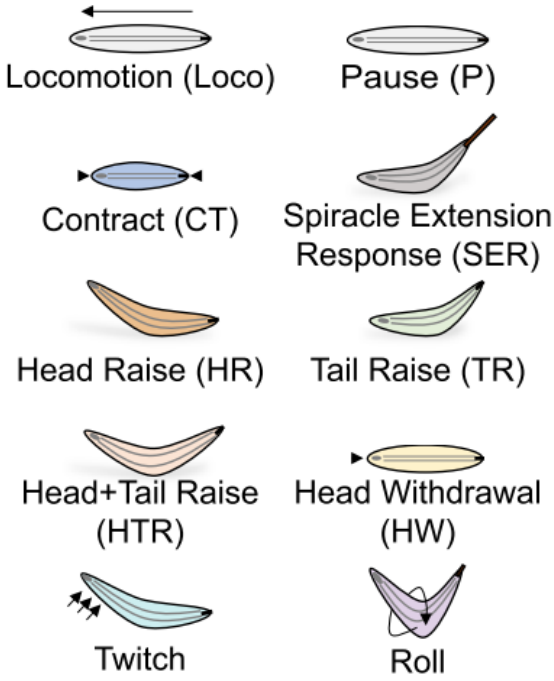

Figure 2. Cold evoked behaviours in third instar larvae. Figure adapted from Himmel et al. (2021) (61).

The prevalence of these behaviours increases with further cooling, yet each behaviour peaks at slightly different temperatures (58).

5.7.5 Chill coma in insect larvae

At present, no studies have directly demonstrated chill coma in *Drosophila* larvae, nor elucidated its underlying mechanism. However, chill coma has been documented in larval stages of several other species. Andersen et al. (2017) examined last instar larvae of the Lepidopteran species *Manduca sexta*, *Bombyx mori* and *Heliconius cyndo* to investigate chill coma mechanisms in insects with an atypical haemolymph ionic composition (62). Similarly, Ramadan et al. (2020) reported chill coma in *Tribolium castaneum* larvae following acute low-temperature shocks (63). Regarding cellular mechanisms in *Drosophila* larvae, the findings of Frolov & Singh (2013) showed that, in absence of muscle depolarization, low temperature impairs the activation of the L-type Ca^{2+} channels responsible for generating action potentials in larval muscle fibres (64). Therefore, it is reasonable to hypothesize that *Drosophila* larvae also experience a chill-coma-like physiological state under sufficiently low temperatures.

5.7.6 Behavioural assays for cold responsiveness

Few behavioural studies have been performed concerning noxious cold in *Drosophila* larvae. Two assays have been described before, specifically implementing a cold probe or cold plate.

The only studies using a cold probe are published by the group of Turner et al. (2016) (58,65). The custom-built probe was applied by hand to the dorsal midline, and cold evoked behaviours were recorded per stimulated segment (58).

Various research groups use a cold plate, of whom most reference the set-up of Turner et al. (2016)(58,65). The cold plate assay of Turner et al. (2016) consists of a thin metal plate (2 mm), sprayed with a fine mist of water, where larvae were placed ventral side down. This metal plate was transferred

to a Peltier-controlled plate that was pre-cooled to a temperature of interest and each larva was recorded individually (58,65).

The two temperature choice assay, previously mentioned in adults, has also been implemented using larvae in the study of Kwon et al. (2010) (59).

Currently, there are no published behavioural studies using an arena that allows comparison of cold sensitivity across larvae with different genotypes. This research gap was addressed in this project.

5.8 Genetic architecture of *Drosophila*

Since *Drosophila* was first used to elucidate the chromosome theory of inheritance, its broad genetic tool kit was the basis for its wide use as a genetic model organism.

The long time use as model organism and the small genome size made that the *Drosophila* genome was the second fully sequenced metazoan genome (37,66,67). Annotation of the genome identified 17.728 genes, of which 13.907 are protein-coding that translate to 21.953 unique polypeptides, and the remaining 3821 loci are RNA noncoding genes (67). Although exact numbers vary per source, an estimated 60% of all human genes and 65-75% of human disease genes have a *Drosophila* homologue (35,38,68). Protein coding genes are identified by the "CG" starting the annotation ID, while noncoding gene IDs begin with "CR" (37). Integrated genetic and genomic data can be found in the publicly accessible database FlyBase (https://flybase.org/), while expression and enrichment data of each gene can be located in FlyAtlas2 (https://flyatlas.gla.ac.uk/FlyAtlas2/index.html?page=gene). One of the more recent projects is that of Li et al. (2022) called Fly Cell Atlas, in which the *Drosophila* w1118 single nuclei transcriptome of head, body and isolated organs of both male and female was sequenced and mapped (69). The original datasets of each snRNA sequencing run are publicly available. The results are also accessible via the platform SCope and ASAP, and the integrated viewer in FlyBase.

5.9 *Drosophila* genetic toolkit

The main strategies to study human diseases using a fly model is via forward or reverse genetics. Forward genetics are based on inducing random mutations by mutagens or transposons, followed by screening for a particular phenotype. This strategy has the advantage of being unbiased and therefore able to identify uncharacterized mutations in known disease genes, also known as phenotypic expansion, or linking previously unknown genes (38).

In contrast, in reverse genetics approaches one starts from the fly homologue of human genes to study their phenotypes in vivo. Three possible ways can be implemented to reduce or eliminate expression of a certain gene of interest, namely targeted gene disruption by using CRISPR/Cas9, transposon-mediated mutagenesis, and gene silencing via RNA interference or CRISPR/Cas9 (38).

In this project, the 21 genes of interest were studied by gene silencing in the *Drosophila* fat body, the equivalent of the mammalian liver and adipose tissue, using RNA interference.

5.9.1 Reverse genetics using gene silencing

RNA interference (RNAi) has become a widely used strategy to investigate gene function in *Drosophila*, particularly when combined with the GAL4/UAS system to enable tissue-specific control. Unlike mutational approaches, RNAi enables targeted gene silencing without altering the endogenous copy, making it a flexible tool for functional genomics (70). The RNAi pathway is initiated by double stranded RNA (dsRNA), which can be experimentally introduced by injection or expressed from transgenes

designed to produce hairpin structures complementary to the gene of interest (71). Once present in the cytoplasm, dsRNA is processed by the Dicer-2 enzyme into short fragments of 21-25 nucleotides (72,73). These fragments are then incorporated into Argonaute 2, which binds the ‘3- and ‘5 terminus of the guide strand in its domains to generate the pre-RNA-induced silencing complex (pre-RISC) (72). Once bound, the passenger strand is cleaved and thereby dissociated from the complex, resulting in the formation of the mature RISC (71,74). RISC uses the guide strand to identify complementary mRNA sequences and cleaves them, thereby preventing translation (72). Importantly, RISC does not require perfect sequence complementarity to initiate cleavage, meaning that transcripts with partial homology to the gene of interest can also be targeted, resulting in off-target effects (71,72).

In this project, *Drosophila* strains are used from the Vienna Drosophila Resource Center (VDRC) and Bloomington Drosophila Stock Center (BL) (see Table 2). Each centre uses different techniques to generate genetically altered strains expressing the hairpin dsRNA construct (71). The GD library of VDRC was constructed using gene-specific inverted repeats of around 300 bp downstream of the Upstream Activating Sequence (UAS) promotor. Integration of these constructs was done by P-element-mediated transposition (71). P-elements are a particular type of mobile genetic elements and can be further classified in autonomous or nonautonomous based on their ability to transpose (75). While P-element transposition is not site-specific, it occurs in regions around gene promotors and in general has a preference for more open chromatin (76). The more recent KK library of VDRC uses PhiC31-mediated site-specific integration. The PhiC31 recombinase recognizes attP attachment sites engineered into the *Drosophila* genome and the attB sites that flank the transgene in the donor plasmid, subsequently catalysing site-specific recombination (77). The hybrid sites change after recombination, creating a unidirectional and irreversible reaction, allowing the construct to be stable and heritable. As there are no cofactors required, such as host recombination machinery, this technique can also be implemented in embryos and germlines (77). All BL lines were generated by PhiC31 mediated integration(71).

5.9.2 Spatial and temporal control via the GAL4/UAS system

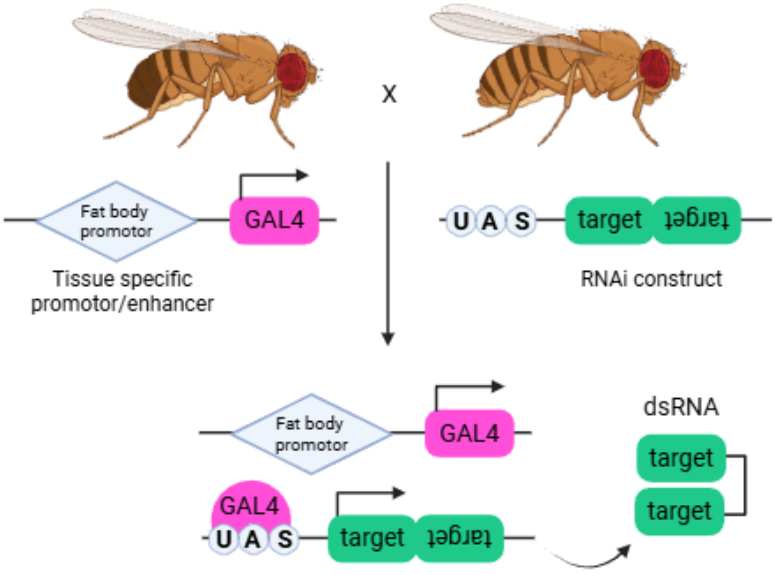

Figure 3. GAL4/UAS system to implement RNAi. Figure adapted from Hales et al. (2015), created in https://BioRender.com (37).

The GAL4/UAS system is used for tissue-specific gene regulation (71). The system relies on transcription factor GAL4, originally identified in *Saccharomyces cerevisiae,* which lacks endogenous binding sites in the *Drosophila* genome (70,78). As this transcription factor is derived from another species, its activity is restricted to the genes of interest that have been cloned under the regulation of the Upstream Activating Sequence (UAS), which has been optimized to achieve high affinity binding (78). Depending on the cloned genetic construct, both gene knock-down and overexpression are possible using this system. In the case of gene silencing by RNAi, the UAS promotor will regulate expression of the dsRNA construct. Another advantage of this system is the ability of spatial and temporal control, achieved by linking the GAL4 expression to tissue-specific promotors (78).

The combination of the GAL4/UAS system and the RNAi method was implemented in this project to study the different gene functions related to lipid metabolism in the fat body and their possible role in cold resistance and recovery during acute cold exposure.

6 AIMS

Recent GWAS in human populations living in extreme environments has identified candidate liver enriched genes putatively associated with cold adaptation.

This project aims to elucidate the functional role in cold tolerance of their homologous genes, utilizing *Drosophila melanogaster* as an *in vivo* model.

Specifically, our objectives are to:

- Silence the genes of interest in the fat body via targeted, tissue-specific knockdown (RNAi) and assess their contribution to cold stress responses in adult flies. Knockdown flies and genetic controls will be evaluated based on cold recovery and resistance phenotypes using the standardized chill coma recovery time and cold susceptibility assays.
- Analyse lipid composition and morphological characteristics of the fat body to determine whether they are correlated with cold recovery kinetics.
- Implement a nervous system-specific knockdown of TRP channel encoding candidate genes. Behavioural assays will be conducted to evaluate the impact of neural gene silencing on cold resistance and recovery.
- Establish a comparative behavioural assay in third instar wandering larvae enabling robust detection of cold associated phenotypes.

7 MATERIAL AND METHODS

7.1 *Drosophila* stocks and fly husbandry

Drosophila stocks were reared at 25°C using the lab's standard fly food recipe (Table 1), while exposed to a light-dark cycle of 12h/12h. Vials to collect virgin females from were stored overnight at 18°C. Collected virgin females of each strain were maintained at 18°C until crossed, at which time they were returned to 25°C. A minimum of five crosses, seen as biological replicates, were implemented and flipped after 24-48h of egg laying to create technical replicates. All *Drosophila* stocks used are listed in Table 2.

Component	Quantity
MilliQ water	12 L
Cornmeal	1000 g
Yeast	400 g
Agar	112.5 g
Dextrose	270 g
Molasses	600 mL
Propionic acid	150 mL
10% Hydroxybenzoate	22.5 g
99.8% Ethanol	225 mL

Table 1. Standard fly food recipe

Genotype	FlybaseID	Source	Stock number
UAS-Aldh-III-RNAi	FBgn0010548	VDRC	V107110
UAS-ATPsynBeta-RNAi	FBgn0010217	VDRC	V37812
UAS-Arr-RNAi	FBgn0000119	VDRC	V6707
UAS-CG14230-RNAi	FBgn0031062	VDRC	V104096
UAS-CG4168-RNAi	FBgn0028888	VDRC	v100080
UAS-Egr-RNAi	FBgn0033483	VDRC	V108814
UAS-Hyd-RNAi	FBgn0002431	VDRC	V44675
UAS-Galk-RNAi	FBgn0263199	VDRC	V103656
UAS-Iav-RNAi	FBgn0086693	VDRC	V100701
UAS-IleRS-RNAi	FBgn0027086	BL	58176
UAS-Klp68D-RNAi	FBgn0004381	VDRC	V101058
UAS-Mhc-RNAi	FBgn0264695	VDRC	V105355
UAS-Nan-RNAi	FBgn0036414	VDRC	V100090
UAS-ND23-RNAi	FBgn0017567	VDRC	V11097
UAS-Ndae1-RNAi	FBgn0259111	VDRC	V102707
UAS-Nep1-RNAi	FBgn0029843	VDRC	V108660
UAS-Nep7-RNAi	FBgn0039564	VDRC	V108266
UAS-NonAL-RNAi	FBgn0015520	VDRC	V101567
UAS-Pll-RNAi	FBgn0010441	VDRC	V103774
UAS-Pten-RNAi	FBgn0026379	VDRC	V101475
UAS-Rbfox1-RNAi	FBgn0026379	VDRC	V110518
PPL-GAL4	FBgn0027945	BL	58768
LSP2-GAL4	FBgn0002565	BL	6357
ELAV-GAL4	FBgn0260400	BL	4c8
UAS-CD8-GFP		BL	5137
Canton SB		Trudy Mackay	-
w1118		VDRC	60000

Table 2. Fly stocks used in this project. FlybaseID adapted from flybase.org. Stock numbers derived from designated resource center.

7.2 Novel chill coma susceptibility in adult flies

Individual adult flies of 5-7 days were aspirated into an arena containing 16 wells (5 mm diameter, 1 mm depth) and covered with a plastic petri dish. The arena was secured to white tissue to enhance contrast, with a sheet of aluminium foil underneath to optimize temperature conductance. To remove residual odour traces, both arena and cover were incubated overnight in 1% sodium dodecyl sulphate (SDS, #11667289001; *Roche, Indianapolis, IN, USA*) on a shaking platform at room temperature (RT) and subsequently washed. Avoidance of cold exposure by climbing was prevented by additionally treating the cover with Sigmacote (SL2; *Sigma-Aldrich*, *St. Louis, MO, USA*).

Each arena accommodated four flies per sex in both experimental and control condition, separated at least two days prior using CO_2. Three biological replicates were performed per assay, each conducted within a consistent 30 minute time window across experiments. After fly loading and a minimum 2 minute acclimatisation period, the arena was transferred to a precooled Peltier module equipped with a fan to dissipate residual heat. Settings to induce a stable 7,2-8,2°C temperature range were estimated using the PeakTech 4980 Dual Laser IR-Thermometer, requiring a 0,1A increase per replicate (79). Equal current and voltage settings were used per assay.

Response times were recorded using the Raspberry Pi High Quality Camera set-up and scored manually. Endpoint of chill coma was defined as the loss of upright posture accompanied by no further movement.

7.3 Chill coma recovery in adult flies

Chill coma was induced in 5-7 day-old adult flies by placing their rearing vials in ice in a 4°C environment. After 30 minutes, flies were transferred with a brush to the same arena design as described in the susceptibility assay, pre-cooled to 4°C to maintain chill coma. For each biological replicate, two arenas were used, yielding a total of 8 flies per sex per condition. Both arenas were positioned on a metal plate that was returned to ice immediately after loading, to ensure identical cold exposure. Based on Gerken et al. (2016), flies were subjected to 3h of cold exposure (55).

Following the cold treatment, arenas were returned to room temperature and covered with an SDS- (1%, #11667289001; *Roche, Indianapolis, IN, USA*) and Sigmacote- (SL2; *Sigma-Aldrich*, *St. Louis, MO, USA*) treated petri dish. Behaviour was recorded for 30 min using a Raspberry Pi High Quality Camera set-up, and recovery timepoints were scored manually. Recovery was defined as the return to an upright posture. Individuals that displayed leg or wing movement but failed to regain an upright position were assigned a recovery time of 30 min, corresponding to the full recording duration. Non-responders and casualties were excluded from the dataset.

7.4 Lipid quantification via sulfo-phospho-vanillin assay

Assay adapted from Van Handel (1985) (80). Snap frozen adult flies were sampled at a fixed time point (ZT5.5), to control for circadian variability in metabolic state. During collection, snap-frozen individuals of each cross were pooled to minimize potential batch effects, with each replicate consisting of 5 adult flies per sex. The adult abdominal fat body was dissected and tissues were mechanically homogenized using pestles and a motor in 250 µl PBS. All samples were stored at -80°C until further processing. 4 biological replicates were analysed per genotype. Homogenized samples were transferred to glass tubes (B20020; *M.L.S., Menen, Belgium*), to which Folch solution was added, consisting of chloroform:methanol in a 2:1 ratio. The standard curve was prepared using triolein solution (1000

µg/ml) diluted in Folch solution, to yield the following concentrations: 1000 µg/ml, 500 µg/ml, 250 µg/ml, 125 µg/ml, 100 µg/ml, 75 µg/ml, 50 µg/ml, 25 µg/ml and 12,5 µg/ml. Samples and lipid standards were incubated in a shaking incubator for 1h (37°C, 100 rpm). After incubation, the upper hydrophilic phase containing tissue debris was removed. The samples and lipid standards were placed in a heated water bath (65°C) until complete evaporation of the Folch solution. Lipids were activated by adding 200 µl of 95-98% sulfuric acid and boiled for 10 min using the heated water bath (95°C). Vanillin reagent was prepared in a ratio of 1 ml H_2O:4ml phosphoric acid (85%):6 mg vanillin (W310700; *Sigma-Aldrich*, *St. Louis, MO, USA*). Further processing was performed in reduced light exposure, as vanillin reagent is light sensitive. After cooling, 2 mL of the vanillin reagent was added to the samples and lipid standards. After incubating for 15 min at room temperature, 200 µl of both samples and lipid standards was loaded in a 96-well Greiner plate (650101) and absorbance was measured at 540 nm.

7.5 Fat body staining

Protocol adapted from De Groef et al. (2021) and Bradshaw (2023) (81,82). Adult fat body was dissected in ice cold PBS as described in De Groef et al. (2021) and fixed for 1h in 3.7% formaldehyde (#252549; *Sigma-Aldrich, Taufkirchen, Germany*) at RT. Fixed fat bodies were washed in ice cold PBS and incubated in Rhodamine Phalloidin (25 µg/mL, #P1951; *Sigma-Aldrich, St. Louis, MO, USA*) overnight at 4°C. After washing in PBS, lipid droplets were stained with BODIPY (1.25 µg/mL, #D3922; *Life Technologies, Carlsbad, CA, USA*) for 2 hours (RT), followed by a final PBS wash. Fixation, washing and staining steps were performed on a shaking platform. Tissues were mounted in VECTASHIELD Antifade Mounting Medium (H-1000-10; *Vector Laboratories, Burlingame, CA, USA*), visualized using the Olympus Fluoview FV1000 confocal microscope and processed using ImageJ.

7.6 RT-qPCR

Total RNA was extracted from tissue samples using NucleoZOL reagent (740404.200; *Macherey-Nagel, Düren, Germany*) according to the manufacturer's protocol with minor modifications. Samples consisted of 10 snap frozen adult flies collected at a fixed timepoint (ZT5.5) to minimize potential circadian differences in gene expression. Samples were homogenized in 500 µl NucleoZOL using a bead-based homogenizer executing 3 cycles of 30 s at 4 m/s (FastPrep-24 5G Bead beating grinder and lysis system; *MP Biomedicals*). Subsequently, 200 µl RNAse-free water was added per 500 µl NucleoZOL, and samples were vigorously shaken for 15s followed by 5 minutes incubation at room temperature. Samples were centrifuged (15 min, 12000 rpm, RT), after which the supernatant containing the RNA was transferred to a fresh RNAse-free tube. RNA precipitation was achieved by adding an equal volume of isopropanol and incubating overnight at 4°C. After centrifugation (10 min, 12000 rpm, 4°C), the RNA pellet was washed twice with 75% ethanol, including centrifugation (8000 rpm, 3 min, 4°C) between washes. After washing, ethanol was removed and the RNA pellet was resuspended in RNAse-free water. Samples were incubated overnight at 4°C to ensure complete solubilization.

cDNA synthesis of the extracted total RNA was performed using the SensiFast cDNA Synthesis Kit (BIO-65253; *Bioline, Waddinxveen, The Netherlands*). NanoDrop (*Thermo Fisher Scientific*) measured concentration per sample was used to synthesize 1000 ng cDNA. Reverse transcription was performed according to the cDNA Sensifast program in the Eppendorf Mastercycler Nexus x2 (*Sigma-Aldrich*).

Quantitative real-time PCR (qPCR) was performed using the protocol of NIPPON Genetics. Each reaction contained qPCR Universal Master Mix (5 µl, LS4050; *NIPPON Genetics, Düren, Germany*),

forward and reverse primer (0.5 µl, 250 nM; *IDTDNA, Leuven, Belgium*), cDNA template (2.5 µl, 20 ng/µl) and 2.5 µl RNase-free water. The 384-well plate was loaded according to the experimental design, sealed and briefly centrifuged to ensure proper mixing. The PCR of 40 cycli via the "Standard Curve with Melt (Run mode: Fast)" template was performed using the QuantStudio 6 Pro Real-Time PCR system (*Thermo Fisher Scientific*). Plates were analysed using the Design & Analysis Software 2.8.0 (*Thermo Fisher Scientific*).

Primer efficiency was determined using serial cDNA dilutions (1:1, 1:5, 1:10, 1:50, 1:100, 1:1000 and 1:10000). Results of primer efficiency are summarized in Supplementary table 1.

7.7 Statistics

Data analysis and subsequent graph construction were performed in R (version 4.4.1) using GenAI-generated code (83). The complete set of Rscripts are available upon request.

Differential expression between control and experimental groups was evaluated per gene using two-sided Welch's t-tests, robust to unequal variances between groups. Chill coma recovery time comparisons were analysed using Cox proportional hazards model per sex, accounting for variability per assay and nesting per replicate within the assay. Data generated in the chill coma susceptibility assay were analysed separately for males and females using a linear mixed model, testing induction time, assay and their interaction as fixed effects. Replicate nesting within assay was included as random factor to account for non-independent measurements obtained within replicates. The sulfo-phospho-vanillin assay values were modelled using a linear model per females and males. Within each sex, genotypes were compared to the negative control via treatment-versus-control contrasts. Resulting p-values of each implemented statistical test or model were adjusted for multiple testing using the Benjamini-Hochberg method. Statistical significance was defined as adjusted $p < 0.05$.

8 RESULTS

8.1 Genes of interest short list and their expression in the fat body

The liver has a notable impact in chronic cold adaptation across multiple mammalian species, potentially including humans. Hence, liver expression and enrichment divided by maximum expression of the 756 protein coding genes was determined according to the Genotype-Tissue Expression (GTEx) data of 2019. Of that list, genes with relatively highest liver expression, meaning a score of > 0.5, were queried for potential *Drosophila melanogaster* homologues. Using the criteria of most significant p-value in Siberian populations, non-significance in reference populations, elevated liver expression, and a representative *Drosophila melanogaster* homologue, the top 20 candidate genes were selected (Table 3). Additionally, the known *D. melanogaster* TRP channel *inactive* was included, as previous research has reported its relevance in cold perception of *Drosophila* larvae (59).

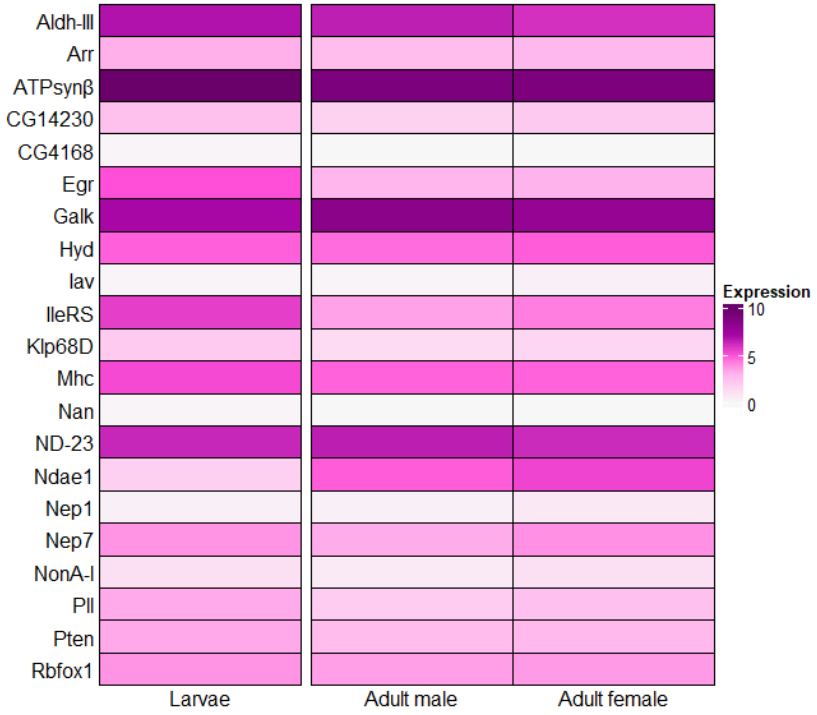

Figure 4. Log transformed FPKM *Drosophila* fat body expression values. Values adapted from FlyAtlas2.

8.2 DGRPool of chill coma recovery

The chill coma recovery phenotype of the DGRPool resource was queried to evaluate whether the candidate genes of interest have associated single nucleotide polymorphisms (SNPs) in wildtype strains. Based on 160 DGRP lines, the dataset of MacKay et al. (2012) reported two SNPs within the Mhc gene (84). Similarly, Morgante et al. (2016) identified three SNPs in Mhc and one SNP in Ndae1 in a cohort of 174 inbred wildtype strains (85). However, all SNPs showed a high false discovery rate (FDR ≈ 0.999), indicating loss of genome wide significance after multiple testing correction.

Human gene	GeneID	Function	*Drosophila melanogaster* homologue	FlybaseID	Function
UBR5	51366	Progestin-induced E3 ubiquitin-protein ligase targeting specific proteins for ubiquitin-mediated proteolysis	Hyd	FBgn0002431	Ubiquitin ligase that enables the transcription of Wnt targets
TPTE2	93492	Membrane-associated phosphatase with substrate specificity for the 3-position phosphate of inositol phospholipids	Pten	FBgn0026379	Dual lipid and protein phosphatase that inhibits cell growth, cell proliferation and cellular events controlling cytoskeletal and junctional rearrangements
PSPC1	55269	Nucleolar protein found in subnuclear structures occurring close to splicing speckles in transcriptionally active cells. It localizes to unique cap structures at the nucleolar periphery when RNA polymerase II transcription is inhibited, or during telophase	NonAL	FBgn0015520	Predicted to enable RNA binding activity and predicted to be involved in DNA-templated transcription regulation
ATP5F1B	506	Beta subunit of the mitochondrial ATP synthase catalytic core (Complex V)	ATPsynβ	FBgn0010217	Beta subunit of the mitochondrial membrane ATP synthase catalytic core (Complex V)
LRP5	4041	Transmembrane low-density lipoprotein receptor that binds and internalizes ligands. Also acts as co-receptor to transduce signals by Wnt proteins. Key role in skeletal homeostasis	Arr	FBgn0000119	Type I trans-membrane protein functioning as obligate coreceptor in the canonical Wnt signalling pathway
IARS1	3376	Isoleucine-tRNA synthetase, catalyses the aminoacylation of tRNA by their cognate amino acid	IleRS	FBgn0027086	Part of aminoacyl-tRNA synthetase multienzyme complex
NOL8	55035	Binding to Ras-related GTP-binding proteins, plays a role in cell growth	CG14230	FBgn0031062	Predicted to be involved in regulation of alternative mRNA splicing
TRPV5	56302	Member of the transient receptor family, specifically the TRPV subfamily. Activated by low internal calcium levels	Nan	FBgn0036414	Member of the Transient Receptor Potential (TRP) channel family, responding to stimuli such as startle, humidity and sound
			Iav	FBgn0086693	Member of Transient Receptor Potential (TRP) channel family, involved in response to different stimuli, such as startle, heat and sound
KEL	3792	Type II transmembrane glycoprotein, known as highly polymorphic Kell blood group antigen. Encoded protein	Nep7	FBgn0039564	Predicted to enable metal ion binding activity and metalloendopeptidase activity, predicted to be involved in proteolysis

		contains sequence and structural similarity to members of the neprilysin (M13) family of zinc endopeptidases			
KIF3C	3797	Predicted to be part of kinesin complex. Predicted to be active in cytoplasm and microtubule. Predicted to enable ATP hydrolysis activity, microtubule binding activity and microtubule motor activity	Klp68D	FBgn0004381	kinesin-2β motor subunit of the heterotrimeric kinesin-2. Essential role in sensory cilia assembly, microtubule organization in dendrites, and axonal transport
MYH15	22989	Predicted to enable actin filament binding activity and microfilament motor activity. Predicted to be involved in extraocular skeletal muscle development	Mhc	FBgn0264695	Motor protein that drives muscle contraction through its ATP-dependent interaction with actin filaments
GALK2	2585	N-acetylgalactosamine (GalNAc) kinase that becomes active during high galactose concentrations	Galk	FBgn0263199	Enzyme that phosphorylates alpha-D-galactose to form alpha-D-galactose 1-phosphate
ALDH3B1	221	Member of the aldehyde dehydrogenase protein family. Encoded protein is able to oxidize long-chain fatty aldehydes in vitro, and may play a role in protection from oxidative stress	Aldh-III	FBgn0010548	Protein that oxidises aromatic aldehydes and neutralizes lipid aldehydes formed due to reactive oxygen species and radicals
NDUFS8	4728	Subunit of mitochondrial mitochondrial NADH:ubiquinone oxidoreductase, also known as Complex I. Encoded protein is involved in binding iron-sulfur clusters of Complex I, thereby required in the electron transfer process	ND-23	FBgn0017567	Core subunit of the mitochondrial membrane respiratory chain NADH dehydrogenase (Complex I), among minimal assembly to enable catalysis
IRAK2	3656	Serine/threonine kinases that becomes associated with the interleukin-1 receptor (IL1R) upon stimulation	Pll	FBgn0010441	Tyrosine kinase-like family serine-threonine protein kinase that functions in the Toll pathway
SLC4A10	57282	Member of sodium-coupled bicarbonate transporters (NCBTs) family that regulate the intracellular pH of neurons, the secretion of bicarbonate ions across the choroid plexus, and the pH of the brain extracellular fluid.	Ndae1	FBgn0259111	Intrinsic membrane protein that reversibly mediates the exchange of 1 Na^+ and 2 HCO_3^- for 1 Cl^- at basolateral membranes of gut, renal epithelia and CNS neurons
RBFOX2	23543	RNA binding protein predicted to be a key regulator of alternative exon splicing in the nervous system and other cell types. The protein binds to a conserved UGCAUG and promotes inclusion of the alternative exon in mature transcripts. The protein also interacts with the oestrogen receptor 1 transcription factor,	Rbfox1	FBgn0052062	RNA-binding proteins that bind to (U)GCAUG elements. Nuclear isoforms regulate tissue specific alternative splicing, while cytoplasmic isoforms regulate mRNA translation

		thereby regulating oestrogen receptor 1 transcriptional activity			
ECM2	1842	Protein sharing extensive similarity with known extracelluar matrix proteins	CG4168	FBgn0028888	Function unknown
EDA	1896	Type II membrane protein that belongs to the tumour necrosis factor family and may be involved in cell-cell signaling during the development of ectodermal organs. Encoded protein can be cleaved by furin to produce a secreted form	Egr	FBgn0033483	TNF superfamily ligand that activates the intracellular JNK pathway. Roles include cell death, tumour suppression, tumour promotion, growth regulation, host defence, pain sensitization, and nutrient response
MMEL1	79258	Type II transmembrane protein that is member of the neutral endopeptidase (NEP) or membrane metalloendopeptidase (MME) family	Nep1	FBgn0029843	Plasma membrane bound metallopeptidase considered to cleave and inactivate signalling peptides

Table 3. Genes of interest. Human genes organized based on most significant p-value with their corresponding *Drosophila* homologue. GeneID and function of the human genes are derived from the NCBI Gene database. FlybaseID and *Drosophila* gene function are adapted from flybase.org

8.3 GAL4-driver potency measured using GFP expression

To determine the efficiency of the GAL4 driver that will be used to implement the knockdown, the available fat body specific GAL4 lines were crossed with UAS-CD8-GFP. In third instar larvae, LSP2-GAL4 had visually strongest GFP signal (Supplementary figure 1). Expression of LSP2-GAL4 and PPL-GAL4 was also determined in adult fat body. Individuals harbouring only the LSP2-GAL4 driver showed no measurable GFP expression (Supplementary figure 2), while GFP expression was present in both males and females containing the PPL-GAL4 driver (Figure 5). Based on these results, the PPL-GAL4 driver was selected to induce the fat body specific knockdown in adults.

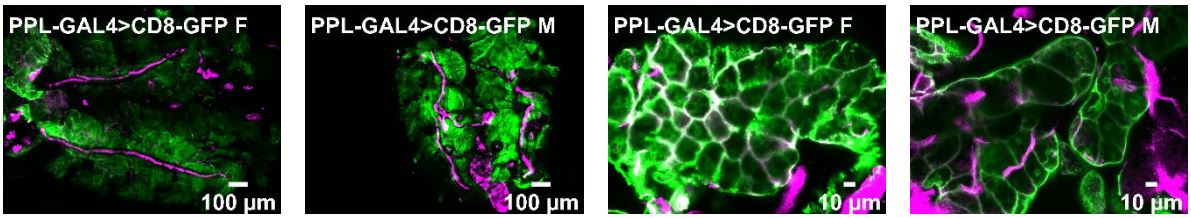

Figure 5. PPL-GAL4 induced GFP expression in female (F) and male (M) adult fat body. Dissected fat bodies were stained with Rhodamine Phalloidin to visualize actin in cell membranes.

8.4 Relative gene of interest expression in whole flies

To evaluate the knockdown efficiency of the PPL-GAL4 driven RNAi, the expression of the targeted gene was evaluated in control and knockdown flies using RT-qPCR.

First, primer efficiency was determined using serial cDNA dilutions. Primers with an efficiency of 80-130% percent were selected (Supplementary table 1). Three sets of primers were tested to measure gene expression of CG4168, Nan, Nep1 and Rbfox1, but none achieved optimal efficiency. The primer set that best approximated the efficiency criteria was selected.

Significantly reduced gene of interest expression in both females and males was detected in PPL-GAL4>Aldh-III-RNAi, PPL-GAL4>Arr-RNAi, PPL-GAL4>Galk-RNAi, PPL-GAL4>Hyd-RNAi, PPL-GAL4>Mhc-RNAi and PPL-GAL4>Pll-RNAi (Figure 6). PPL-GAL4>Ndae1-RNAi, PPL-GAL4>ND23-RNAi, and PPL-GAL4>Nep1-RNAi presented a significantly reduced gene expression only in males.

Following lines did not display any significant decrease in gene expression of the gene of interest in both sexes: PPL-GAL4>ATPsynBeta-RNAi, PPL-GAL4>CG14230-RNAi, PPL-GAL4>CG4168-RNAi, PPL-GAL4>Egr-RNAi, PPL-GAL4>Iav-RNAi, PPL-GAL4>Klp68D-RNAi, PPL-GAL4>Nan-RNAi, PPL-GAL4>Nep7-RNAi, PPL-GAL4>NonAL-RNAi, PPL-GAL4>Pten-RNAi and PPL-GAL4>Rbfox1-RNAi (Figure 6 & 7). Females of PPL-GAL4>ND23-RNAi, PPL-GAL4>Ndae1-RNAi and PPL-GAL4>Nep1-RNAi did not show a significant gene expression decrease.

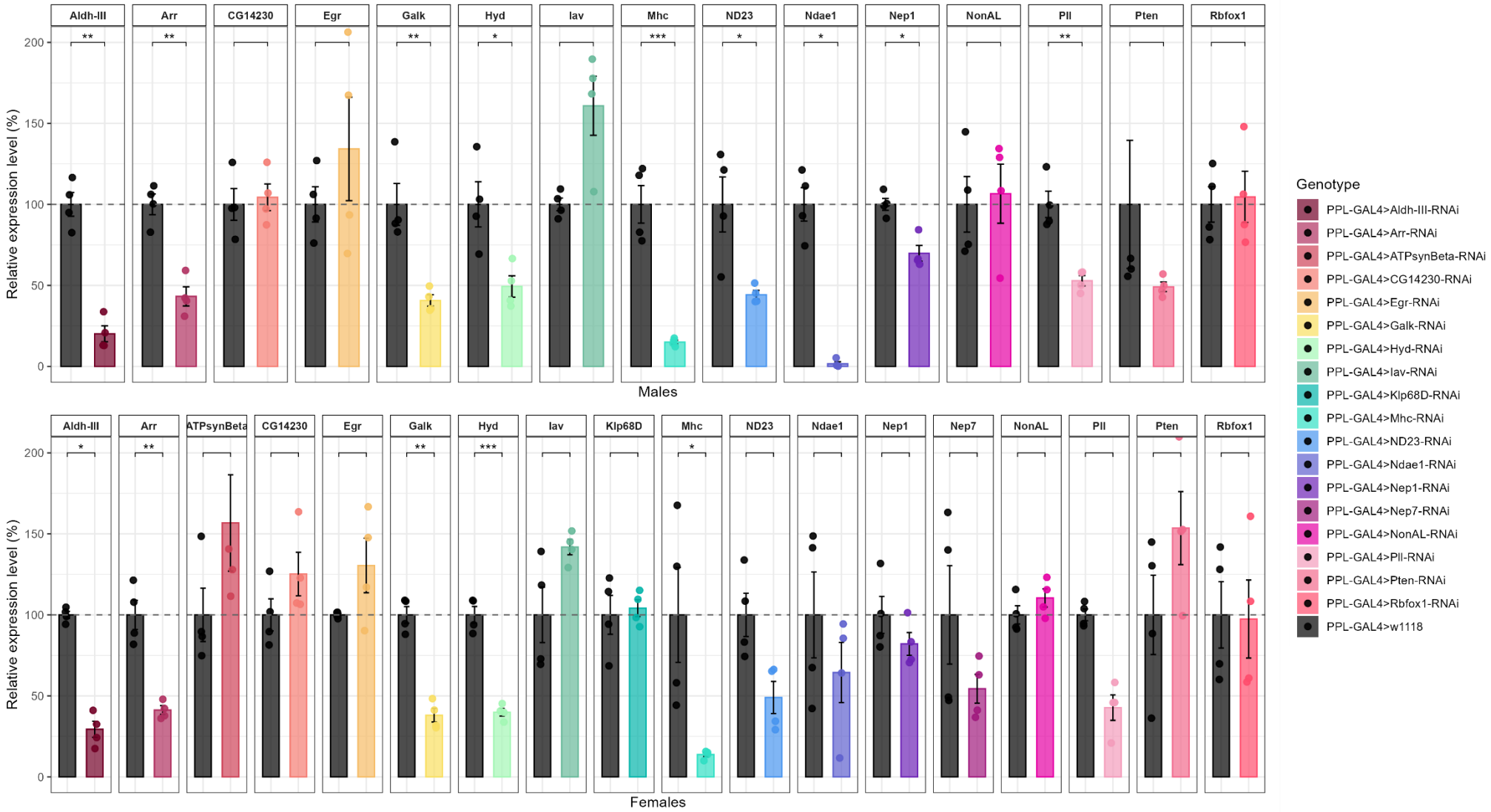

Figure 6. Relative gene expression (< 200% compared to control) following tissue-specific RNAi knockdown in males and females. Relative expression levels were quantified by RT-qPCR. Each genotype is represented by four replicates containing ten flies. Statistical significance was assessed by implementing Welch's t-test with unequal variances on the ΔCt values, and adjusted with Benjamini-Hochberg multiple testing correction. Significance levels are indicated as adjusted p<0.05 (*), adjusted p<0.01 (**), adjusted p<0.001 (***).

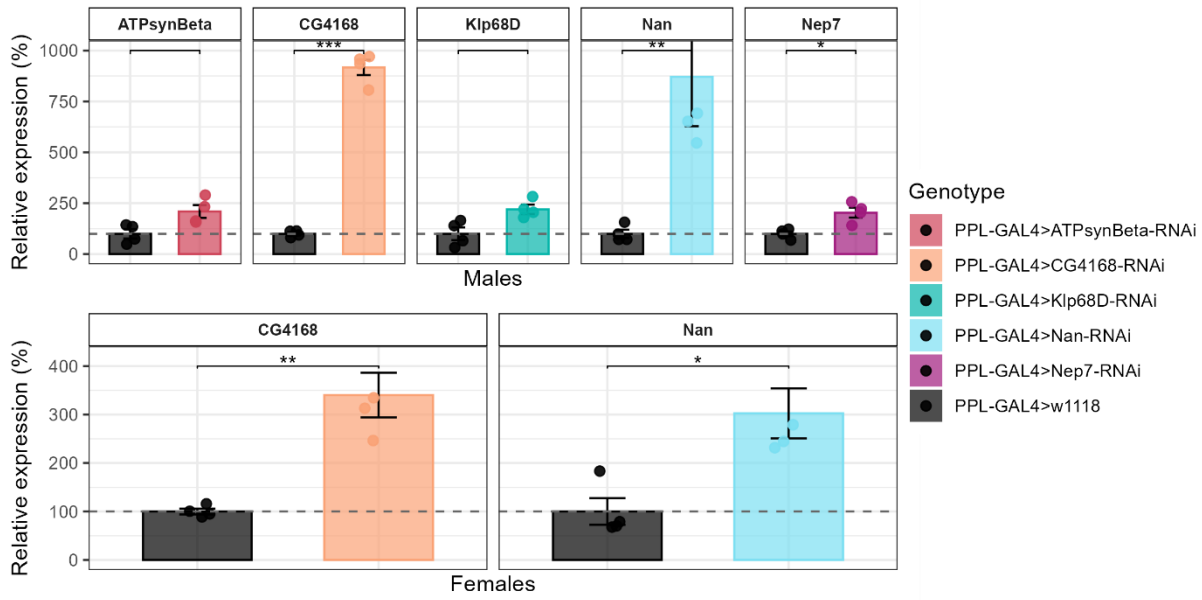

Figure 7. Relative gene expression (> 200% compared to control) following tissue-specific RNAi knockdown in males and females. Relative expression levels were quantified via RT-qPCR. Each genotype is represented by four replicates containing ten flies. Statistical significance was assessed by implementing Welch's t-test with unequal variances on the ΔCt values, and adjusted with Benjamini-Hochberg multiple testing correction. Significance levels are indicated as adjusted p<0.05 (*), adjusted p<0.01 (**), adjusted p<0.001 (***).

8.5 Chill coma recovery in adult flies

8.5.1 Optimisation

To define the parameters of the chill coma recovery assay, I optimized the assay using 8 female and 8 male w1118 flies. The most suitable cold exposure duration was determined by testing three potential cooling durations, specifically two, three and four hours. Recovery defined as return of upright position after two hours on ice required an average of 7,23 min (females: 7,88 min, males: 6,59 min), three hours shifted recovery to 12,27 min (females: 11,57, males: 13,22 min), and four hours cooling caused a mean recovery of 11,72 min (females: 11,95 min, males: 11,48 min) (Figure 8A).

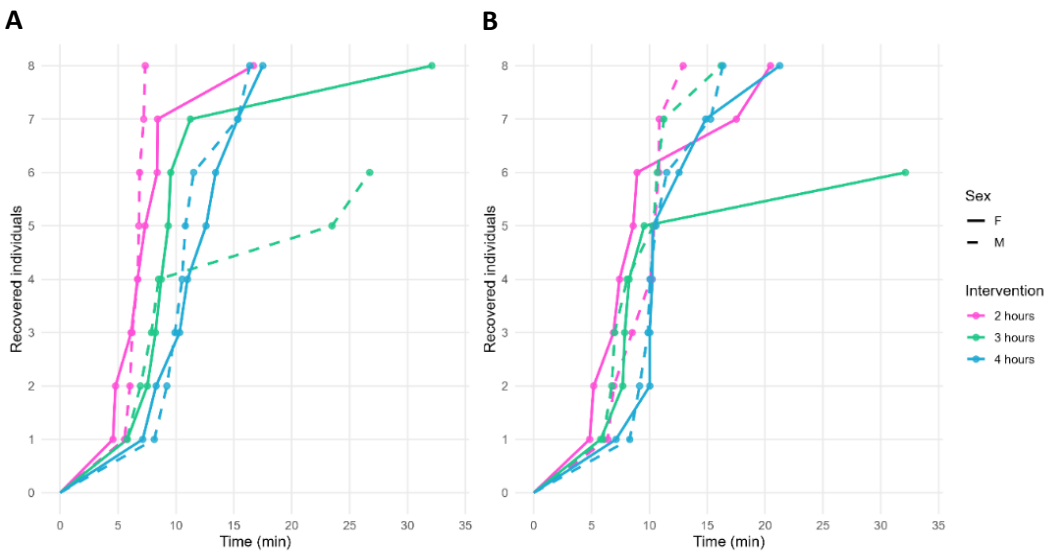

Figure 8. Change in recovery time following different cooling durations. Three potential cold exposures were tested, specifically 2 hours, 3 hours and 4 hours on ice, using 8 female (solid line) and 8 male (dotted line) w1118 flies. A) Recovery defined as return of upright position. B) Recovery defined as first locomotive movement following upright posture.

When defining recovery as return of upright position and first locomotive movement, mean recovery after two hours cooling on ice was 9,80 min (females: 9,98 min, males: 9,62 min), three hours 11,10 min (females: 11,88 min, males: 10,58 min), while four hours 11,72 min (females: 12,05 min, males: 11,39 min) (Figure 8B). Due to minimal shift in both definitions of recovery between the different cooling durations, the three hour intervention as described in Gerken et al. (2016) was selected (55). As resumption of locomotion is largely based on the incentive to move, recovery seen as return of upright position is more robust in determining muscle function regain and requires less subjective interpretation. Based on this data, the experimental genotypes were tested compared to the negative control using a cold exposure of three hours and their recovery defined as regaining upright posture.

8.5.2 Prolonged chill coma recovery in knockdown genotypes

To determine the contribution of the fat body specific gene of interest knockdown to cold stress responses, the chill coma recovery after three hour cold exposure was measured.

The PPL-GAL4>IleRS-RNAi genotype is not represented in this dataset, as there was no F1 progeny containing the gene knockdown succeeding each cross.

Chill coma recovery time was significantly impacted in both females and males in the following genotypes: PPL-GAL4>Aldh-III-RNAi, PPL-GAL4>ATPsynBeta-RNAi, PPL-GAL4>CG14230-RNAi, PPL-GAL4>CG4168-RNAi, PPL-GAL4>Egr-RNAi, PPL-GAL4>Iav-RNAi, PPL-GAL4>Klp68D-RNAi, PPL-GAL4>Nan-RNAi, PPL-GAL4>Nep1-RNAi, PPL-GAL4>Nep7-RNAi, PPL-GAL4>NonAL-RNAi, PPL-GAL4>Pll-RNAi, PPL-GAL4, w1118 and Canton SB (Figure 9-11, Supplementary table 2 and 3). Significant female-specific alterations in recovery were seen in PPL-GAL4>Galk-RNAi and PPL-GAL4>Pten-RNAi (Figure 9 and 11, Supplementary table 3). Significant differences only in males were detected in PPL-GAL4>Hyd-RNAi, PPL-GAL4>Mhc-RNAi, PPL-GAL4>ND23-RNAi and PPL-GAL4>Rbfox1-RNAi (Figure 9 and 10, Supplementary table 2). PPL-GAL4>Arr-RNAi and PPL-GAL4>Ndae1-RNAi did not generate any significant alterations in recovery duration. Only PPL-GAL4>Pten-RNAi presented an enhanced recovery time, yet only females attained statistical significance. Significantly faster recovery was also

detected in the control genotypes w1118 and Canton SB females. Significant alterations in other tested genotypes were due to prolonged recovery compared to the negative control within the assay.

Pairwise log rank comparisons within the control genotype PPL-GAL4>w1118 across the different assays displayed significant variation in recovery time per assay, occurring more frequently in females (Supplementary figure 3).

Most genotypes containing a targeted, tissue-specific gene of interest knockdown demonstrated a significant chill coma recovery delay compared to the negative control.

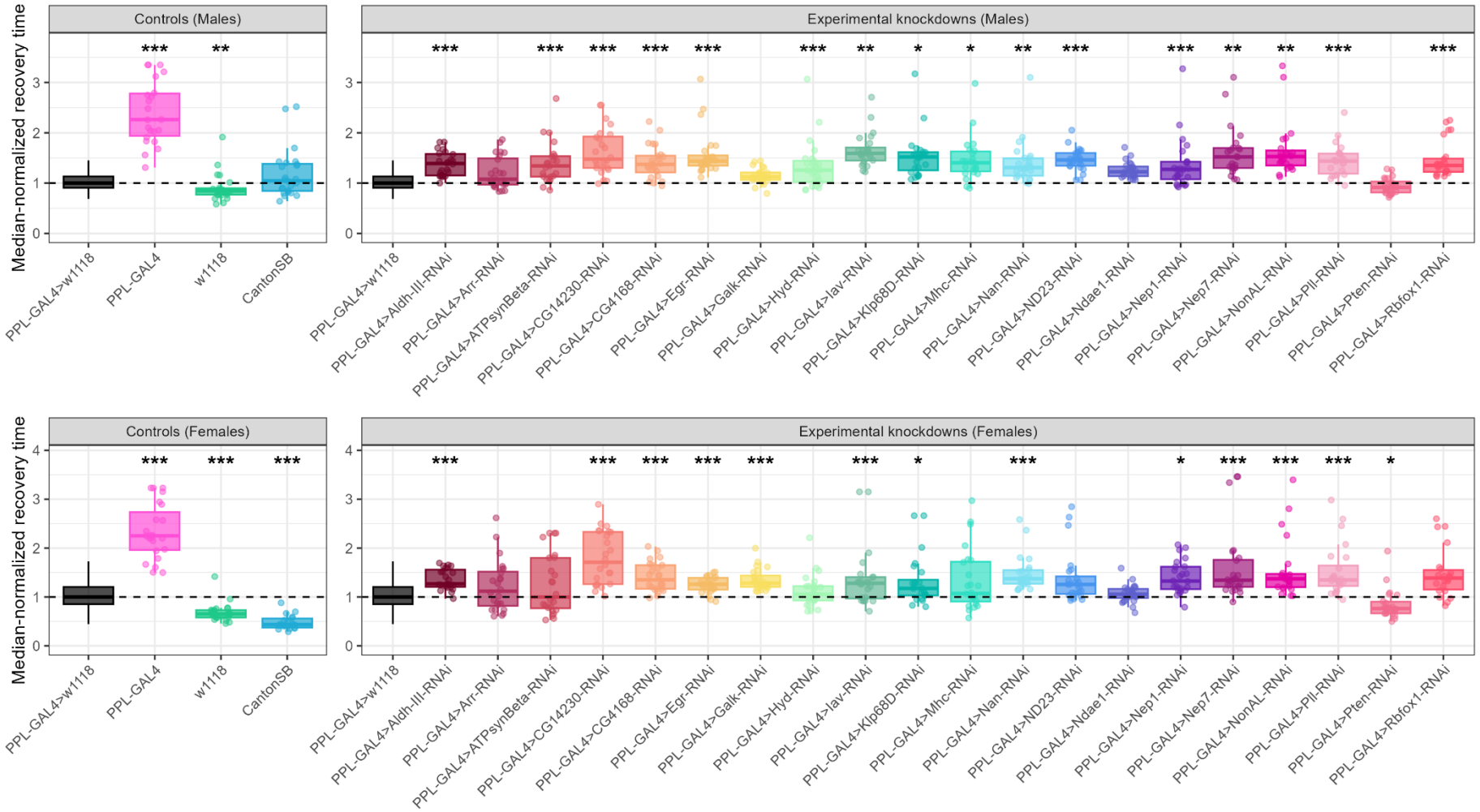

Figure 9. Median-normalized chill coma recovery of experimental genotypes containing fat body-specific gene of interest knockdown compared to the negative control. Each assay consisted of three replicates containing 8 flies per sex within the experimental and control condition. Three hour cold exposure was applied by maintaining the individuals on ice in a 4°C environment. Recovery was manually scored as the time necessary to regain an upright posture. Individuals that displayed movement but did not manage an upright position within the recording duration of 30 minutes, were scored a recovery time of 30 minutes. Cox proportional hazards model was implemented to perform pairwise comparisons of the experimental genotype to the assay's control survival distributions, accounting for variability per assay and nesting within replicate. Multiple testing was corrected by applying Benjamini-Hochberg correction. Significance is indicated by adjusted $p<0.05$ (*), adjusted $p<0.01$ (**) and adjusted $p<0.001$ (***).

A

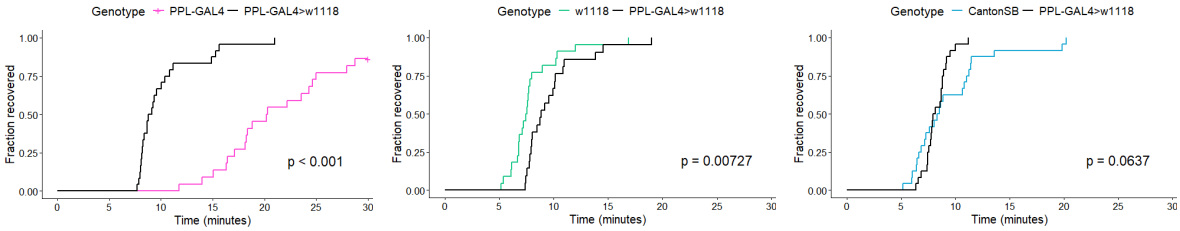
Genotype PPL-GAL4 PPL-GAL4>w1118
Fraction recovered
Time (minutes)
p < 0.001
Genotype w1118 PPL-GAL4>w1118
p = 0.00727
Genotype CantonSB PPL-GAL4>w1118
p = 0.0637

B

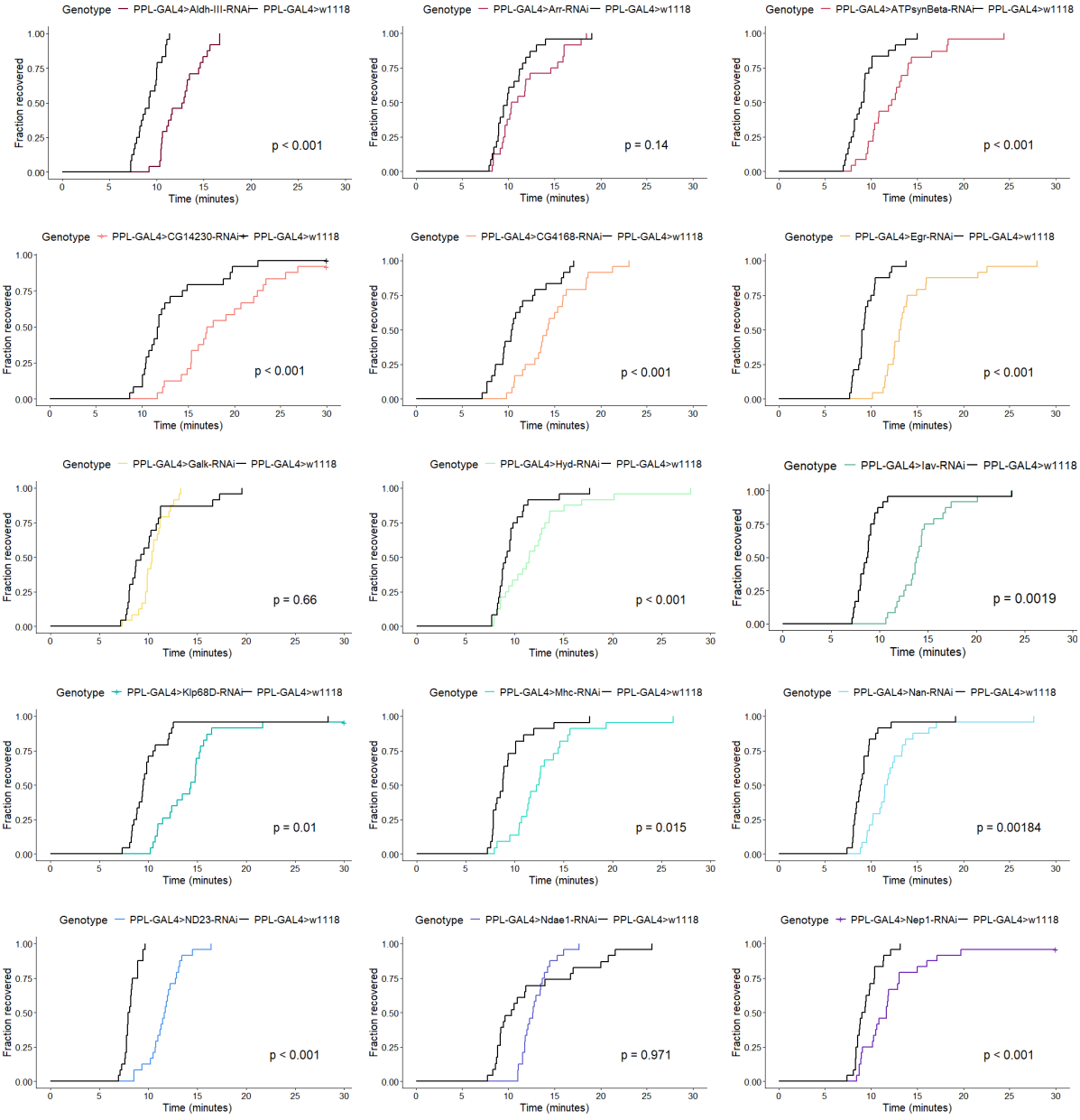
Genotype PPL-GAL4>Aldh-III-RNAi PPL-GAL4>w1118
p < 0.001
Genotype PPL-GAL4>Arr-RNAi PPL-GAL4>w1118
p = 0.14
Genotype PPL-GAL4>ATPsynBeta-RNAi PPL-GAL4>w1118
p < 0.001
Genotype PPL-GAL4>CG14230-RNAi PPL-GAL4>w1118
p < 0.001
Genotype PPL-GAL4>CG4168-RNAi PPL-GAL4>w1118
p < 0.001
Genotype PPL-GAL4>Egr-RNAi PPL-GAL4>w1118
p < 0.001
Genotype PPL-GAL4>Galk-RNAi PPL-GAL4>w1118
p = 0.66
Genotype PPL-GAL4>Hyd-RNAi PPL-GAL4>w1118
p < 0.001
Genotype PPL-GAL4>Iav-RNAi PPL-GAL4>w1118
p = 0.0019
Genotype PPL-GAL4>Klp68D-RNAi PPL-GAL4>w1118
p = 0.01
Genotype PPL-GAL4>Mhc-RNAi PPL-GAL4>w1118
p = 0.015
Genotype PPL-GAL4>Nan-RNAi PPL-GAL4>w1118
p = 0.00184
Genotype PPL-GAL4>ND23-RNAi PPL-GAL4>w1118
p < 0.001
Genotype PPL-GAL4>Ndae1-RNAi PPL-GAL4>w1118
p = 0.971
Genotype PPL-GAL4>Nep1-RNAi PPL-GAL4>w1118
p < 0.001
Fraction recovered
Time (minutes)

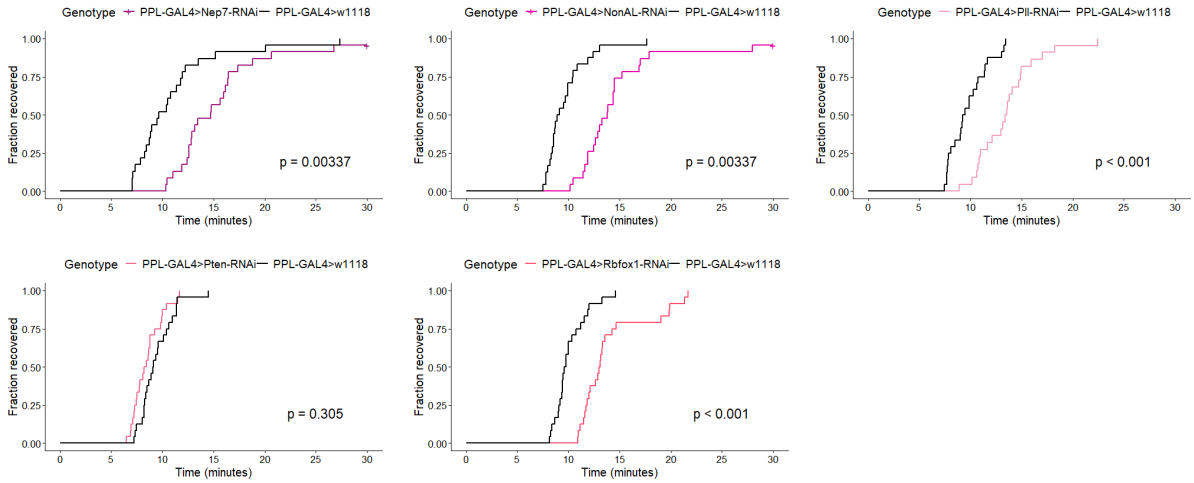

Figure 10. Kaplan-Meier analyses of male control and experimental genotypes compared to the negative control. Distributions of the experimental and control genotype within the assay were compared using Cox proportional hazards model, accounting for variability between assays and nesting within replicate. Benjamini-Hochberg correction for multiple testing was implemented and adjusted p-values are shown. A) Distributions in male control genotypes. B) Distributions in male experimental genotypes containing fat body-specific gene of interest knockdown.

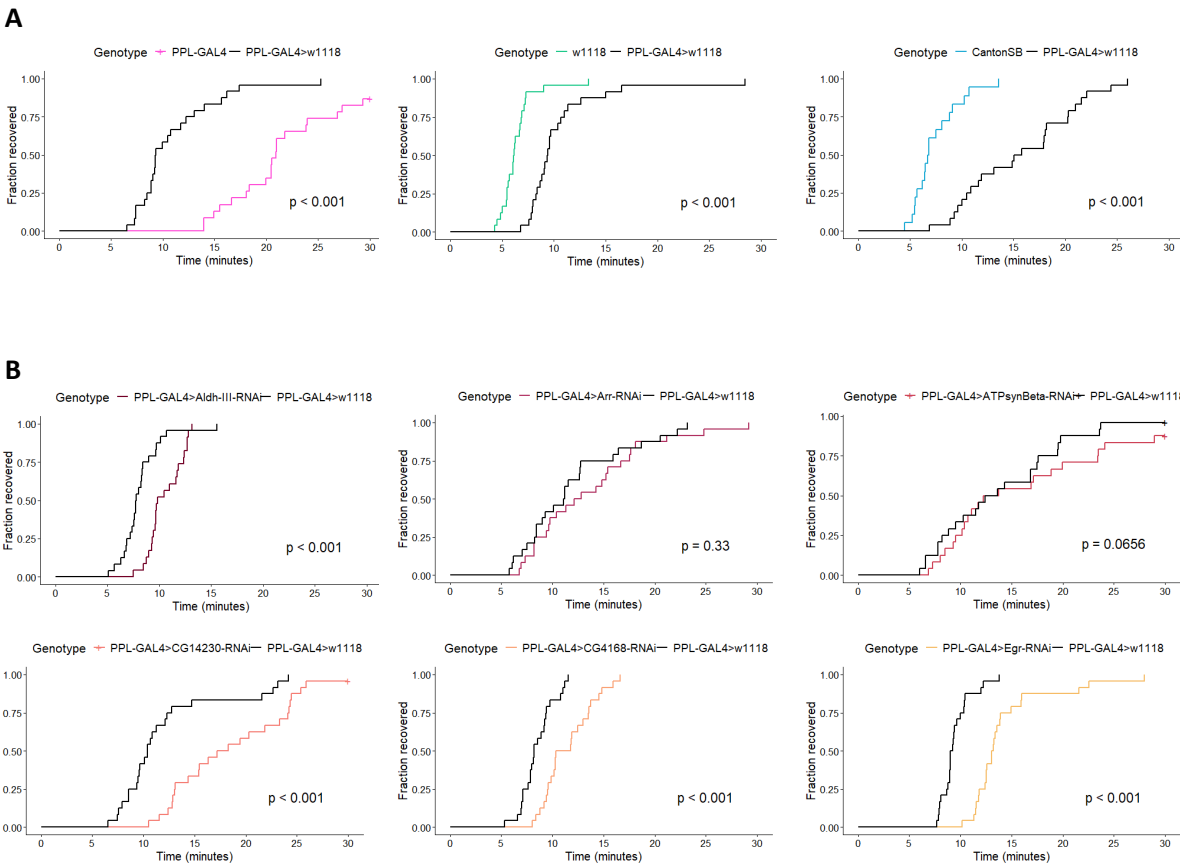

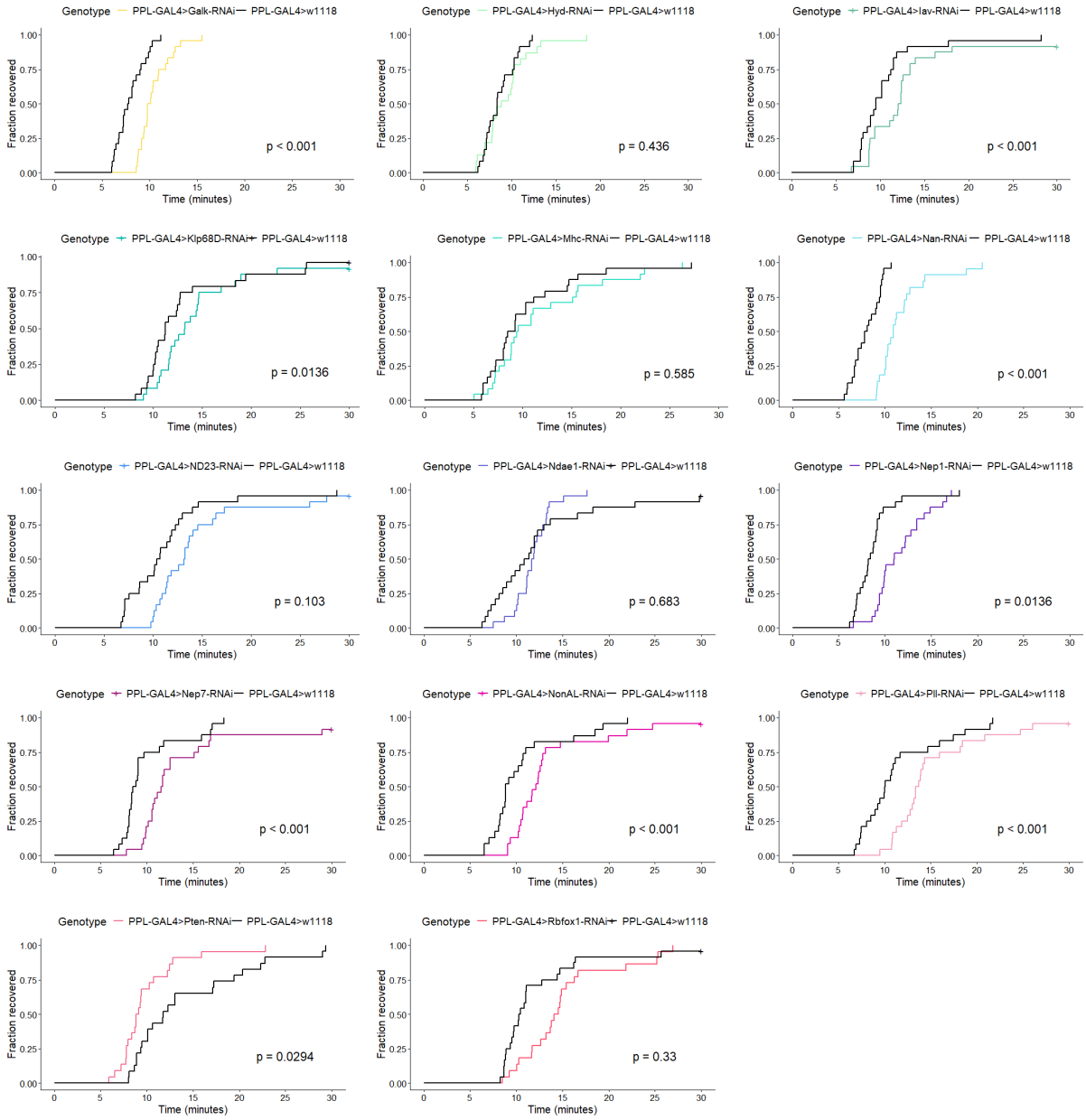

Figure 11. Kaplan-Meier analysis of female control and experimental genotypes compared to the negative control. Distributions of the experimental and negative genotype within the assay were compared using Cox proportional hazard model, accounting for variability between assays and nesting within replicate. Benjamini-Hochberg correction for multiple testing was implemented and adjusted p-values are shown. A) Distributions in female control genotypes. B) Distributions in female experimental genotypes containing fat body-specific gene of interest knockdown.

8.6 Chill coma susceptibility in adult flies

To determine whether the fat body-specific targeted knockdown changes chill coma susceptibility, translating to altered cold resistance, adult flies were exposed to a temperature range below the average chill coma threshold of flies reared at 25°C.

8.6.1 Optimisation

The main objective of the chill coma susceptibility assay optimization was to evaluate whether the Peltier module was able to reliably induce chill coma in different replicates within a single session. The required current and voltage settings to induce a stable temperature range of 7,2°C-8,2°C were estimated using the PeakTech 4980 Dual Laser IR-Thermometer, demanding a 0,1A increase per sequential replicate. Across two consecutive replicates using the recorded current and voltage settings, w1118 flies exhibited a similar chill-coma induction response (mean replicate 1: 3,73 min, mean replicate 2: 1,89 min) (Figure 12). Chill coma onset showed an observable drift, yet the implemented cooling parameters were sufficient to induce chill coma reliably within a replicate. Completion of two consecutive replicates within a defined time window indicates that the assay is operationally feasible for a multiple replicate experimental design. These findings confirm that the Peltier module enables sufficient thermal control to induce chill coma and the workflow can be executed sequentially.

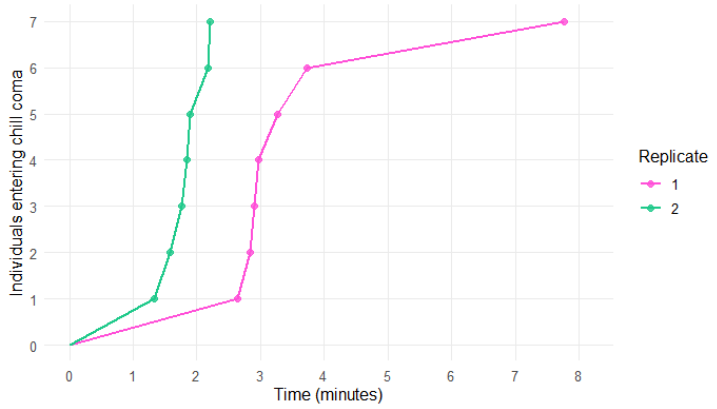

Figure 12. Response variability across two consecutive replicates using standardized Peltier module settings. Surface temperature of the Peltier element was estimated using the PeakTech 4980 Dual Laser IR-Thermometer. Settings that induced a stable temperature range of 7,2°C-8,2°C were recorded for further implementation. Chill coma occurrence and its required induction time in w1118 flies was recorded and manually scored. Performing consecutive replicates within one time window induces variability in chill coma induction time.

8.6.2 Chill coma induction responses in flies containing fat body-specific gene silencing

Within the experimental genotypes, PPL-GAL4>Egr-RNAi and PPL-GAL4>ATPsynBeta-RNAi presented a significantly altered chill coma induction time that was inverse between both sex (Figure 14). Knockdown of Egr caused reduced chill coma susceptibility in females, while enhanced in males, compared to the negative control. Contrary, in comparison to the negative control, females of the PPL-GAL4>ATPsynBeta-RNAi genotype entered chill coma faster, while males had a reduced chill coma susceptibility. Male-specific significantly altered chill coma susceptibility was detected in PPL-GAL4>Arr-RNAi and PPL-GAL4>Pll-RNAi, both generating a delayed chill coma induction time. Significantly modified susceptibility only occurring in females was seen in PPL-GAL4>CG4168-RNAi, PPL-GAL4>Galk-RNAi, PPL-GAL4>Nan-RNAi and PPL-GAL4>NonAL-RNAi. Knockdowns causing female-

specific alterations induced significantly prolonged chill coma induction time compared to the negative control.

When comparing the negative control PPL-GAL4>w1118 to its parental strains, PPL-GAL4 flies had significant differences in both females and males compared to PPL-GAL4>w1118 (Figure 13). The inverse significant alterations between females and males were present here as well, as the vast majority of females had a reduced chill coma susceptibility, while males entered chill coma quicker.

Chill coma induction was significantly altered in various genotypes, with three genotypes presenting sexual dimorphism compared to the negative control.

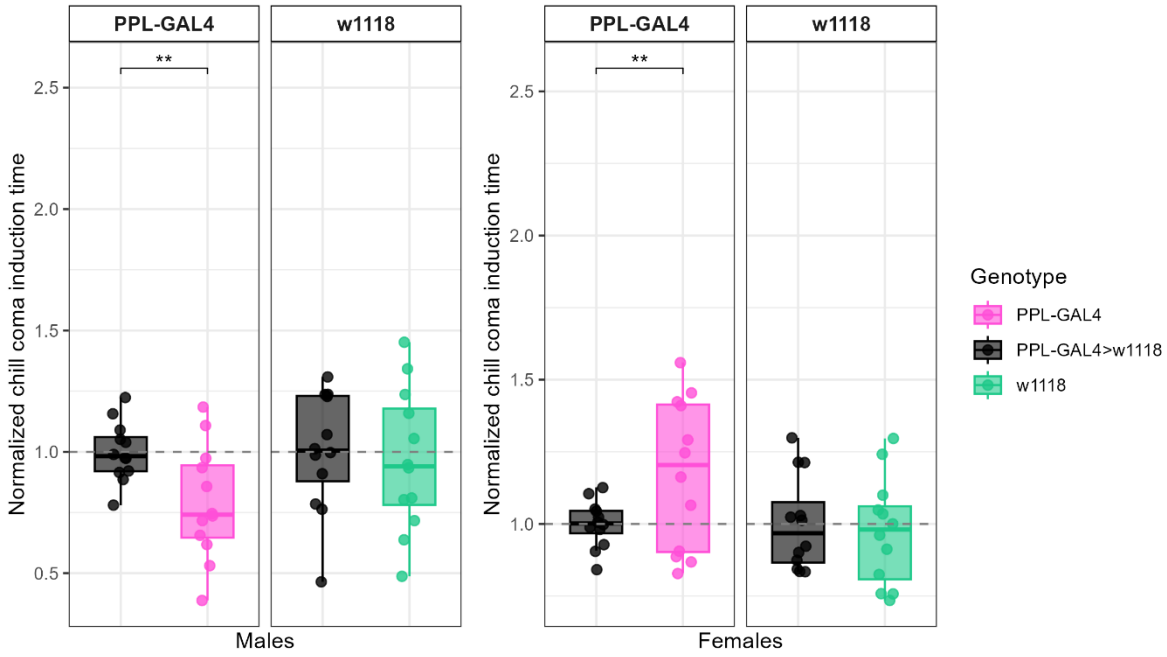

Figure 13. Normalized per replicate chill coma induction time of the negative control compared to its parental strains. Three replicates containing four female and four male flies of both genotypes were exposed to a precooled Peltier element. Time necessary to induce chill coma was manually scored. Linear mixed model per sex was used to pairwise compare chill coma induction time of both genotypes, while accounting for variability between assays and between replicates within the assay. Multiple testing was corrected using Benjamini-Hochberg method. Statistical significance is indicated as adjusted $p<0.05$(*), adjusted $p<0.01$ (**), adjusted $p<0.001$ (***). Chill coma induction time was normalized by the mean of the negative control per replicate, thereby normalizing the spread induced by temperature variability between replicates.

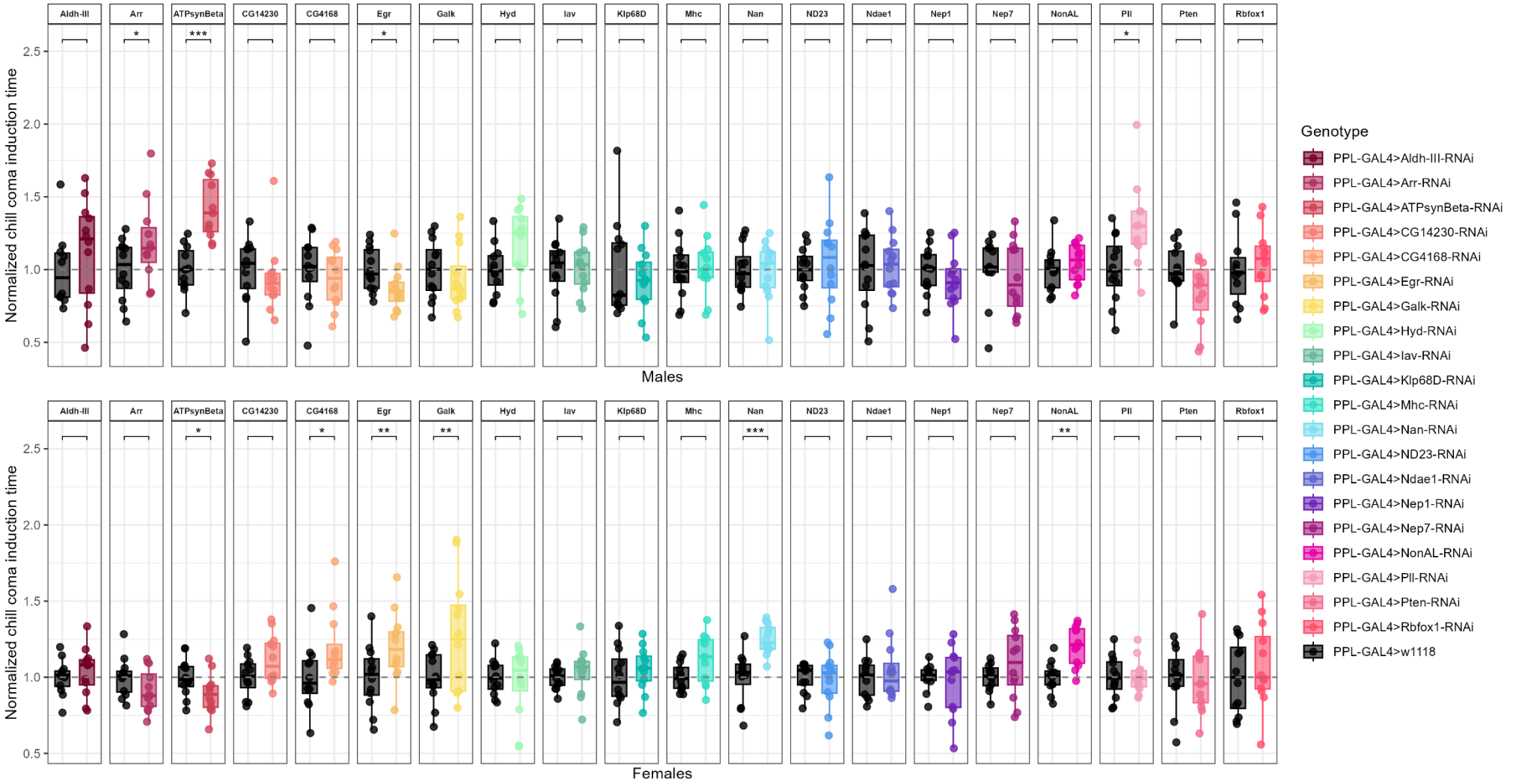

Figure 14. Normalized per replicate chill coma induction time per sex. Each genotype is represented by a total of 12 flies per sex, measured in three replicates. Time necessary to induce chill coma after exposure to a precooled Peltier element, defined as loss of upright posture, was manually scored. Data was analysed using a linear mixed model per sex computing pairwise comparisons, while accounting for variability between assays and between replicates within the assay. Benjamini-Hoch correction was implemented, and significance is presented as adjusted p<0.05 (*), adjusted p<0.01 (**), adjusted p<0.001 (***). Presented data is normalized using mean induction time of the negative control per replicate, thereby normalizing spread caused by temperature variability between replicates.

8.7 Significant changes in abdominal fat body lipid content

As these gene of interest knockdowns are induced in the fat body, we aimed to determine if the significant changes in chill coma recovery were due to modifications in the lipid metabolism. Genotypes that presented a significantly altered chill coma recovery time in males were further analysed regarding lipid content of the abdominal fat body and dorsal fat body lipid droplet morphology (Supplementary figure 4 and 5).

In the following genotypes significant differences in lipid content were detected in both sex: PPL-GAL4>Aldh-III-RNAi, PPL-GAL4>Egr-RNAi and PPL-GAL4>Nep1-RNAi (Figure 15, Supplementary table 6 and 7). The genotypes PPL-GAL4>CG4168-RNAi and PPL-GAL4>NonAL-RNAi presented solely significant differences in females (Supplementary table 7), while lipid content of PPL-GAL4>ATPsynBeta-RNAi, PPL-GAL4>Hyd-RNAi, PPL-GAL4>Nan-RNAi and CantonSB were significantly altered exclusively in males compared to the negative control (Supplementary table 6).

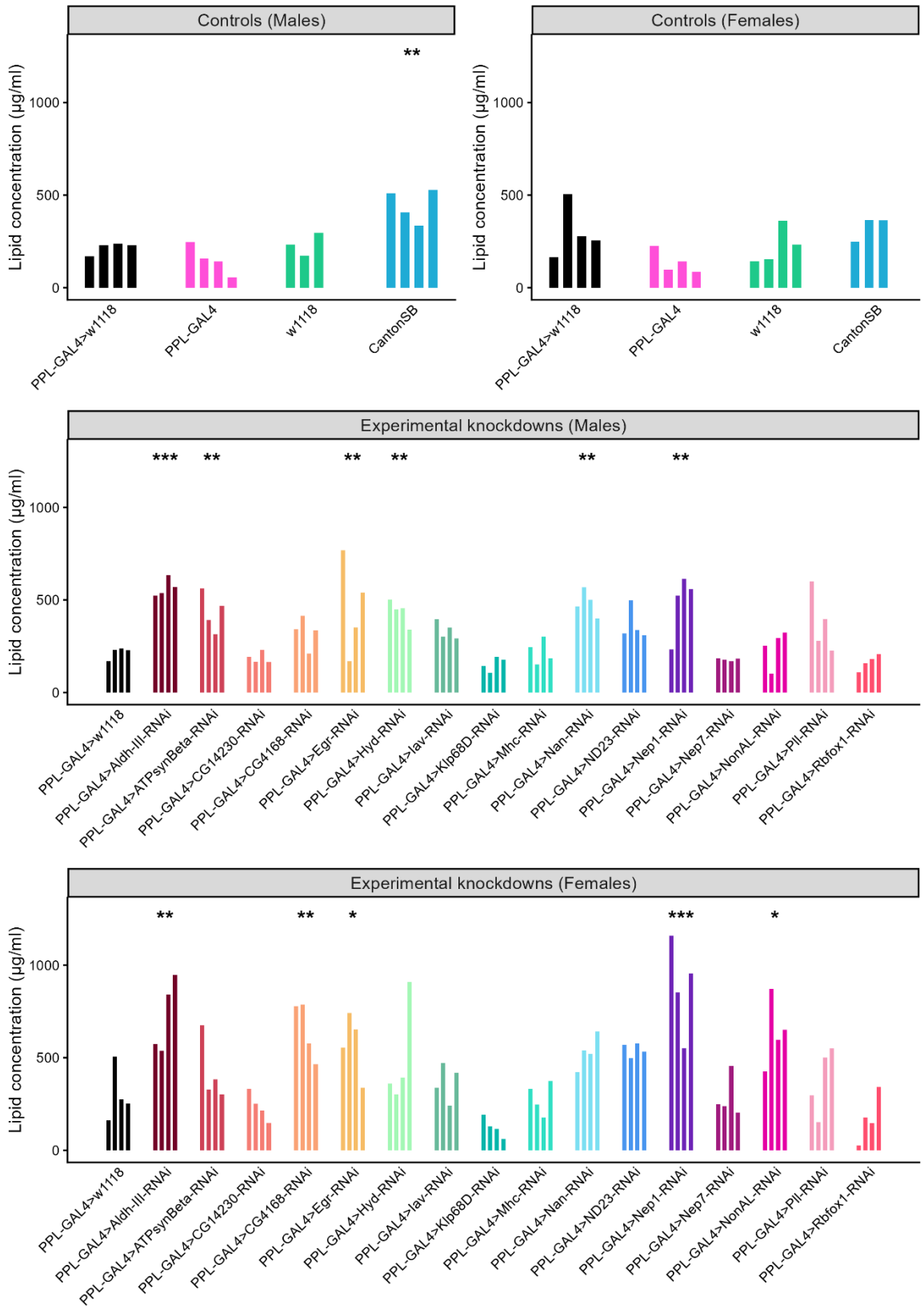

Figure 15. Abdominal fat body lipid content across genotypes in females and males. Lipid content of each genotype was tested using four independent replicates of five dissected abdominal fat bodies per sex, except Canton SB females and w^{1118} males represented by three replicates. Sex-specific linear model was implemented to compare each genotype to the negative control PPL-GAL4>w1118. Significance is indicated as $p < 0.05$ (*), $p < 0.01$ (**), and $p < 0.001$ (***), based on model-generated Benjamini-Hochberg adjusted p-values.

8.8 Development of gradual cooling assay in third instar larvae

Multiple set-ups were tested aiming to establish a comparative cold sensitivity assay in third instar wandering larvae using the cold-evoked behaviours as described by Himmel et al. (2021) (61). Due to the gentle touch stimulation, manual transfer by brush to a precooled agar plate induced similar behaviour, thereby impacting the behavioural signal. Similarly, immersion in PBS or liquified food medium generated altered behavioural movement prior to cold exposure. Arenas with agar induced climbing behaviour during the normalization period, which greatly increased when transferring the arena to the precooled Peltier element. Addition of a thermoneutral zone, based on the minimal temperature conductance of plastic, in a camera-visible plane did not prevent recording unfavourable locomotion/climbing.

8.9 Novel locomotion recovery assay in third instar larvae

While third instar larvae do not freeze at 0°C, there is a visible movement arrest when transferring larvae on ice. This phenotype was used to create a comparative assay to study whether differences in cold stress responses are also present in larval stages.

A series of optimization experiments were performed to determine the most effective assay set-up, cooling duration and response variable for reliably detecting genotype-dependent differences in cold recovery.

To evaluate the influence of the physical setting, five female and five male w1118 larvae were cooled on a petri dish (55 mm diameter) containing 10 ml agar or PBS wet tissue taped to aluminium foil for optimal temperature conductance. Across three cooling durations, larvae placed on 2% agar more consistently resumed locomotor activity, supporting smoother post-chill movement initiation. Wet tissue introduced more exaggerated movements, such as moving head or tail completely off the surface.

Two potential response variables were tested: first head movement and first full body movement. First head movement was defined as contraction or sideways movement seen in real-time. Locomotion resumption or cold evoked behaviour as described by Himmel et al. (2021), with clear movement of both head and tail, were set as criteria to score first full body movement (61). Manual scoring of first head movement required certain personal interpretation, especially within the 2% agar set-up, as larvae frequently display miniscule head movements that were only clearly visible during accelerated footage. First full body movement provided a more discrete time point with reduced ambiguity during manual scoring, representing a robust transition back to coordinated locomotion. First head movement, as it was scored here, does not indicate an earlier resumed body mobility (Figure 18). Therefore, full body movement was selected as the main response variable of this assay.

Next, the effect of various cooling durations was assessed by exposing w1118 larvae to 15 min, 30 min and 45 min cold exposure by placing the arena on ice in a 4°C environment. All cooling durations induced complete movement arrest, but the 15-min cooling period on 2% agar produced the most informative recovery window (Table 4, Figure 17). Recovery using the wet tissue arena was within a narrow time window, only improving in the 45 min cold exposure. In addition, there were more frequently non-responders on wet tissue, defined as larvae that display head movement, but do not resume full body movement within the recording duration. The 15 min cooling duration using the 2% agar set up already provided a recovery delay that was long enough to capture potential differences while remaining short enough for efficient throughput.

Cooling duration	Set-up	Mean first head movement (min)	Mean first full body movement (min)
15 min	Agar (2%)	Males: 12,04 Females: 8,66	Males: 15,35 Females: 13,60
	Damp tissue	Males: 0,53 Females: 0,66	Males: 0,79 *(3 non-responders)* Females: 0,87 *(1 non-responder)*
30 min	Agar (2%)	Males: 24,20 Females: 13,43	Males: 30,61 Females: 23,95
	Damp tissue	Males: 3,33 Females: 0,95	Males: 5,57 *(1 non-responder)* Females: 5,01
45 min	Agar (2%)	Males: 22,50 Females: 21,78	Males: 32,24 *(2 non-responders)* Females: 23,70
	Damp tissue	Males: 11,87 Females: 9,29	Males: 14,35 Females: 18,92 *(1 non-responder)*

Table 4. Mean response times of the manually scored variables across cooling duration and arena set-up. Five male and female w1118 larvae endured cold exposure of different durations, specifically 15 min, 30 min, 45 min, using two different arena set-ups, namely 2% agar and damp tissue. Recovery was manually scored as first head movement, defined as contraction or sideways movement, and first full body movement, either locomotion resumption or full body cold-evoked behaviour. Larvae were classified as non-responders within the full body response variable when there is clear head movement, but no full body movement within the recording duration.

Together, these findings demonstrate that the 2% agar is the optimal arena for supporting locomotion recovery, and 15 min cold exposure induces a reversible chill-induced arrest that is suitable for comparative studies. Under these conditions, first full body movement is seen as the most practical and reproducible response variable. This combination provides a recovery window sensitive enough to detect differences between experimental and control genotypes while maintaining high assay throughput.

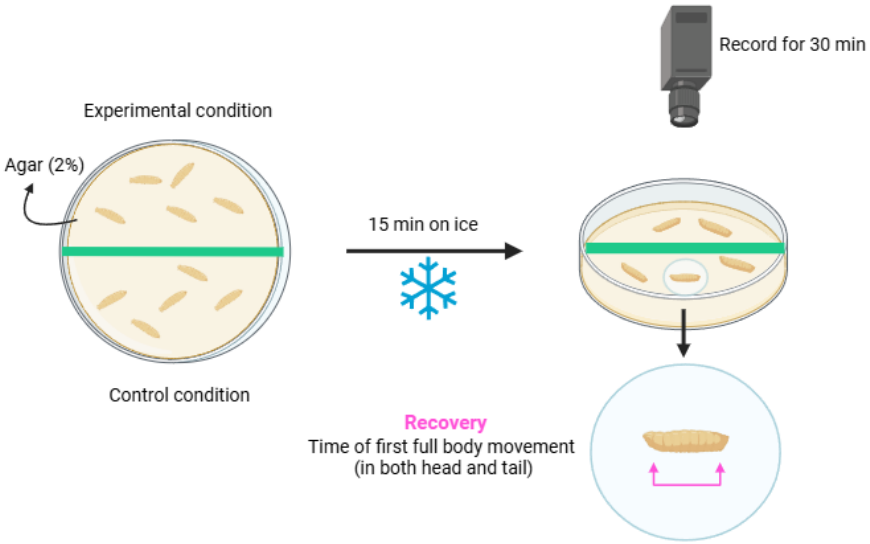

Figure 16. Schematic overview of locomotion recovery assay in third instar wandering larvae. Created in https://BioRender.com

The implementation of this assay to compare cold sensitivity in larvae containing fat body specific gene of interest knockdown was not feasible due to an insufficient number of the genetic control LSP2-GAL4>w1118 larvae to generate three replicates. This issue did not occur in six tested experimental genotypes. Adjustments in number of females per cross, number of crosses per assay, increased surface area by implementation of larger vials, >8 hour earlier cross set-up of control compared to experimental condition, or implementing a delayed light cycle in experimental lines compared to control did not aid in providing sufficient control larvae per sex that were adequately age matched to the experimental genotype.

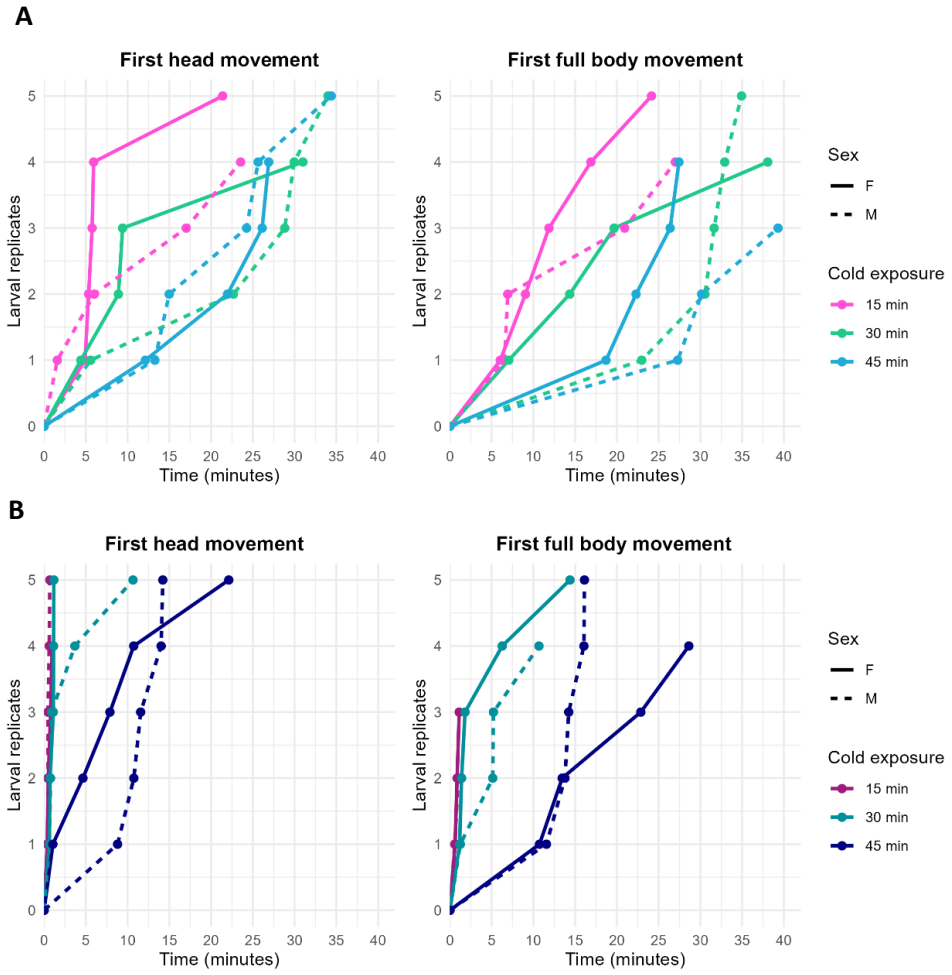

Figure 17. Response variables across different cooling durations per arena set up. Five female (solid line) and male (dotted line) w1118 larvae were exposed to different cooling durations, specifically 15 min, 30 min and 45 min. Cold recovery was scored as first head movement, defined as contraction or sideways movement, and first full body movement, seen as locomotion resumption or full body cold evoked behaviour. A) Response across larvae using the 2% agar arena. B) Response across larvae on wet tissue.

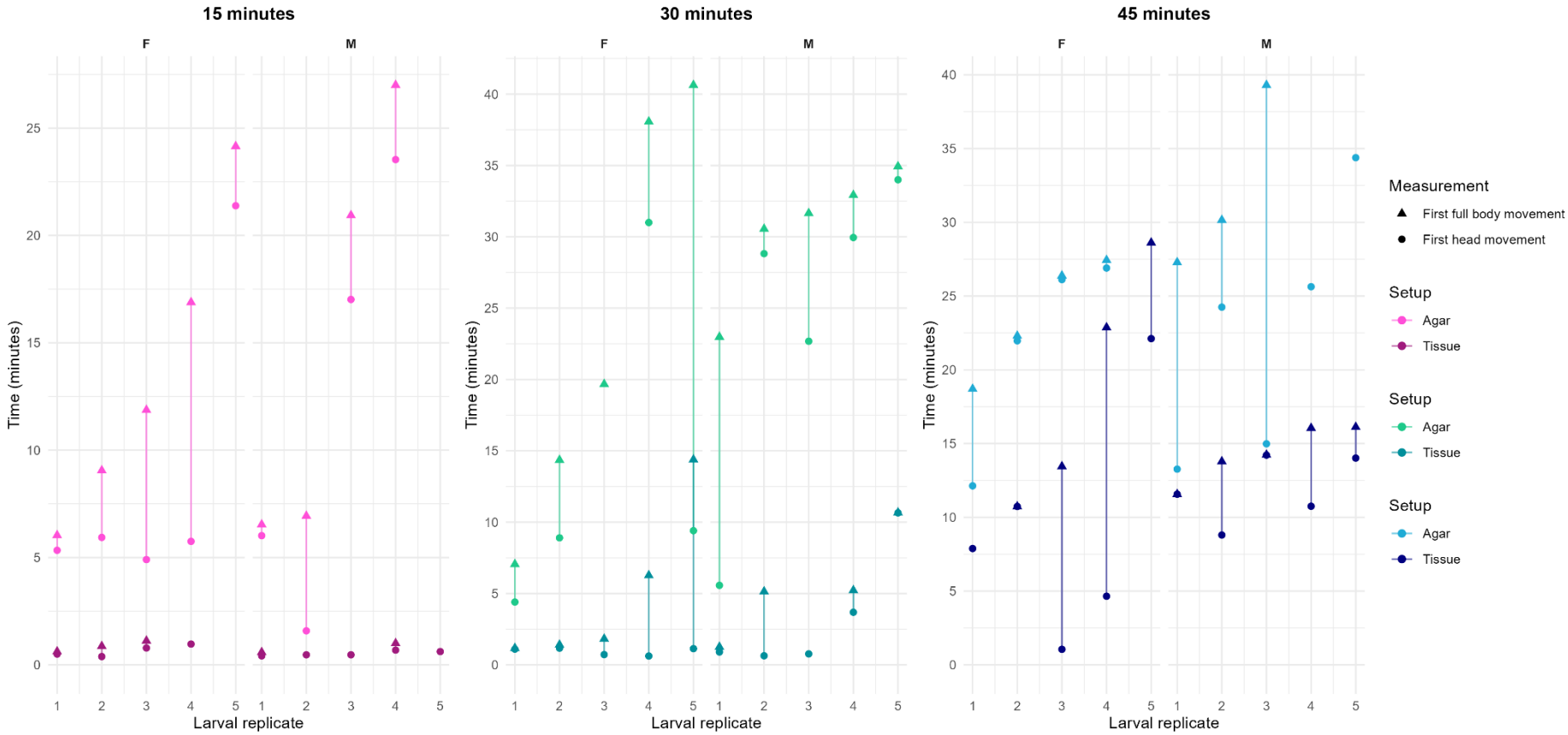

Figure 18. Response variables per larval replicate across different cooling durations and arena set ups. Five female and male w1118 larvae were exposed to different cooling durations, specifically 15 min, 30 min, 45 min, in two different arena setups, namely a petri dish containing 2% agar or wet tissue taped to aluminium foil. Recovery was manually scored as first head movement, defined as contraction or sideways movement, and first full body movement, seen as locomotion or cold-evoked behaviour including both head and tail. Comparison of both response variables across larval replicates indicated that earlier head movement does not equal earlier full body movement. First full body movement required less subjective interpretation and was therefore selected as main response variable of this assay.

9 DISCUSSION AND CONCLUSION

Humans have survived and adapted in extreme climates, such as the Arctic region known for its drastically colder ambient temperatures and overall extreme environment. Understanding how humans adapted to these extreme conditions provides important insight into human evolutionary flexibility and the mechanisms by which populations respond to environmental pressures. Whole genome sequencing revealed that, in comparison to reference populations living in more temperate climates, 418 windows of 200.000 bp in Siberian genomes exhibited a selection signal of $p < 0.01$ in at least one of three statistical tests targeting evolutionary signatures. In total, 756 protein coding genes were identified within the 418 candidate regions. In this project, we used *Drosophila melanogaster* as a model system to functionally characterize the top 20 liver-enriched genes that displayed positive cold selection signatures, with addition of the known cold-responsive TRP channel Iav. Two behavioural assays based on the chill coma phenotype were implemented. Fat body-specific knockdown of the genes Aldh-III, CG14230, CG4168, Egr, Iav, Klp68D, Nan, Nep1, Nep7, NonAL or Pll induced a significantly delayed chill coma recovery in both females and males compared to the negative control. Chill coma recovery delay was detected only in males when silencing ATPsynBeta, Hyd, Mhc, ND23 or Rbfox1. Chill coma recovery alterations were seen in females with a knockdown of Galk or Pten. A significant recovery delay was seen with Galk-RNAi while Pten-RNAi were more susceptible. Cold sensitivity via the chill coma susceptibility assay indicated a significantly delayed chill coma induction in males with a knockdown of Arr, ATPsynBeta or Pll, while enhanced susceptibility was detected in Egr-RNAi males. In females, knockdown of CG4168, Egr, Galk or NonAL induced a significantly reduced chill coma susceptibility, while ATPsynBeta-RNAi females presented a significantly faster chill coma induction. In genotypes presenting significant chill coma recovery alterations in males, abdominal fat body lipid content was analysed. Compared to the genetic control, knockdown of Aldh-III, Egr or Nep1 induced a significant lipid content increase in both sex. ATPsynBeta-RNAi, Hyd-RNAi or Nan-RNAi generated a significant lipid concentration increase in males, whereas knockdown of CG4168 or NonAL induced a significant increase in females. Finally, a novel behavioural assay for third instar wandering larvae was established to test potential differences in cold sensitivity in larval stages.

9.1 Basic mechanisms in cold sensitivity and heat production

This project aimed to determine if liver enriched genes associated with evolutionary selection in humans affect cold stress responses. Results of the chill coma recovery and – susceptibility assay confirm that gene of interest silencing in the fat body significantly alters cold stress responses in *Drosophila*. This suggests that basic mechanisms regarding cold tolerance and sensitivity may be conserved between ecto- and endothermic species.

In humans, chronic cold exposure induces an increased basal resting metabolism via BAT activation. BAT is able to generate heat due to the enrichment of mitochondria containing UCP1 (19). Fatty acids are seen as the primary fuel for mitochondrial uncoupling respiration. However, PET/CT data in humans during cold exposure indicated that the 18F-FDG tracer metabolite uptake is significantly increased in BAT, indicating increased glucose uptake (86,87). In addition, glucose tracing in cold-activated BAT leads to increased glucose oxidation and enhanced glucose flux to the mitochondrial tricarboxylic acid cycle (87).

Similarly, insect mitochondria have a high capacity for oxidative phosphorylation while low levels of proton leak at benign temperatures (88). In artificially selected *Drosophila* lines based on fast or slow chill coma recovery, cold-adapted flies with a faster recovery had a greater metabolic turnover before cold exposure, similar rate during cold exposure, and increased metabolic rate again during recovery. Additionally, cold tolerant flies had higher rates of glucose and leucine oxidation prior to cold exposure and during recovery (89). In *Drosophila* flight muscle, oxidative phosphorylation inhibitors caused a significantly reduced heat production during glucose supply, associating glycolytic flux during heat generation (90).

These findings indicate that similar metabolic pathways are required during cold responses in humans and flies.

9.2 Fat body is associated with cold stress responses

Although there is no consensus mechanism available yet, it is postulated that chill coma induction and its recovery are based on two different mechanisms. Evidence about chill coma induction points to neuronal spreading depolarization as mechanism, while chill coma recovery is linked to ion homeostasis reinstatement with subsequent muscle function recovery (53). Currently, the fat body has not been implicated. In this project, significant alterations in chill coma induction and its recovery in flies containing a PPL-GAL4 mediated fat body knockdown were detected, thereby identifying the fat body as potential modulator of cold stress responses.

The hypothesis that chill coma induction versus recovery have different causal mechanisms makes the two behavioural assays that were used complementary. Comparison of the results generated in both assays suggests distinct genetic contributions. Examples are PPL-GAL4>Arr-RNAi males and PPL-GAL4>ATPsynBeta females that did not have an altered chill coma recovery, yet did show a significantly modified chill coma induction compared to the negative control.

The genes of interest are enriched for the insulin signalling pathway. The gene Pten is a very important human tumor suppressor protein and inhibits the conserved insulin signalling pathway via dephosphorylation of PIP3. Knockdown of Pten tends to shift the metabolism towards growth, nutrient storage and insulin responsiveness (91). Pten is the only gene of which the fat body targeted knockdown caused an enhanced chill coma recovery, albeit only significant in females compared to the negative control. Another gene linked to this pathway is Egr, as it has been shown that Egr produced by adipose cells remotely acts on brain neurosecretory cells that produce insulin. Egr activates the JNK pathway, thereby repressing the insulin gene expression (92). In this project, female and male flies containing a fat body-specific Egr knockdown presented significantly increased fat body lipid content, indicating a metabolic shift towards nutrient storage. However, prior research states that knockdown of Pten also shifts the metabolism towards nutrient storage, yet chill coma recovery kinetics between knockdowns of Pten and Egr were vastly different. A potential explanation could be that Pten-RNAi is cell-autonomous, meaning it modulates how the fat body responds to insulin, whereas Egr acts via endocrine signalling, thereby potentially changing the systemic effects of insulin signalling. Another potential connection to insulin signalling pathway is CG4168, previously associated with hyperglycemia and overall glucose metabolism. Interestingly, CG4168 has been proposed as the *Drosophila* ortholog of human IGFALS, encoding a serum protein that binds to circulating insulin-like growth factors (93). Finally, CG14230 has previously been shown to be insulin responsive in RNAseq analyses of insulin-stimulated *Drosophila* S2R+ (94). Insulin signalling pathway affects the glucose

metabolism, which in turn might alter the glycolytic flux during heat generation, potentially explaining the significant differences in chill coma kinetics.

There is an interesting interplay between several genes of interest and dFOXO, a key transcription factor that activates up- and downstream targets of the insulin signalling pathway (95,96). It has been shown that fat body-specific knockdown of Pll promotes nuclear localization of dFOXO, while evidence indicates that Pten is able to regulate the nuclear entry of dFOXO (91,97). Induced deficiencies in several complexes of the mitochondrial respiration chain in *Drosophila* intestinal stem cells caused elevated dFOXO activity, associating ND23 as part of the Complex I minimal assembly to the transcription factor (98). It has been shown via ChIP-seq in 7-day old females that dFOXO is significantly enriched in the Aldh-III gene region (95). Transcription of the lipase *brummer* is induced via dFOXO, thereby providing a link to fat metabolism (45).

Knockdown of the TRP genes, Iav and Nan, induced significantly prolonged chill coma recovery when targeting the fat body using PPL-GAL4 and the nervous system via ELAV-GAL4. A significantly delayed chill coma induction was detected in PPL-GAL4>Nan-RNAi females and ELAV-GAL4>Nan-RNAi males compared to the control. Literature to date has only associated Iav to cold perception in chordotonal neurons of third instar larvae, while not yet to cold stress responses or potential mechanisms in the fat body (59). There is no prior evidence available linking the TRP channel Nan to cold stress behaviour or fat metabolism, as fat body specific knockdown induced a significant lipid content increase in the abdominal fat body of males. Additionally, pan-neuronal knockdown of these TRP channels induced an adverse phenotype in females, specifically reduced viability and failed post-eclosion wing expansion. This phenotype has also been reported in flies carrying a Dβ1 nAchR subunit deletion, which was partially attributed to the CCAP neuronal circuit and loss of peptide hormone bursicon (99). At present, there is no evidence that the TRP channels Iav or Nan are present/enriched in CCAP neurons or if designated gene silencing affects another, potentially indirect, neuronal circuit related to wing expansion or viability. In addition, there is no explanation available why this adverse phenotype solely impacted females.

9.3 Increased abdominal fat body content in genotypes with a delayed chill coma recovery

The lipid content of the abdominal fat body was analysed in those experimental genotypes with an altered chill coma recovery in males. Significantly increased lipid concentration was detected in a subset of experimental genotypes that also presented a significantly delayed chill coma recovery. This finding is in line with previous research showing that female w1118 flies on a high fat diet which induced significantly increased whole body triglyceride content, had significantly reduced survival of 20% compared to 80% in control flies when enduring 2 hours severe cold exposure (100). This inverse relation between lipid content and chill coma recovery suggests that elevated lipid content is not protective during cold stress recovery in flies.

When comparing to the chill coma susceptibility assay, the significantly increased fat body lipid content of females with knockdown of CG4168, Egr or NonAL corresponds to a significantly delayed chill coma induction time compared to the genetic control. However, Nep1-RNAi presented a significantly increased lipid content as well but did not generate alterations in chill coma susceptibility. Knockdown of ATPsynBeta in males induced a significant increase in fat body lipid content corresponding with a significantly prolonged chill coma induction time, while Egr-RNAi also presented significantly increased lipid content, yet an accelerated chill coma induction compared to the control. At present, no prior

studies have correlated a higher abdominal fat body lipid content, corresponding to more fat reserves, to alterations in chill coma induction time or the critical temperature to induce the phenotype. These results suggest that contrary to the expectation that increased abdominal fat body lipid content would provide better insulation or protection in chill coma susceptibility, this is not the case. This is consistent with the observation that cold exposure results in increased glucose oxidation and enhanced glucose flux to the mitochondrial tricarboxylic acid cycle in humans and flies (see section 9.1).

9.4 Limitations

The relative gene expression measured by RT-qPCR indicated relative gene silencing for most genotypes. However, occasionally no changes in expression and even apparent overexpression were measured. A potential explanation is the fact that whole flies were used to extract RNA, while the knockdown was fat body-specific. For genes that are broadly expressed in other tissues, the RNAi effect in the fat body could be masked by the unchanged expression in other tissues. In genotypes PPL-GAL4>Nan-RNAi and PPL-GAL4>CG4168-RNAi a significantly high overexpression was measured. The most likely explanation for this observation is that the gene expression level in controls was at the detection limit. A second possible reason is that the primer set used to amplify these particular genes did not achieve optimal efficiency.

In this project, two behavioural assays based on the chill coma phenotype were used to detect potential differences in cold-stress responses. A limitation of the chill coma susceptibility assay was the temperature fluctuations of the Peltier module per replicate and between assays. The current and voltage settings were standardized, but possible fluctuations in the environment, such as ambient temperature, humidity, differences in airflow, that impact the cooling kinetics of the Peltier module were not accounted for. Another limitation is the small sample size per condition (n = 12) due to the available surface area of the module, thereby restricting the statistical power.

The sulfo-phospho-vanillin assay provides a broad estimate of lipid abundance without specificity in different lipid classes, as triglycerides, phospholipids, free fatty acids and other compounds may react differently to sulfuric acid and vanillin. This factor is considered a limitation as the assay only provides a relative estimate of total lipid content rather than an absolute measurement.

9.5 Future perspectives

These findings indicate that *Drosophila* is a suitable model organism to study the role of genes associated with cold adaptation. Future perspectives to further strengthen these results are the inclusion of a scrambled RNAi genotype, to account for potential cold response variability due to the active RNAi machinery, and the use of alternative RNAi lines to account for potential off target effects due to sequence homology of the hairpin construct.

In the future, validation and quantification of the knockdown efficiency of the gene of interest should ideally be done in RNA derived from dissected fat bodies. Alternatively, if using whole flies is recommended, a ubiquitously expressed GAL4-driver to induce whole body gene knockdown would be preferred.

To further investigate these gene functions in cold tolerance, fat body-specific gene overexpression should rescue the detected cold stress response alterations, or even reverse the phenotype, thereby providing a clear genetic association.

The assays constructed in this project enable future more in-depth studies of these gene functions. The chill coma susceptibility assay allows a better detection of cold sensitive or - resistant phenotypes. The comparative locomotion recovery assay in third instar wandering larvae enables discovery of altered cold stress responses in the larval stages. To further strengthen the current results of the behavioural assays, the addition of a technical control assay comparing individuals of the same genetic control background within the same assay would be beneficial to document variability induced by technical manipulations. To further strengthen the larval behavioural assay composition, calcium signalling in larval cuticle muscle fibres would enable determination of maintained muscle contractility or if a potential chill coma-like paralysis phenotype is induced. Moreover, determination of the physiological effect due to the selected cold severity and cooling duration would give insight into potential confounding factors and create additional ways of explaining potential cold stress differences measured in this assay.

The interpretation of lipid content measurements would be further strengthened by normalization using protein content or body weight, enabling true biological lipid accumulation detection rather than differences in sample quantity. As the sulfo-phospho-vanillin assay measures all fatty acids, an additional future perspective is specifically examining triglyceride reserves via enzymatic detection or quantitative lipid droplet analysis of the fat body microscopic images as described in De Groef et al. (2021)(82).

9.6 Conclusion

This project aimed to functionally characterize genes associated with human liver-related cold adaptation using an *in vivo Drosophila* model. The *Drosophila* homologue of the genes of interest was silenced in the fat body by RNAi, and their cold stress responses, specifically chill coma susceptibility and recovery, and fat body lipid content were measured. Knockdown of several genes of interest induced a delayed chill coma recovery, while also inducing alterations in chill coma induction time. In several genotypes, an increased abdominal fat body lipid content was measured. These findings identify the fat body as potential modulator of cold stress responses. Finally, my results also show that the *Drosophila* homologues of genes previously linked with cold adaptation in humans also have a role in *Drosophila* cold physiology.

10 DUTCH SUMMARY

Evolutionaire genetica van humane koude adaptatie gebruikmakende van het modelorganisme *Drosophila melanogaster*

10.1 Inleiding

Volgens het *out of Africa*-model is de anatomisch moderne mens ontstaan in een tropisch klimaat, gekenmerkt door warme omgevingstemperaturen. Archeologisch en genetisch bewijsmateriaal suggereert dat ongeveer 60.000 jaar geleden een relatief kleine groep Afrika verliet en zich verspreidde over Eurazië (1). De eerste sporen van een menselijke habitat in de Arctische regio dateren van circa 45.000 jaar geleden (3). Aangezien het Arctische klimaat gekenmerkt wordt door extreem lage temperaturen, met minima tussen de -54°C en -46°C, zullen fysiologische, gedragsmatige en culturele aanpassingsmechanismes van uitermate belang geweest zijn om te kunnen overleven in zo een drastisch ander klimaat(2).

Een vorm van fysiologische adaptatie tijdens chronische koude blootstelling is het geobserveerd verhoogd basaal metabolisme, wat toelaat om warmere huidtemperaturen te behouden (16). Dit fenomeen wordt in verband gebracht met een verhoogde metabolische activiteit van bruin vetweefsel door maximalisatie van β-oxidatie, oxidatieve fosforylering en UCP1 expressie (20,21). Daarnaast tonen observationele studies bij Arctische inheemse populaties een consistente daling van cholesterol en serumlipiden (23,26). Deze bevindingen suggereren dat er ook een potentiële hepatische bijdrage is in chronische koude adaptatie. Tot op heden komt het bewijs hiervoor voornamelijk uit proefdieronderzoek. In pasgeboren geiten induceerde een 24h blootstelling aan 6°C een significante daling van serum vrije vetzuren en triglyceriden, met vergelijkbare resultaten bij melkgeiten die gedurende 21 dagen werden blootgesteld aan koude (27,28). Bij ratten induceerde een 4°C koude blootstelling en gewijzigd dag-nachtritme gedurende vier weken een significant daling in serum triglyceriden, terwijl *ex vivo* hepatische perfusie een 23% verhoogde opname van vrije vetzuren aantoonde (29). Naast deze fysiologische aanpassingen is het redelijk om aan te nemen dat deze langdurige koude blootstelling over meerdere generaties ook geleid heeft tot een evolutionaire genetische selectie in inheemse populaties.

Whole genome sequencing van Siberische individuen toonde dat, in vergelijking met populaties afkomstig uit warmere klimaten, 418 regio's van 200.000 bp een significant selectiesignaal vertoonden op basis van drie evolutiegerelateerde statistische testen. Binnen deze regio's werden er 756 eiwitcoderende genen geïdentificeerd (niet-gepubliceerde resultaten, Anna Kolesnikova & Toomas Kivisild). Op basis van de geassocieerde hepatische invloed in chronische koude adaptatie, werd deze genenlijst gesorteerd op leververrijking en vervolgens gezocht naar een representatieve *Drosophila melanogaster* homoloog. De top 20 genen uit deze selectie werden in dit project onderzocht, met toevoeging van het gekende koude responsief TRP kanaal *inactive* (59).

Drosophila melanogaster, hierna *Drosophila* genoemd, werd gebruikt als modelorganisme om deze genen functioneel te karakteriseren in koude stressreacties. Het orgaan van interesse is de menselijke lever, waarbij het *Drosophila* vetlichaam wordt beschouwd als functionele equivalent voor vetmetabolisme (44). De expressie van de geselecteerde genen werd gereduceerd via RNAi, gebaseerd op mRNA degradatie door het RISC-complex (72). Om weefselspecifieke knockdown te bekomen werd

het GAL4/UAS systeem toegepast (78). Als ectotherm organisme ervaart *Drosophila* bij voldoende ernstige koude blootstelling een fenomeen dat bekend staat als *chill coma*, een reversibele staat van verlamming waarvan het onderliggend mechanisme nog niet volledig is opgehelderd (53,101). Dit fenotype werd gebruikt om potentiële verschillen in koude stressreacties tussen genotypes te detecteren.

10.2 Doelstelling

Het doel van deze thesis is het functioneel karakteriseren van de geselecteerde genen met betrekking tot koude adaptatie, gebruikmakende van het modelorganisme *Drosophila melanogaster*.

10.3 Materialen en methoden

10.3.1 Chill coma herstel

Drie replicaten van acht vrouwelijke en acht mannelijke fruitvliegen per experimentele en controle conditie werden drie uur op ijs geplaatst in een 4°C omgeving, waarna hun *chill coma* herstel werd gefilmd en manueel gescoord. *Chill coma* herstel werd gedefinieerd als het tijdstip wanneer de rechtopstaande houding werd hersteld. Vliegen die beweging vertoonden, maar geen rechtopstaande houding behaalden binnen de videoduur, werden een hersteltijd van 30 minuten toegewezen.

10.3.2 Chill coma inductie

Vier vrouwelijke en vier mannelijke fruitvliegen per experimentele en controle conditie werden blootgesteld aan een Peltier element dat gekoeld werd tot onder de gekende *chill coma* grens van vliegen die werden gekweekt in 25°C. Drie replicaten van deze opstelling werden gefilmd en manueel gescoord. *Chill coma* inductie werd gedefinieerd als het tijdstip waarop de vlieg omvalt en geen verdere beweging meer vertoont.

10.3.3 Vet meting van het abdominale vetlichaam

5 tot 7 dagen oude vliegen van alle experimentele en controle lijnen werden gevriesdroogd op eenzelfde tijdstip en het abdominale vetlichaam werd gedissecteerd van 4 replicaten bestaande uit 5 vrouwelijke of mannelijke vliegen. Het lipidengehalte werd gemeten via de sulfo-fosfo-vanilline *assay* dat een colometrisch resultaat vertoont op basis van het vetzuurgehalte.

10.3.4 Immunofluorescente *staining* van het abdominale vetlichaam

De morfologie van het vetlichaam werd gevisualiseerd door middel van dissectie, fixatie in formaldehyde, toevoeging van BODIPY voor het visualiseren van de vetdruppels, en toevoeging van Rhodamine Phalloïdine om de actine in celmembranen te kenmerken. Deze microscopische foto's werden genomen met een confocale fluorescentiemicroscoop.

10.3.5 Relatieve genexpressie via RT-qPCR

De vetlichaam-specifieke knockdown werd gevalideerd met RT-qPCR. Totale RNA werd geëxtraheerd uit vier replicaten bestaande uit 10 gevriesdroogde vrouwelijk of mannelijke vliegen. Het RNA werd omgezet tot cDNA via reverse transcriptie. Efficiëntie van de gebruikte primers werd bepaald aan de hand van seriële verdunningen. De geselecteerde primers werden samen geladen met het cDNA en PCR van 40 cycli werd voltooid.

10.3.6 Statistiek

De statistische analyse en grafiek constructie werd uitgevoerd in R met behulp van *GenAI* gegenereerde code (83). De herstel tijdspunten werden gemodelleerd via een Cox proportionele gevaren model per geslacht, waarin rekening gehouden werd met variabiliteit per *assay* en gepaarde metingen binnen een replicaat. De *chill coma* inductie tijdspunten werden geanalyseerd via een lineair gemend model per geslacht, waarbij het effect van genotype werd vergeleken, terwijl er rekening gehouden werd met variabiliteit per replicaat binnen een *assay*. De lipidenconcentraties afkomstig uit de vetmeting werden geanalyseerd via een lineair model. De RT-qPCR ΔCt waarden werden vergeleken met de genetische controle via Welsh t-test met ongelijke varianties. Alle p-waarden verkregen uit statistische testen en modellen werden gecorrigeerd voor meervoudige testing via de Benjamini-Hochberg methode en significantie werd gedefinieerd als gecorrigeerde $p<0.05$.

10.4 Resultaten

10.4.1 Significante vertraging in vetlichaam specifieke knockdown genotypes

Volgende genotypes hadden een significant aangepaste *chill coma* hersteltijd in zowel in vrouwelijk als mannelijke vliegen ten opzichte van de genetische controle PPL-GAL4>w1118: PPL-GAL4>Aldh-III-RNAi, PPL-GAL4>ATPsynBeta-RNAi, PPL-GAL4>CG14230-RNAi, PPL-GAL4>CG4168-RNAi, PPL-GAL4>Egr-RNAi, PPL-GAL4>Iav-RNAi, PPL-GAL4>Klp68D-RNAi, PPL-GAL4>Nan-RNAi, PPL-GAL4>Nep1-RNAi, PPL-GAL4>Nep7-RNAi, PPL-GAL4>NonAL-RNAi, PPL-GAL4>Pll-RNAi. Significante veranderingen enkel in mannelijke vliegen werd gedetecteerd in PPL-GAL4>Hyd-RNAi, PPL-GAL4>Mhc-RNAi, PPL-GAL4>ND23-RNAi en PPL-GAL4>Rbfox1-RNAi. *Chill coma* herstel respons was significant veranderd enkel in de vrouwelijke vliegen van PPL-GAL4>Galk-RNAi en PPL-GAL4>Pten-RNAi. Uitgezonderd PPL-GAL4>Pten-RNAi vertoonde een versneld herstel, terwijl andere genotypes een significante vertraging presenteerden.

10.4.2 *Chill coma* inductie variatie in experimentele genotypes

Deze *assay* werd ontwikkeld en geoptimaliseerd met behulp van w1118 vliegen. In vergelijking met de negatieve controle werd in mannelijke vliegen een significante vertraging van *chill coma* inductie gedetecteerd in PPL-GAL4>Arr-RNAi, PPL-GAL4>ATPsynBeta-RNAi en PPL-GAL4>Pll-RNAi, terwijl PPL-GAL4>Egr-RNAi een verhoogde chill coma vatbaarheid vertoonde. In vrouwelijke vliegen van PPL-GAL4>CG4168, PPL-GAL4>Galk-RNAi, PPL-GAL4>Nan-RNAi en PPL-GAL4>NonAL-RNAi werd een significant gereduceerde *chill coma* vatbaarheid gedetecteerd ten opzichte van de controle, terwijl in PPL-GAL4>ATPsynBeta-RNAi vrouwtjes net een significant versnelde inductie werd gemeten.

10.4.3 Significante verandering in lipidengehalte van het abdominale vetlichaam van experimentele genotypes

Van genotypes die in mannelijke vliegen significante veranderingen in *chill coma* herstel induceerden werd het vetgehalte van abdominaal vetlichaam bepaald. In vergelijking met de genetische controle werd een significant verhoogd lipidengehalte gemeten in PPL-GAL4>Aldh-III-RNAi, PPL-GAL4>Egr-RNAi en PPL-GAL4>Nep1-RNAi mannelijke en vrouwelijke vliegen. Significante vettoename werden enkel in mannelijke vliegen van PPL-GAL4>ATPsynBeta-RNAi, PPL-GAL4>Hyd-RNAi, PPL-GAL4>Nan-RNAi gemeten. In vrouwelijke vliegen van het genotype PPL-GAL4>CG4168-RNAi en PPL-GAL4>NonAL-RNAi werd een significante toename in vetgehalte gemeten ten opzichte van de negatieve controle.

10.4.4 Koude-geïnduceerd bewegingsherstel in derde instar larves

Larves vertonen geen beweging meer wanneer ze blootgesteld worden aan een voldoende ernstige temperatuurdaling. Dit fenotype werd gebruikt om een vergelijkende *assay* op te stellen die toelaat veranderingen in koude sensitiviteit/tolerantie te meten. Gebruik makende van telkens 5 vrouwelijke en 5 mannelijke w1118 larves werden twee verschillende arena constructies getest, namelijk een petrischaal gevuld met 2% agar en een nat papieren zakdoek vastgemaakt aan aluminiumfolie, over verschillende tijden van koude blootstelling. De 15 minuten koude blootstelling gebruik makende van de 2% agar arena zorgde voor voldoende vertraging in bewegingsherstel dat toelaat potentiële veranderingen te meten.

10.5 Besluit

Genen die werden geselecteerd op basis van een vermoedelijke associatie in menselijke koude adaptatie induceren significante veranderingen in koude stressreacties van volwassen vliegen via vetlichaam specifieke knockdown. Meerdere genen vertonen in *Drosophila* een link met *insulin signalling pathway* en de transcriptiefactor dFOXO. De ontworpen gedragsstudies, namelijk chill coma inductie *assay* en koude geïnduceerd bewegingsherstel in derde instar larves, creëren bijkomende mogelijkheden tot het studeren van potentiële veranderingen in koude stress responsen.

REFERENCE LIST

1. Abood S, Oota H. Human dispersal into East Eurasia: ancient genome insights and the need for research on physiological adaptations. J Physiol Anthropol. 2025 Dec 1;44(1):5. doi:10.1186/S40101-024-00382-3 PubMed PMID: 39953642.

2. Britannica Encyclopedia. Arctic [Internet]. 2025 [cited 2025 Sep 18]. Available from: https://www.britannica.com/place/Arctic

3. Pitulko V V., Tikhonov AN, Pavlova EY, Nikolskiy PA, Kuper KE, Polozov RN. Paleoanthropology: Early human presence in the Arctic: Evidence from 45,000-year-old mammoth remains. Science (1979). 2016;351(6270):260–3. doi:10.1126/science.aad0554 PubMed PMID: 26816376.

4. Tan CL, Knight ZA. Regulation of Body Temperature by the Nervous System. Neuron. 2018. p. 31–48. doi:10.1016/j.neuron.2018.02.022 PubMed PMID: 29621489.

5. Tveita T, Sieck GC. Physiological Impact of Hypothermia: The Good, the Bad, and the Ugly. Physiology. 2022 Mar 1;37(2):69–87. doi:10.1152/physiol.00025.2021 PubMed PMID: 34632808.

6. Imray C, Grieve A, Dhillon S. Cold damage to the extremities: Frostbite and non-freezing cold injuries. Postgrad Med J. 2009 Sep;85(1007):481–8. doi:10.1136/pgmj.2008.068635 PubMed PMID: 19734516.

7. Haman F, Souza SCS, Castellani JW, Dupuis MP, Friedl KE, Sullivan-Kwantes W, et al. Human vulnerability and variability in the cold: Establishing individual risks for cold weather injuries. Temperature. 2022;9(2):158–95. doi:10.1080/23328940.2022.2044740 PubMed PMID: 36106152.

8. Heil K, Thomas R, Robertson G, Porter A, Milner R, Wood A. Freezing and non-freezing cold weather injuries: A systematic review. Br Med Bull. 2016 Mar 1;117:79–93. doi:10.1093/bmb/ldw001 PubMed PMID: 26872856.

9. King M, Carnahan H. Revisiting the brain activity associated with innocuous and noxious cold exposure. Neurosci Biobehav Rev. 2019 Sep 1;104:197–208. doi:10.1016/j.neubiorev.2019.06.021 PubMed PMID: 31283953.

10. Davis KD, Pope GE. Noxious cold evokes multiple sensations with distinct time courses. Pain. 2002;98(1):179–85. doi:10.1016/S0304-3959(02)00043-X PubMed PMID: 12098630.

11. Lewis CM, Griffith TN. The mechanisms of cold encoding. Curr Opin Neurobiol. 2022 Aug 1;75:102571. doi:10.1016/j.conb.2022.102571 PubMed PMID: 35679808.

12. Filingeri D. Neurophysiology of Skin Thermal Sensations. Compr Physiol. 2016 Jul 1;6:1429–91. doi:10.1002/CPHY.C150040 PubMed PMID: 27347898.

13. Lewis CM, Griffith TN. Ion channels of cold transduction and transmission. Journal of General Physiology. 2024 Oct 7;156(10):e202313529. doi:10.1085/jgp.202313529 PubMed PMID: 39051992.

14. Buijs TJ, McNaughton PA. The Role of Cold-Sensitive Ion Channels in Peripheral Thermosensation. Front Cell Neurosci. 2020 Aug 20;14:262. doi:10.3389/fncel.2020.00262 PubMed PMID: 32973456.

15. Daanen HAM, Van Marken Lichtenbelt WD. Human whole body cold adaptation. Temperature. 2016 Jan 2;3(1):104–18. doi:10.1080/23328940.2015.1135688 PubMed PMID: 27227100.

16. Castellani JW, Young AJ. Human physiological responses to cold exposure: Acute responses and acclimatization to prolonged exposure. Auton Neurosci. 2016 Apr 1;196:63–74. doi:10.1016/j.autneu.2016.02.009 PubMed PMID: 26924539.

17. Yurkevicius BR, Alba BK, Seeley AD, Castellani JW. Human cold habituation: Physiology, timeline, and modifiers. Temperature. 2022;9(2):122–57. doi:10.1080/23328940.2021.1903145 PubMed PMID: 36106151.

18. Wakabayashi H, Sakaue H, Nishimura T. Recent updates on cold adaptation in population and laboratory studies, including cross-adaptation with nonthermal factors. J Physiol Anthropol. 2025 Dec 1;44(1):7. doi:10.1186/s40101-025-00387-6 PubMed PMID: 39972479.

19. Sabatino L, Vassalle C. Thyroid Hormones and Metabolism Regulation: Which Role on Brown Adipose Tissue and Browning Process? Biomolecules. 2025 Mar 1;15(3):361. doi:10.3390/BIOM15030361 PubMed PMID: 40149897.

20. Yau WW, Yen PM. Thermogenesis in Adipose Tissue Activated by Thyroid Hormone. Int J Mol Sci. 2020 Apr 2;21(8):3020. doi:10.3390/IJMS21083020 PubMed PMID: 32344721.

21. Motzfeldt Jensen M, Jørgensen MG, Elberling Almasi C, Andersen S. Effect of habitual cold exposure on brown adipose tissue activity in Arctic adults: a systematic review. Int J Circumpolar Health. 2025;84(1):2545059. doi:10.1080/22423982.2025.2545059 PubMed PMID: 40804739.

22. Yoneshiro T, Matsushita M, Sakai J, Saito M. Brown fat thermogenesis and cold adaptation in humans. J Physiol Anthropol. 2025 Dec 1;44(1):11. doi:10.1186/s40101-025-00391-w PubMed PMID: 40259336.

23. Leonard WR, Snodgrass JJ, Sorensen M V. Metabolic adaptation in indigenous Siberian populations. Annu Rev Anthropol. 2005;34:451–71. doi:10.1146/annurev.anthro.34.081804.120558

24. Bligh J, Johnson KG. Glossary of terms for thermal physiology. J Appl Physiol. 1973;35(6):941–61. doi:10.1152/jappl.1973.35.6.941 PubMed PMID: 4765838.

25. Motzfeldt Jensen M, Elberling Almasi C, Kjærgaard B, Rasmussen BS, Haunstrup T, Ulrik Thomsen S, et al. Cross-over comparative study of cold-induced brown adipose tissue activity in Greenlandic Inuit and Danes: rationale, design, and methodology. Int J Circumpolar Health. 2025 Dec 1;84(1):2545662. doi:10.1080/22423982.2025.2545662 PubMed PMID: 40820950.

26. Vlasova O, Bichkaeva F, Shengof B, Nesterova E, Strelkova A, Baranova N. Features of lipid metabolism in Arctic residents depending on ethnicity and lifestyle. Rural Remote Health. 2025 May 29;25(2):9140. doi:10.22605/RRH9140 PubMed PMID: 40441777.

27. Zhang Z, Cheng L, Ma J, Wang X, Zhao Y. Chronic Cold Exposure Leads to Daytime Preference in the Circadian Expression of Hepatic Metabolic Genes. Front Physiol. 2022 May 17;13:865627. doi:10.3389/fphys.2022.865627

28. Coloma-García W, Mehaba N, Such X, Caja G, Salama AAK. Effects of Cold Exposure on Some Physiological, Productive, and Metabolic Variables in Lactating Dairy Goats. Animals (Basel). 2020 Dec 1;10(12):2383. doi:10.3390/ANI10122383 PubMed PMID: 33322635.

29. Hauton D, Richards SB, Egginton S. The role of the liver in lipid metabolism during cold acclimation in non-hibernator rodents. Comparative Biochemistry and Physiology - B Biochemistry and Molecular Biology. 2006;144(3):372–81. doi:10.1016/j.cbpb.2006.03.013 PubMed PMID: 16730468.

30. Pagani L, Lawson DJ, Jagoda E, Mörseburg A, Eriksson A, Mitt M, et al. Genomic analyses inform on migration events during the peopling of Eurasia. Nature. 2016 Jul 1;538(7624):238–42. doi:10.1038/nature19792 PubMed PMID: 27654910.

31. Goodwin S, McPherson JD, McCombie WR. Coming of age: Ten years of next-generation sequencing technologies. Nat Rev Genet. 2016 Jun 1;17(6):333–51. doi:10.1038/nrg.2016.49 PubMed PMID: 27184599.

32. Voight BF, Kudaravalli S, Wen X, Pritchard JK. A map of recent positive selection in the human genome. PLoS Biol. 2006;4(3):0446–58. doi:10.1371/JOURNAL.PBIO.0040072 PubMed PMID: 16494531.

33. Ferrer-Admetlla A, Liang M, Korneliussen T, Nielsen R. On detecting incomplete soft or hard selective sweeps using haplotype structure. Mol Biol Evol. 2014;31(5):1275–91. doi:10.1093/molbev/msu077 PubMed PMID: 24554778.

34. Tajima F. Statistical method for testing the neutral mutation hypothesis by DNA polymorphism. Genetics. 1989;123(3):585–95. doi:10.1093/genetics/123.3.585 PubMed PMID: 2513255.

35. Giansanti MG, Frappaolo A, Piergentili R. Drosophila melanogaster: How and Why It Became a Model Organism. Int J Mol Sci. 2025 Aug 2;26(15):7485. doi:10.3390/ijms26157485 PubMed PMID: 40806617.

36. Prokop A. droso4schools [Internet]. Available from: https://droso4schools.wordpress.com/

37. Hales KG, Korey CA, Larracuente AM, Roberts DM. Genetics on the fly: A primer on the drosophila model system. Genetics. 2015 Nov 1;201(3):815–42. doi:10.1534/genetics.115.183392 PubMed PMID: 26564900.

38. Ugur B, Chen K, Bellen HJ. Drosophila tools and assays for the study of human diseases. DMM Disease Models and Mechanisms. 2016 Mar 1;9(3):235–44. doi:10.1242/dmm.023762 PubMed PMID: 26935102.

39. Arrese EL, Soulages JL. Insect fat body: Energy, metabolism, and regulation. Annu Rev Entomol. 2010 Jan 1;55:207–25. doi:10.1146/annurev-ento-112408-085356 PubMed PMID: 19725772.

40. Tsuyama T, Hayashi Y, Komai H, Shimono K, Uemura T. Dynamic de novo adipose tissue development during metamorphosis in Drosophila melanogaster. Development (Cambridge). 2023 May 1;150(10). doi:10.1242/dev.200815 PubMed PMID: 37092314.

41. Li S, Yu X, Feng Q. Fat body biology in the last decade. Annu Rev Entomol. 2019 Jan 7;64:315–33. doi:10.1146/annurev-ento-011118-112007 PubMed PMID: 30312553.

42. Kühnlein RP. Thematic review series: Lipid droplet synthesis and metabolism: From Yeast to man. Lipid droplet-based storage fat metabolism in Drosophila. J Lipid Res. 2012 Aug;53(8):1430–6. doi:10.1194/jlr.R024299 PubMed PMID: 22566574.

43. Azeez OI, Meintjes R, Chamunorwa JP. Fat body, fat pad and adipose tissues in invertebrates and vertebrates: The nexus. Lipids Health Dis. 2014 Apr 23;13(1):71. doi:10.1186/1476-511X-13-71 PubMed PMID: 24758278.

44. Moraes KCM, Montagne J. Drosophila melanogaster: A Powerful Tiny Animal Model for the Study of Metabolic Hepatic Diseases. Front Physiol. 2021 Sep 16;12:728407. doi:10.3389/fphys.2021.728407 PubMed PMID: 34603083.

45. Heier C, Kühnlein RP. Triacylglycerol metabolism in drosophila melanogaster. Genetics. 2018 Dec 1;210(4):1163–84. doi:10.1534/genetics.118.301583 PubMed PMID: 30523167.

46. Bi J, Xiang Y, Chen H, Liu Z, Grönke S, Kühnlein RP, et al. Opposite and redundant roles of the two Drosophila: Perilipins in lipid mobilization. J Cell Sci. 2012 Aug 1;125(15):3568–77. doi:10.1242/jcs.101329 PubMed PMID: 22505614.

47. Boukal DS, Ditrich T, Kutcherov D, Sroka P, Dudová P, Papáček M. Analyses of developmental rate isomorphy in ectotherms: Introducing the dirichlet regression. PLoS One. 2015 Jun 26;10(6):e0129341. doi:10.1371/journal.pone.0129341 PubMed PMID: 26114859.

48. Pool JE, Braun DT, Lack JB. Parallel Evolution of Cold Tolerance within Drosophila melanogaster. Mol Biol Evol. 2017;34(2):349–60. doi:10.1093/molbev/msw232 PubMed PMID: 27777283.

49. MacMillan HA, Knee JM, Dennis AB, Udaka H, Marshall KE, Merritt TJS, et al. Cold acclimation wholly reorganizes the Drosophila melanogaster transcriptome and metabolome. Sci Rep. 2016 Jun 30;6(1):28999-. doi:10.1038/srep28999 PubMed PMID: 27357258.

50. Li K, Gong Z. Feeling Hot and Cold: Thermal Sensation in Drosophila. Neurosci Bull. 2017 Jun 1;33(3):317–22. doi:10.1007/s12264-016-0087-9 PubMed PMID: 27995563.

51. Montell C. Drosophila sensory receptors-a set of molecular Swiss Army Knives. Genetics. 2021 Jan 1;217(1). doi:10.1093/GENETICS/IYAA011 PubMed PMID: 33683373.

52. Sayeed O, Benzer S. Behavioral genetics of thermosensation and hygrosensation in Drosophila. Proc Natl Acad Sci U S A. 1996 Jun 11;93(12):6079–84. doi:10.1073/pnas.93.12.6079 PubMed PMID: 8650222.

53. Andersen MK, Overgaard J. The central nervous system and muscular system play different roles for chill coma onset and recovery in insects. Comp Biochem Physiol A Mol Integr Physiol. 2019 Jul 1;233:10–6. doi:10.1016/j.cbpa.2019.03.015 PubMed PMID: 30910613.

54. Overgaard J, Macmillan HA. The Integrative Physiology of Insect Chill Tolerance. Annu Rev Physiol. 2017;79:187–208. doi:10.1146/annurev-physiol-022516-034142 PubMed PMID: 27860831.

55. Gerken AR, Mackay TFC, Morgan TJ. Artificial selection on chill-coma recovery time in Drosophila melanogaster: Direct and correlated responses to selection. J Therm Biol. 2016;59:77–85. doi:10.1016/j.jtherbio.2016.04.004 PubMed PMID: 27264892.

56. Garcia MJ, Teets NM. Cold stress results in sustained locomotor and behavioral deficits in Drosophila melanogaster. J Exp Zool A Ecol Integr Physiol. 2019 Mar 1;331(3):192–200. doi:10.1002/jez.2253 PubMed PMID: 30609298.

57. Frazier MR, Harrison JF, Kirkton SD, Roberts SP. Cold rearing improves cold-flight performance in Drosophila via changes in wing morphology. Journal of Experimental Biology. 2008 Jul;211(13):2116–22. doi:10.1242/jeb.019422 PubMed PMID: 18552301.

58. Turner HN, Landry C, Galko MJ. Novel Assay for Cold Nociception in Drosophila Larvae. J Vis Exp. 2017;(122):e55568. doi:10.3791/55568 PubMed PMID: 28448025.

59. Kwon Y, Shen WL, Shim HS, Montell C. Fine thermotactic discrimination between the optimal and slightly cooler temperatures via a TRPV channel in chordotonal neurons. Journal of Neuroscience. 2010 Aug 4;30(31):10465–71. doi:10.1523/JNEUROSCI.1631-10.2010 PubMed PMID: 20685989.

60. Patel AA, Cardona A, Cox DN. Neural substrates of cold nociception in Drosophila larva. Elife. 2025 Jun 13;12:RP91582. doi:10.7554/elife.91582 PubMed PMID: 40512662.

61. Himmel NJ, Letcher JM, Sakurai A, Gray TR, Benson MN, Donaldson KJ, et al. Identification of a neural basis for cold acclimation in Drosophila larvae. iScience. 2021;24(6):102657. doi:10.1016/j.isci.2021.102657

62. Andersen MK, Jensen SO, Overgaard J. Physiological correlates of chill susceptibility in Lepidoptera. J Insect Physiol. 2017 Apr 1;98:317–26. doi:10.1016/j.jinsphys.2017.02.002 PubMed PMID: 28188725.

63. Ramadan MM, Abdel-Hady AAA, Guedes RNC, Hashem AS. Low temperature shock and chill-coma consequences for the red flour beetle (Tribolium castaneum) and the rice weevil (Sitophilus oryzae). J Therm Biol. 2020 Dec 1;94:102774. doi:10.1016/j.jtherbio.2020.102774 PubMed PMID: 33293005.

64. Frolov R V., Singh S. Temperature and functional plasticity of L-type Ca2+ channels in Drosophila. Cell Calcium. 2013;54(4):287–94. doi:10.1016/j.ceca.2013.07.005 PubMed PMID: 23993048.

65. Turner HN, Armengol K, Patel AA, Himmel NJ, Sullivan L, Iyer SC, et al. The TRP Channels Pkd2, NompC, and Trpm Act in Cold-Sensing Neurons to Mediate Unique Aversive Behaviors to Noxious Cold in Drosophila. Current Biology. 2016 Dec 5;26(23):3116–28. doi:10.1016/j.cub.2016.09.038 PubMed PMID: 27818173.

66. Adams MD, Celniker SE, Holt RA, Evans CA, Gocayne JD, Amanatides PG, et al. The genome sequence of Drosophila melanogaster. Science (1979). 2000 Mar 24;287(5461):2185–95. doi:10.1126/science.287.5461.2185 PubMed PMID: 10731132.

67. Kaufman TC. A short history and description of Drosophila melanogaster classical genetics: Chromosome aberrations, forward genetic screens, and the nature of mutations. Genetics. 2017 Jun 1;206(2):665–89. doi:10.1534/genetics.117.199950 PubMed PMID: 28592503.

68. Hope KA, Reiter LT. Understanding human genetic disease with the fly. In: Cellular and Animal Models in Human Genomics Research. Academic Press; 2019. p. 69–87. doi:10.1016/B978-0-12-816573-7.00004-3

69. Li H, Janssens J, de Waegeneer M, Kolluru SS, Davie K, Gardeux V, et al. Fly Cell Atlas: A single-nucleus transcriptomic atlas of the adult fruit fly. Science (1979). 2022 Mar 4;375(6584). doi:10.1126/science.abk2432 PubMed PMID: 35239393.

70. Ryder E, Russell S. Transposable elements as tools for genomics and genetics in Drosophila. Brief Funct Genomic Proteomic. 2003 Apr;2(1):57–71. doi:10.1093/BFGP/2.1.57 PubMed PMID: 15239944.

71. Heigwer F, Port F, Boutros M. RNA interference (RNAi) screening in Drosophila. Genetics. 2018 Mar 1;208(3):853–74. doi:10.1534/genetics.117.300077 PubMed PMID: 29487145.

72. Wilson RC, Doudna JA. Molecular mechanisms of RNA interference. Annu Rev Biophys. 2013 May;42(1):217–39. doi:10.1146/ANNUREV-BIOPHYS-083012-130404 PubMed PMID: 23654304.

73. Kim K, Lee YS, Harris D, Nakahara K, Carthew RW. The RNAi pathway initiated by Dicer-2 in Drosophila. Cold Spring Harb Symp Quant Biol. 2006;71:39–44. doi:10.1101/sqb.2006.71.008 PubMed PMID: 17381278.

74. Matranga C, Tomari Y, Shin C, Bartel DP, Zamore PD. Passenger-strand cleavage facilitates assembly of siRNA into Ago2-containing RNAi enzyme complexes. Cell. 2005 Nov 18;123(4):607–20. doi:10.1016/j.cell.2005.08.044 PubMed PMID: 16271386.

75. Dahmann C. Drosophila: Methods and Protocols. Dahmann C, editor. Methods in Molecular Biology. Totowa (NJ): Humana Press; 2008. 201–201 p. doi:10.1086/603491

76. Ghanim GE, Rio DC, Teixeira FK. Mechanism and regulation of P element transposition. Open Biol. 2020;10(12):200244. doi:10.1098/RSOB.200244 PubMed PMID: 33352068.

77. FlyC31. Why PhiC31? [Internet]. [cited 2025 Dec 31]. Available from: https://www.flyc31.org/why_phic31.php

78. Brand AH, Perrimon N. Targeted gene expression as a means of altering cell fates and generating dominant phenotypes. Development. 1993;118(2):401–15. doi:10.1242/DEV.118.2.401 PubMed PMID: 8223268.

79. Andersen JL, Manenti T, Sørensen JG, Macmillan HA, Loeschcke V, Overgaard J. How to assess Drosophila cold tolerance: Chill coma temperature and lower lethal temperature are the best predictors of cold distribution limits. Funct Ecol. 2015;29(1):55–65. doi:10.1111/1365-2435.12310

80. Van Handel E. Rapid determination of total lipids in mosquitoes. J Am Mosq Control Assoc. 1985;1(3):302–4.

81. Bradshaw TW. The Role of Insulin Signaling in Controlling Oogenesis In Drosophila Melanogaster. Theses and Dissertations [Internet]. 2023 Oct 1 [cited 2026 Apr 29]. Available from: https://scholarcommons.sc.edu/etd/7647

82. De Groef S, Wilms T, Balmand S, Calevro F, Callaerts P. Sexual dimorphism in metabolic responses to western diet in drosophila melanogaster. Biomolecules. 2022 Jan 1;12(1):33. doi:10.3390/biom12010033 PubMed PMID: 35053181.

83. AI created; ChatGPT, OpenAI, database dates from May 2026, last consulted on 19.05.26. Available at: https://chatgpt.com/

84. MacKay TFC, Richards S, Stone EA, Barbadilla A, Ayroles JF, Zhu D, et al. The Drosophila melanogaster Genetic Reference Panel. Nature. 2012;482(7384):173–8. doi:10.1038/nature10811 PubMed PMID: 22318601.

85. Morgante F, Sørensen P, Sorensen DA, Maltecca C, Mackay TFC. Genetic Architecture of Micro-Environmental Plasticity in Drosophila melanogaster. Sci Rep. 2015;5:09785. doi:10.1038/srep09785 PubMed PMID: 25943032.

86. Chondronikola M, Volpi E, Børsheim E, Porter C, Annamalai P, Enerbäck S, et al. Brown adipose tissue improves whole-body glucose homeostasis and insulin sensitivity in humans. Diabetes. 2014;63(12):4089–99. doi:10.2337/DB14-0746 PubMed PMID: 25056438.

87. Shinde AB, Song A, Wang QA. Brown Adipose Tissue Heterogeneity, Energy Metabolism, and Beyond. Front Endocrinol (Lausanne). 2021;12. doi:10.3389/FENDO.2021.651763 PubMed PMID: 33953697.

88. Lebenzon JE, Overgaard J, Jørgensen LB. Chilled, starved or frozen: insect mitochondrial adaptations to overcome the cold. Curr Opin Insect Sci. 2023;58:101076. doi:10.1016/j.cois.2023.101076 PubMed PMID: 37331596.

89. Williams CM, Mccue MD, Sunny NE, Szejner-Sigal A, Morgan TJ, Allison DB, et al. Cold adaptation increases rates of nutrient flow and metabolic plasticity during cold exposure in Drosophila melanogaster. Proceedings of the Royal Society B: Biological Sciences. 2016;283:20161317. doi:10.1098/rspb.2016.1317 PubMed PMID: 27605506.

90. Lerchner J, Reis YA, Lucio T, Oliveira MF. Energy dissipation via the glycerol phosphate shuttle: coupling glycolysis to mitochondrial thermogenesis in Drosophila melanogaster

flight muscle. Journal of Comparative Physiology B. 2026;1–7. doi:10.1007/S00360-026-01653-4

91. Biglou SG, Bendena WG, Chin-Sang I. An overview of the insulin signaling pathway in model organisms Drosophila melanogaster and Caenorhabditis elegans. Peptides (NY). 2021;145:170640. doi:10.1016/J.PEPTIDES.2021.170640 PubMed PMID: 34450203.

92. Agrawal N, Delanoue R, Mauri A, Basco D, Pasco M, Thorens B, et al. The Drosophila TNF Eiger is an adipokine that acts on insulin-producing cells to mediate nutrient response. Cell Metab. 2016;23:675–84. doi:10.1016/j.cmet.2016.03.003 PubMed PMID: 27076079.

93. Palu RAS, Owings KG, Garces JG, Nicol A. A natural genetic variation screen identifies insulin signaling, neuronal communication, and innate immunity as modifiers of hyperglycemia in the absence of Sirt1. G3 Genes|Genomes|Genetics. 2022;12(6):jkac090. doi:10.1093/G3JOURNAL/JKAC090 PubMed PMID: 35435227.

94. Zirin J, Ni X, Sack LM, Yang-Zhou D, Hu Y, Brathwaite R, et al. Interspecies analysis of MYC targets identifies tRNA synthetases as mediators of growth and survival in MYC-overexpressing cells. Proc Natl Acad Sci U S A. 2019;116(29):14614–9. doi:10.1073/PNAS.1821863116 PubMed PMID: 31262815.

95. Alic N, Andrews TD, Giannakou ME, Papatheodorou I, Slack C, Hoddinott MP, et al. Genome-wide dFOXO targets and topology of the transcriptomic response to stress and insulin signalling. Mol Syst Biol. 2011;7:502. doi:10.1038/MSB.2011.36 PubMed PMID: 21694719.

96. Puig O, Marr MT, Ruhf ML, Tjian R. Control of cell number by Drosophila FOXO: downstream and feedback regulation of the insulin receptor pathway. Genes Dev. 2003 Aug 15;17(16):2006–20. doi:10.1101/GAD.1098703 PubMed PMID: 12893776.

97. Wu C, Chen Y, Wang F, Chen C, Zhang S, Li C, et al. Pelle Modulates dFoxO-Mediated Cell Death in Drosophila. PLoS Genet. 2015;11(10):e1005589. doi:10.1371/JOURNAL.PGEN.1005589 PubMed PMID: 26474173.

98. Zhang F, Pirooznia M, Xu H. Mitochondria regulate intestinal stem cell proliferation and epithelial homeostasis through FOXO. Mol Biol Cell. 2020 Jul 1;31(14):1538–49. doi:10.1091/MBC.E19-10-0560 PubMed PMID: 32374658.

99. Christesen D, Yang YT, Chen W, Batterham P, Perry T. Loss of the Dβ1 nicotinic acetylcholine receptor subunit disrupts bursicon-driven wing expansion and diminishes adult viability in Drosophila melanogaster. Genetics. 2021;219(1):iyab112. doi:10.1093/GENETICS/IYAB112 PubMed PMID: 34849910.

100. Heinrichsen ET, Haddad GG. Role of High-Fat Diet in Stress Response of Drosophila. PLoS One. 2012;7(8):e42587. doi:10.1371/journal.pone.0042587

101. Overgaard J, Macmillan HA. The Integrative Physiology of Insect Chill Tolerance. Annu Rev Physiol. 2017 Feb 10;79:187–208. doi:10.1146/annurev-physiol-022516-034142 PubMed PMID: 27860831.

APPENDIX

10.6 Fat body specific silencing of candidate interest

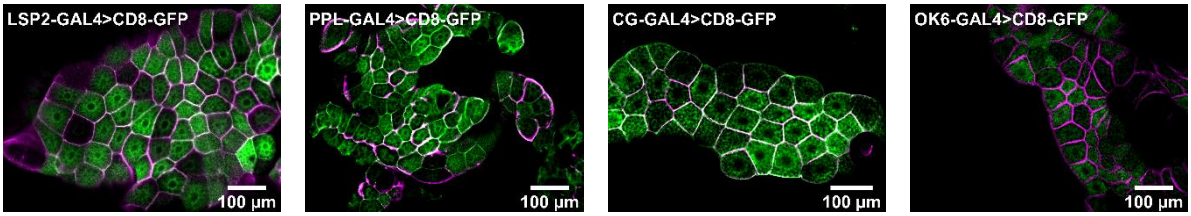

Supplementary figure 1. GFP expression in larval fat body. Various fat body specific GAL4-drivers were tested using GFP-expression in L3 larval fat body. Dissected fat bodies were stained with Rhodamine Phalloidin to visualize actin in cell membranes. PPL-GAL4>CD8-GFP image was adapted with permission from Broos Nijs.

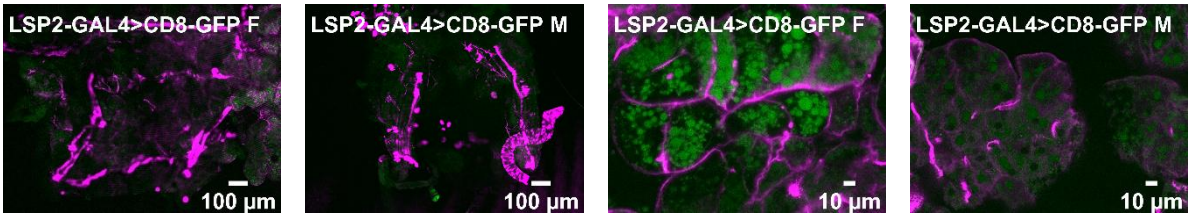

Supplementary figure 2. LSP2-GAL4 induced GFP expression in the adult fat body of females (F) and males (M). Dissected fat bodies were stained with Rhodamine Phalloidin to visualize actin in cell membranes.

Gene	Primer (Forward – Reverse)	Efficiency (%)
Aldh-III	5'- TCATCCGGAGGCCAATGGAG -3' 5'- TCGGTTTCTGGTTCTGGTTCAAT -3'	127,38
Arr	5'- ACCAATTGTGCCAACGGTCA -3' 5'- GGCCGAGATGCAGAGCTTGT -3'	121,69
ATPsynBeta	5'- TACGTGCTGCATCTAAAGCC -3' 5'- GCAGCATGGCTACGAGACAA -3'	103,61
CG14230	5'- ATCCTCGTCTCAAGGAGGGC -3' 5'- AGGCGGTTCTTCACTTGGTC -3'	91,36
CG4168	5'- CACGATGACACACTCGCTCA -3' 5'- GGTTATGTGGTTGCGTTGCG -3'	167,08
Egr	5'- TCCTAGTCCGCAAAGGTGAA -3' 5'- CAAGTGGAAATGGGCTGCTG -3'	106,77
Galk	5'- AGTGCCAGGAAGGGTCAACA –3' 5'- GGCCACTGCAAGGAAAATGC -3'	113,62
Hyd	5'- ATCGTCGAATCTGGATAACTCTGA -3' 5'- AGACTCCACGTTAGAGGGGG- 3'	112,76

Inactive	5’- CTCAAGCAGCTGTCCCATGC -3’ 5’- ATCGGTGTCGCCAATCAAAC -3’	124,18
Klp68D	5’- CAGGTGGGCAACAAGAACCG -3’ 5’- AAATGGCGTGGGATCTTGAACT –3’	96,50
Mhc	5’- GGTTTTGAGATCTTCGAGTACAACG -3’ 5’- AGTCAATGCCTTCCCTCTTGTAT -3’	114,11
Nan	5’- CGATGTTGGCTACGAGGTTG -3’ 5’- CCAAAGTAAGGGGCGTGAGA -3’	203,61
ND23	5’- CATCGCGCAACGGACAG -3’ 5’- ATCTTTGGGTTCTGCTCGCT -3’	123,53
Ndae1	5’- TGATGGGTCTGCCTTGGTTC -3’ 5’- GCACTCCGACTCCAGTTTCA -3’	104,70
Nep1	5’- ATGAACGCGACAACAAAGCC -3’ 5’- ATTTGAGGAATATCCATGCAGCTC -3’	136,24
Nep7	5’- GGAAGTCGGAGGCGGTATTC -3’ 5’- TCGTCCCTTGTCTCATTGCC -3’	100,95
NonAL	5’- CTCGCTACGAACAGGAGACC -3’ 5’- TCCCACTCCAGTTTCATGCG -3’	102,61
Pll	5’- CGGCACGGCTAGAGGC -3’ 5’- CATTGGTCCAGCAGGATGTTG -3’	123,54
Pten	5’- TGGAAGAGAATCATGCCCAGC -3’ 5’- ACAGCTACTCTCCCGCGAA -3’	99,60
Rbfox1	5’- TGCTTCCGCTGATCCAAATCT -3’ 5’- TAGTCACAGTGCGGCGATTTA -3’	143,58

Supplementary table 1. Efficiency of the utilized primer pairs. Efficiency was measured using serial cDNA dilutions (1:1, 1:5, 1:10, 1:50, 1:100, 1:1000 and 1:10000). Slope was formulated based on the Ct values, representing the necessary cycles to compensate the dilution. Selection criteria of 80-130% efficiency were used. Three sets of primers were tested to measure gene expression of CG4168, Nan, Nep1 and Rbfox1, to which none achieved optimal efficiency. The primer set that best approximated the efficiency criteria was selected.

Experimental genotype	Mean recovery time (min) ± standard deviation		Adjusted p-value
	Experimental group	*Control group*	
PPL-GAL4>Aldh-III-RNAi	12,70 ± 2,14	9,17 ± 1,29	<0,0001
PPL-GAL4>Arr-RNAi	11,92 ± 3,09	10,48 ± 2,44	0,14
PPL-GAL4>ATPsynBeta-RNAi	12,75 ± 3,72	9,37 ± 2,03	<0,0001
PPL-GAL4>CG14230-RNAi	19,14 ± 5,22	13,61 ± 4,96	0,00014
PPL-GAL4>CG4168-RNAi	14,70 ± 3,33	11,09 ± 2,88	<0,0001
PPL-GAL4>Egr-RNAi	14,35 ± 4,01	9,50 ± 1,45	<0,0001
PPL-GAL4>Galk-RNAi	10,54 ± 1,40	10,28 ± 3,18	0,66
PPL-GAL4>Hyd-RNAi	12,29 ± 4,37	9,76 ± 2,18	<0,0001
PPL-GAL4>Iav-RNAi	14,42 ± 2,85	9,24 ± 3,16	0,0019
PPL-GAL4>Klp68D-RNAi	14,53 ± 4,15	10,47 ± 3,99	0,010
PPL-GAL4>Mhc-RNAi	12,98 ± 3,84	9,43 ± 2,39	0,015
PPL-GAL4>Nan-RNAi	12,51 ± 3,77	9,45 ± 2,28	0,0018
PPL-GAL4>ND23-RNAi	11,73 ± 1,74	8,18 ± 0,71	<0,0001
PPL-GAL4>Ndae1-RNAi	12,98 ± 1,64	12,56 ± 5,01	0,97
PPL-GAL4>Nep1-RNAi	12,54 ± 4,59	9,51 ± 1,37	<0,0001
PPL-GAL4>Nep7-RNAi	15,53 ± 4,74	11,04 ± 4,56	0,0034
PPL-GAL4>NonAL-RNAi	14,87 ± 4,78	9,77 ± 2,20	0,0034
PPL-GAL4>Pll-RNAi	13,58 ± 2,97	9,76 ± 1,81	<0,0001
PPL-GAL4>Pten-RNAi	8,52 ± 1,39	9,44 ± 1,64	0,31
PPL-GAL4>Rbfox1-RNAi	14,15 ± 3,36	10,12 ± 1,56	<0,0001
PPL-GAL4	21,42 ± 5,45	10,23 ± 3,21	<0,0001
W1118	8,00 ± 2,49	9,80 ± 2,80	0,0073
Canton SB	9,51 ± 3,83	8,27 ± 1,08	0,064

Supplementary table 2. Mean chill coma recovery time per assay in males.

Experimental genotype	Mean recovery time (min) ± standard deviation		Adjusted p-value
	Experimental group	*Control group*	
PPL-GAL4>Aldh-III-RNAi	10,56 ± 1,61	8,18 ± 2,02	0,00030
PPL-GAL4>Arr-RNAi	13,58 ± 5,70	11,94 ± 4,99	0,33
PPL-GAL4>ATPsynBeta-RNAi	16,35 ± 7,84	14,18 ± 6,24	0,066
PPL-GAL4>CG14230-RNAi	18,61 ± 5,48	12,16 ± 5,13	<0,0001
PPL-GAL4>CG4168-RNAi	11,56 ± 2,40	8,54 ± 1,54	<0,0001
PPL-GAL4>Egr-RNAi	10,92 ± 1,43	8,68 ± 1,56	<0,0001
PPL-GAL4>Galk-RNAi	10,48 ± 1,66	7,97 ± 1,44	<0,0001
PPL-GAL4>Hyd-RNAi	9,42 ± 2,80	8,68 ± 1,71	0,44
PPL-GAL4>Iav-RNAi	13,05 ± 5,70	10,61 ± 4,33	<0,0001
PPL-GAL4>Klp68D-RNAi	14,90 ± 5,51	13,60 ± 5,75	0,013
PPL-GAL4>Mhc-RNAi	11,84 ± 5,50	10,38 ± 4,81	0,59
PPL-GAL4>Nan-RNAi	11,79 ± 2,88	8,04 ± 1,43	<0,0001
PPL-GAL4>ND23-RNAi	14,57 ± 5,45	11,26 ± 4,62	0,10
PPL-GAL4>Ndae1-RNAi	11,85 ± 2,03	12,69 ± 6,43	0,68
PPL-GAL4>Nep1-RNAi	11,63 ± 2,72	8,75 ± 2,37	0,014
PPL-GAL4>Nep7-RNAi	14,00 ± 6,32	10,03 ± 3,37	0,00021
PPL-GAL4>NonAL-RNAi	13,66 ± 5,25	10,69 ± 4,15	0,00044
PPL-GAL4>Pll-RNAi	15,32 ± 5,13	11,48 ± 4,38	<0,0001
PPL-GAL4>Pten-RNAi	10,02 ± 3,60	14,43 ± 6,40	0,029
PPL-GAL4>Rbfox1-RNAi	15,25 ± 5,05	12,30 ± 5,25	0,33
PPL-GAL4	21,68 ± 5,09	11,07 ± 4,12	<0,0001
w1118	6,44 ± 1,75	10,59 ± 4,33	<0,0001
CantonSB	7,41 ± 2,25	15,66 ± 5,30	<0,0001

Supplementary table 3. Mean chill coma recovery time per assay in females.

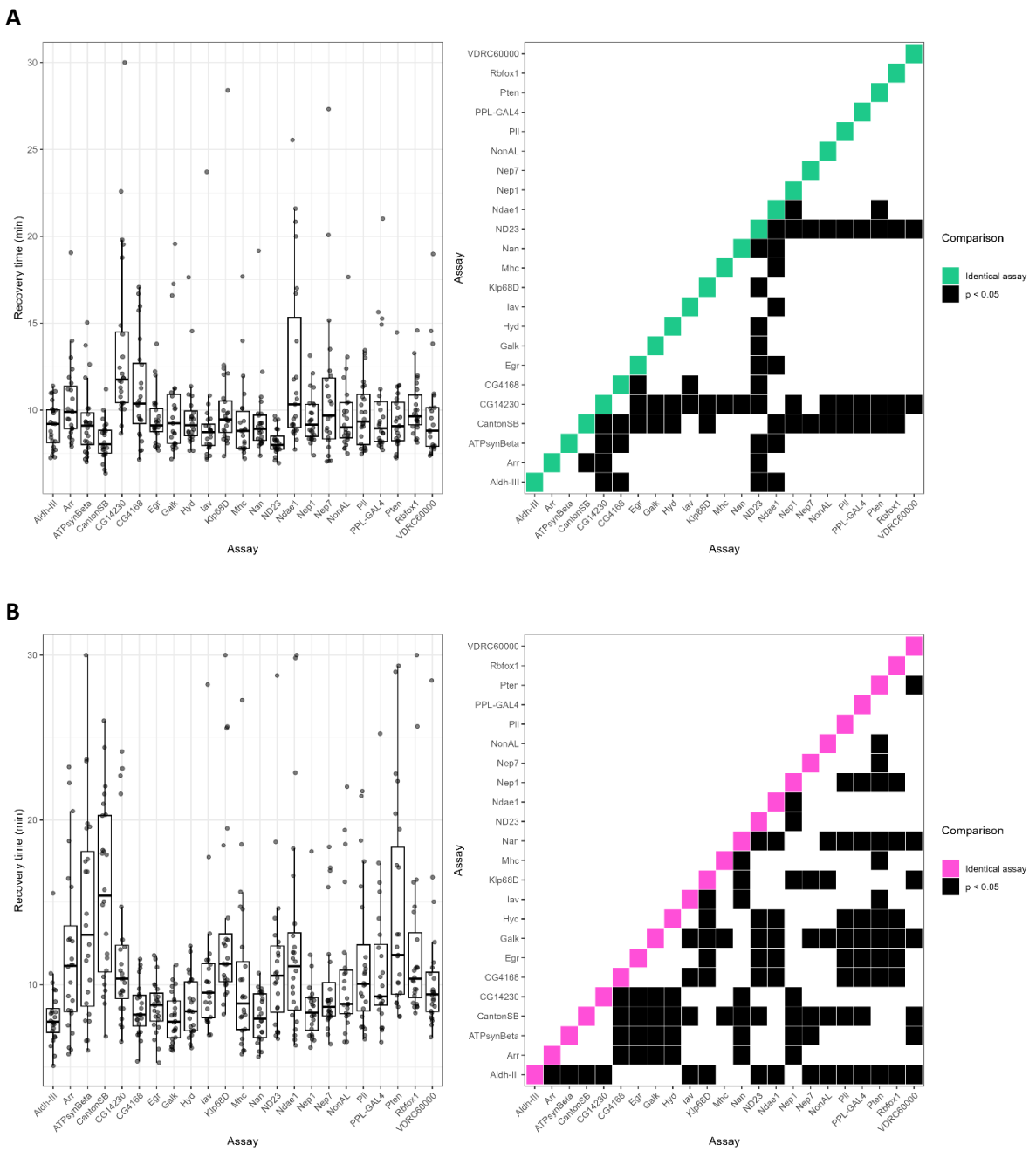

Supplementary figure 3. Across assay comparison of the genetic control PPL-GAL4>w1118. A) Recovery time of PPL-GAL4>w1118 males between assays. B) Recovery time of PPL-GAL4>w1118 females between assays. Each assay consisted of three replicates in which 8 female and 8 male control flies of the same genetic background were measured. Pairwise comparison within the same genotype but between assays indicated significant variability in chill coma recovery time, with a higher frequency in females. This motivates the inclusion of a control condition within each assay.

Experimental genotype	Mean induction time (min) ± standard deviation		Adjusted p-value
	Experimental group	*Control group*	
PPL-GAL4>Aldh-III-RNAi	2,23 ± 0,40	2,24 ± 0,96	0,99
PPL-GAL4>Arr-RNAi	2,32 ± 0,83	2,01 ± 0,72	0,034
PPL-GAL4>ATPsynBeta-RNAi	2,47 ± 0,52	1,74 ± 0,42	<0,0001
PPL-GAL4>CG14230-RNAi	1,83 ± 0,46	1,96 ± 0,44	0,46
PPL-GAL4>CG4168-RNAi	1,82 ± 0,41	1,97 ± 0,53	0,37
PPL-GAL4>Egr-RNAi	2,04 ± 0,42	2,41 ± 0,72	0,027
PPL-GAL4>Galk-RNAi	1,54 ± 0,28	1,74 ± 0,64	0,24
PPL-GAL4>Hyd-RNAi	1,66 ± 0,39	1,42 ± 0,29	0,16
PPL-GAL4>Iav-RNAi	1,89 ± 0,33	1,88 ± 0,49	0,99
PPL-GAL4>Klp68D-RNAi	1,30 ± 0,40	1,43 ± 0,59	0,43
PPL-GAL4>Mhc-RNAi	2,40 ± 0,58	2,34 ± 0,56	0,75
PPL-GAL4>Nan-RNAi	1,97 ± 0,36	2,00 ± 0,42	0,83
PPL-GAL4>ND23-RNAi	1,65 ± 0,70	1,52 ± 0,35	0,44
PPL-GAL4>Ndae1-RNAi	1,95 ± 0,52	1,93 ± 0,70	0,88
PPL-GAL4>Nep1-RNAi	1,62 ± 0,48	1,79 ± 0,52	0,31
PPL-GAL4>Nep7-RNAi	1,92 ± 0,89	1,95 ± 0,61	0,82
PPL-GAL4>NonAL-RNAi	2,35 ± 0,31	2,25 ± 0,36	0,56
PPL-GAL4>Pll-RNAi	1,99 ± 0,60	1,59 ± 0,57	0,01
PPL-GAL4>Pten-RNAi	1,28 ± 0,30	1,59 ± 0,33	0,077
PPL-GAL4>Rbfox1-RNAi	1,25 ± 0,25	1,19 ± 0,30	0,74
PPL-GAL4	1,56 ± 0,40	2,03 ± 0,54	0,0045
w1118	1,97 ± 0,91	2,02 ± 0,80	0,78

Supplementary table 4. Mean chill coma induction time per assay in males.

Experimental genotype	Mean induction time (min) ± standard deviation		Adjusted p-value
	Experimental group	*Control group*	
PPL-GAL4>Aldh-III-RNAi	2,47 ± 0,45	2,38 ± 0,36	0,50
PPL-GAL4>Arr-RNAi	1,83 ± 0,35	2,00 ± 0,34	0,17
PPL-GAL4>ATPsynBeta-RNAi	2,14 ± 0,51	2,39 ± 0,51	0,042
PPL-GAL4>CG14230-RNAi	2,32 ± 0,27	2,10 ± 0,37	0,079
PPL-GAL4>CG4168-RNAi	2,01 ± 0,26	1,72 ± 0,45	0,021
PPL-GAL4>Egr-RNAi	2,49 ± 0,40	2,09 ± 0,46	0,0017
PPL-GAL4>Galk-RNAi	1,86 ± 0,61	1,47 ± 0,26	0,0017
PPL-GAL4>Hyd-RNAi	1,87 ± 0,48	1,91 ± 0,24	0,75
PPL-GAL4>Iav-RNAi	1,93 ± 0,37	1,86 ± 0,27	0,57
PPL-GAL4>Klp68D-RNAi	1,45 ± 0,23	1,38 ± 0,31	0,59
PPL-GAL4>Mhc-RNAi	2,74 ± 0,40	2,55 ± 0,58	0,080
PPL-GAL4>Nan-RNAi	2,23 ± 0,18	1,79 ± 0,30	0,0005
PPL-GAL4>ND23-RNAi	1,57 ± 0,38	1,59 ± 0,25	0,91
PPL-GAL4>Ndae1-RNAi	2,01 ± 0,53	1,90 ± 0,30	0,41
PPL-GAL4>Nep1-RNAi	1,92 ± 0,54	1,95 ± 0,26	0,81
PPL-GAL4>Nep7-RNAi	2,12 ± 0,28	1,96 ± 0,52	0,34
PPL-GAL4>NonAL-RNAi	2,35 ± 0,15	1,96 ± 0,24	0,0020
PPL-GAL4>Pll-RNAi	1,78 ± 0,32	1,77 ± 0,34	0,93
PPL-GAL4>Pten-RNAi	1,53 ± 0,34	1,56 ± 0,35	0,80
PPL-GAL4>Rbfox1-RNAi	1,41 ± 0,28	1,33 ± 0,33	0,507
PPL-GAL4	2,17 ± 0,56	1,83 ± 0,18	0,0074
w1118	2,11 ± 0,78	2,16 ± 0,71	0,69

Supplementary table 5. Mean chill coma induction time per assay in females.

Genotype	**Mean lipid concentration (µg/ml) ± standard deviation**	**Adjusted p-value** *Compared to control*
PPL-GAL4>w1118	217,75 ± 50,45	
PPL-GAL4>Aldh-III-RNAi	566,46 ± 42,76	0,0001
PPL-GAL4>ATPsynBeta-RNAi	434,15 ± 91,30	0,0093
PPL-GAL4>CG14230-RNAi	189,27 ± 26,76	0,79
PPL-GAL4>CG4168-RNAi	325,69 ± 73,19	0,23
PPL-GAL4>Egr-RNAi	456,85 ± 222,39	0,0063
PPL-GAL4>Hyd-RNAi	436,85 ± 59,29	0,0093
PPL-GAL4>Iav-RNAi	335,06 ± 40,57	0,20
PPL-GAL4>Klp68D-RNAi	155,09 ± 32,77	0,56
PPL-GAL4>Mhc-RNAi	221,63 ± 57,39	0,95
PPL-GAL4>Nan-RNAi	483,38 ± 61,02	0,0028
PPL-GAL4>ND23-RNAi	366,46 ± 77,12	0,0849
PPL-GAL4>Nep1-RNAi	482,23 ± 147,70	0,0028
PPL-GAL4>Nep7-RNAi	178,59 ± 6,15	0,75
PPL-GAL4>NonAL-RNAi	243,76 ± 85,05	0,79
PPL-GAL4>Pll-RNAi	376,00 ± 142,77	0,070
PPL-GAL4>Rbfox1-RNAi	164,27 ± 36,08	0,6227
PPL-GAL4	150,24 ± 68,47	0,55
w1118	233,96 ± 50,45	0,88
CantonSB	444,92 ± 78,24	0,0084

Supplementary table 6. Mean lipid concentration in males of experimental genotypes presenting significantly altered chill coma recovery in males.

Genotype	**Mean lipid concentration (µg/ml) ± standard deviation**	**Adjusted p-value** *Compared to control*
PPL-GAL4>w1118	300,24 ± 126,17	
PPL-GAL4>Aldh-III-RNAi	724,92 ± 173,95	0,0016
PPL-GAL4>ATPsynBeta-RNAi	422,23 ± 149,27	0,40
PPL-GAL4>CG14230-RNAi	236,40 ± 66,81	0,65
PPL-GAL4>CG4168-RNAi	652,25 ± 136,92	0,0095
PPL-GAL4>Egr-RNAi	572,23 ± 150,26	0,048
PPL-GAL4>Hyd-RNAi	491,08 ± 242,82	0,18
PPL-GAL4>Iav-RNAi	367,25 ± 87,31	0,65
PPL-GAL4>Klp68D-RNAi	124,79 ± 45,79	0,22
PPL-GAL4>Mhc-RNAi	282,88 ± 76,33	0,90
PPL-GAL4>Nan-RNAi	531,46 ± 77,57	0,089
PPL-GAL4>ND23-RNAi	545,31 ± 31,52	0,076
PPL-GAL4>Nep1-RNAi	880,31 ± 219,22	<0,0001
PPL-GAL4>Nep7-RNAi	287,01 ± 98,45	0,90
PPL-GAL4>NonAL-RNAi	636,71 ± 159,23	0,011
PPL-GAL4>Pll-RNAi	374,75 ± 159,50	0,65
PPL-GAL4>Rbfox1-RNAi	172,83 ± 112,78	0,40
PPL-GAL4	137,88 ± 54,95	0,25
w1118	222,88 ± 86,93	0,65
Canton SB	326,97 ± 54,76	0,90

Supplementary table 7. Mean lipid concentration in females of experimental genotypes presenting significantly altered chill coma recovery in males.

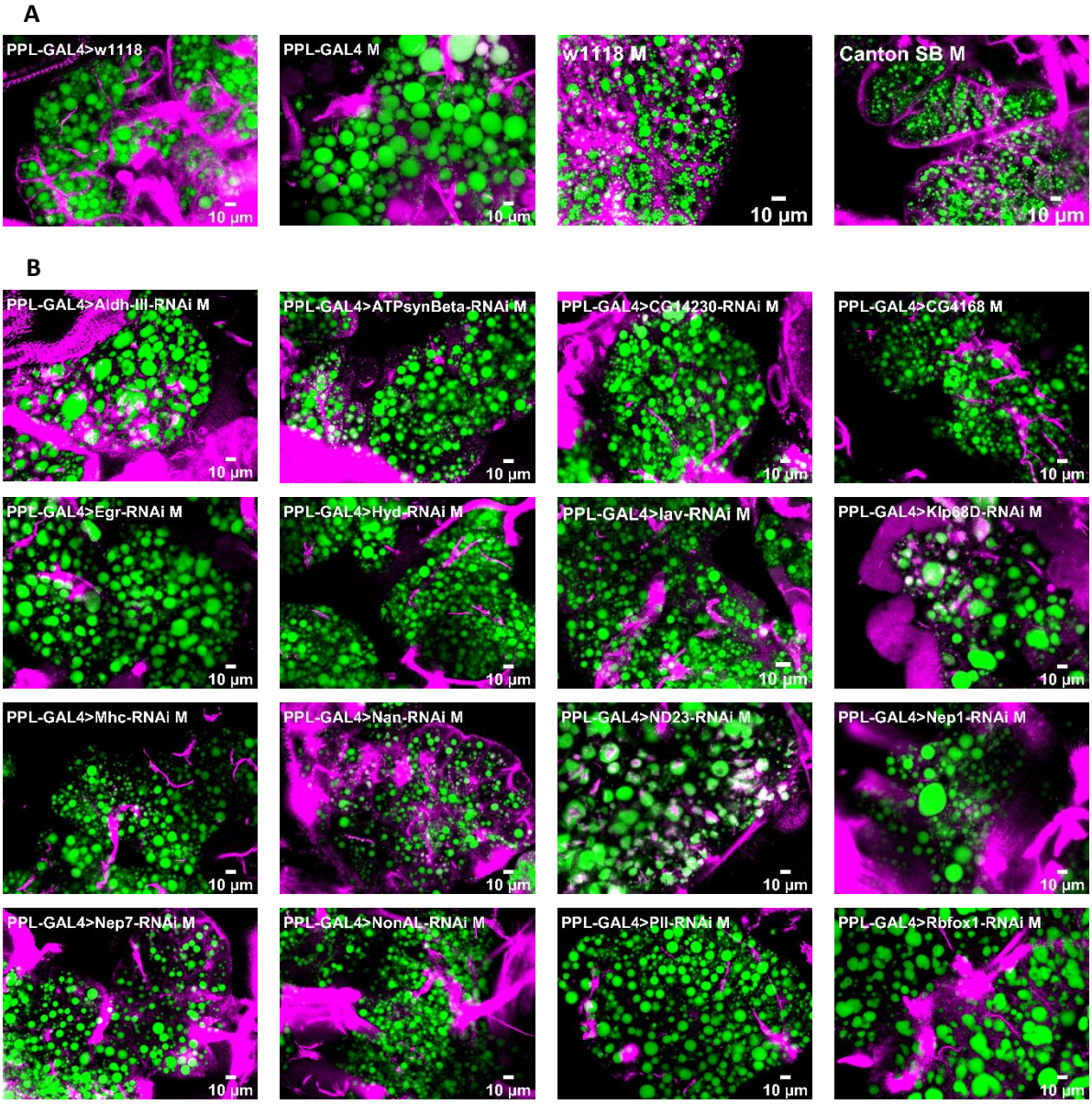

Supplementary figure 4. Lipid droplet morphology of male dorsal fat body in experimental genotype subset. Dissected dorsal fat body of each genotype were stained using BODIPY, to visualize the lipid droplets, and Rhodamine Phalloidin, to indicate actine in cell membranes. A) Control genotypes, B) Experimental genotypes.

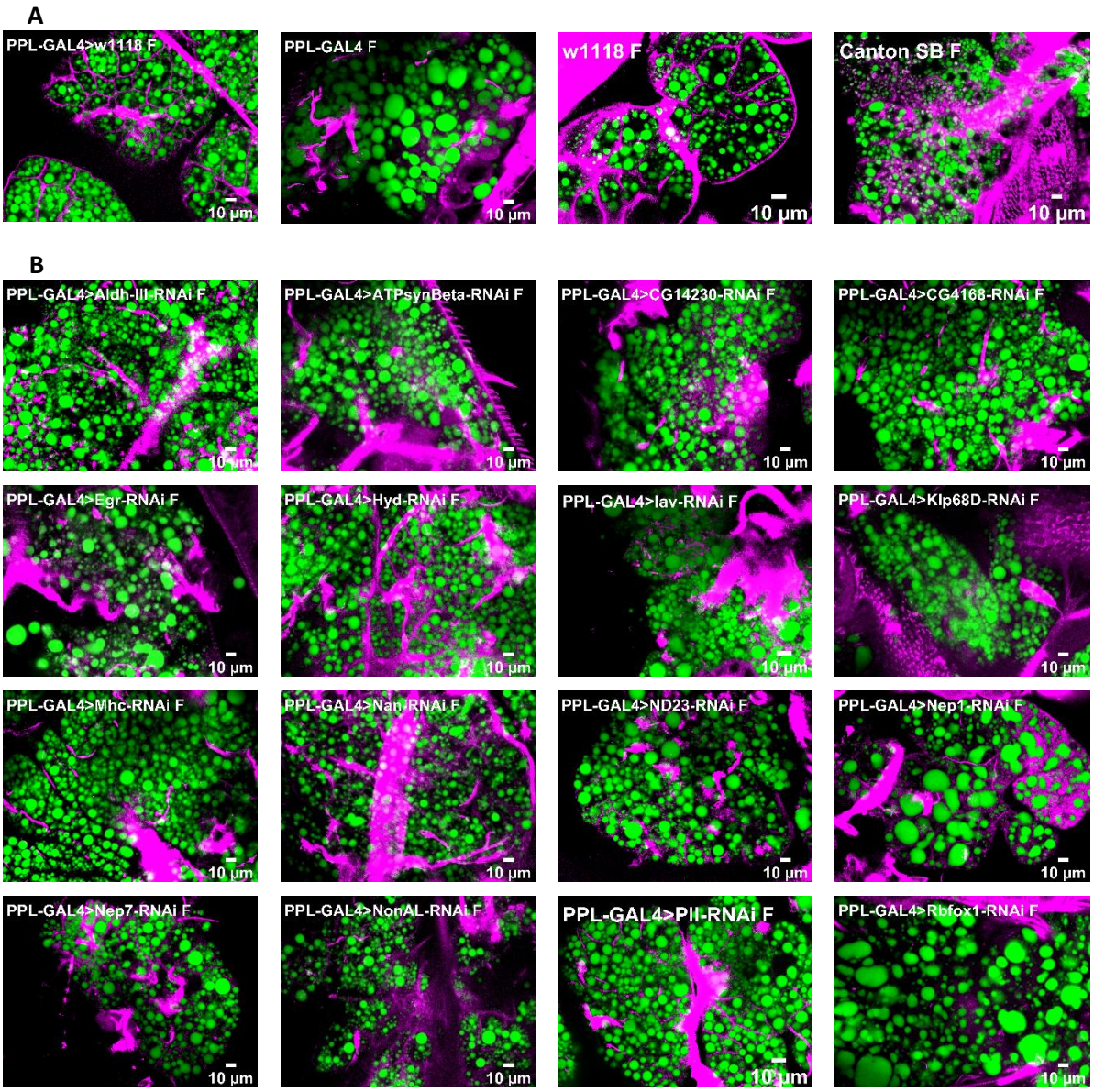

Supplementary figure 5. Lipid droplet morphology of female (F) dorsal fat body in experimental genotype subset. Dissected dorsal fat body of each genotype were stained using BODIPY, to visualize the lipid droplets, and rhodamine phalloidin, to indicate actine in cell membranes. A) Control genotypes, B) Experimental genotypes.

Gene	Relative gene expression	Chill coma recovery time	Chill coma induction time	Lipid content
Aldh-III	Males: ↓ Females: ↓	Males: ↑ Females: ↑	Males: = Females: =	Males: ↑ Females: ↑
Arr	Males: ↓ Females: ↓	Males: = Females: =	Males: ↑ Females: =	
ATPsynBeta	Males: ↑ Females: =	Males: ↑ Females: =	Males: ↑ Females: ↓	Males: ↑ Females: =
CG14230	Males: = Females: =	Males: ↑ Females: ↑	Males: = Females: =	Males: = Females: =
CG4168	Males: ↑ Females: ↑	Males: ↑ Females: ↑	Males: = Females: ↑	Males: ↑ Females: ↑
Egr	Males: = Females: =	Males: ↑ Females: ↑	Males: ↓ Females: ↑	Males: ↑ Females: ↑
Galk	Males: ↓ Females: ↓	Males: = Females: ↑	Males: = Females: ↑	
Hyd	Males: ↓ Females: ↓	Males: ↑ Females: =	Males: = Females: =	Males: ↑ Females: =
Iav	Males: = Females: =	Males: ↑ Females: ↑	Males: = Females: =	Males: = Females: =
Klp68D	Males: ↑ Females: =	Males: ↑ Females: ↑	Males: = Females: =	Males: = Females: =
Mhc	Males: ↓ Females: ↓	Males: ↑ Females: =	Males: = Females: =	Males: = Females: =
Nan	Males: ↑ Females: ↑	Males: ↑ Females: ↑	Males: = Females: ↑	Males: ↑ Females:
ND23	Males: ↓ Females: =	Males: ↑ Females: =	Males: = Females: =	Males: = Females: =
Ndae1	Males: ↓ Females: =	Males: = Females: =	Males: = Females: =	
Nep1	Males: ↓ Females: =	Males: ↑ Females: ↑	Males: = Females: =	Males: ↑ Females: =
Nep7	Males: ↑ Females: ↑	Males: ↑ Females: ↑	Males: = Females: =	Males: = Females: =
NonAL	Males: = Females: =	Males: ↑ Females: ↑	Males: = Females: ↑	Males: = Females: ↑
Pll	Males: ↓ Females: =	Males: ↑ Females: ↑	Males: ↑ Females: =	Males: = Females: =

Pten	Males: = Females: =	Males: = Females: 🡻	Males: = Females: =	
Rbfox1	Males: = Females: =	Males: 🡹 Females: =	Males: = Females: =	Males: = Females: =

Supplementary table 8. Summary of measurements and encountered phenotypes per gene of interest.

10.7 Pan-neuronal knockdown of TRP encoding genes

TRP channels are commonly known for their response-dependent activation in neurons. Therefore, we aimed to test if neuron system specific knockdown of the TRP channel encoding genes of interest caused significant alterations in cold stress responses. We performed pan-neuronal knockdown using the ELAV-GAL4 driver of Iav and Nan and tested their chill coma susceptibility and recovery.

The ELAV-GAL4>Iav-RNAi and ELAV-GAL4>Nan-RNAi generated an adverse phenotype in adult females (Supplementary figure 6). Specifically, wings did not complete post-eclosion expansion and survival was limited to four days.

As females did not reach the age requirement of 5-7 days old, they were not included in the behavioural assay dataset. Although lacking comparison to an experimental genotype, ELAV-GAL4>w1118 females were analysed in both behavioural assays, as to verify that the ELAV-GAL4-driver did not cause enhanced mortality, both prior and post cold exposure.

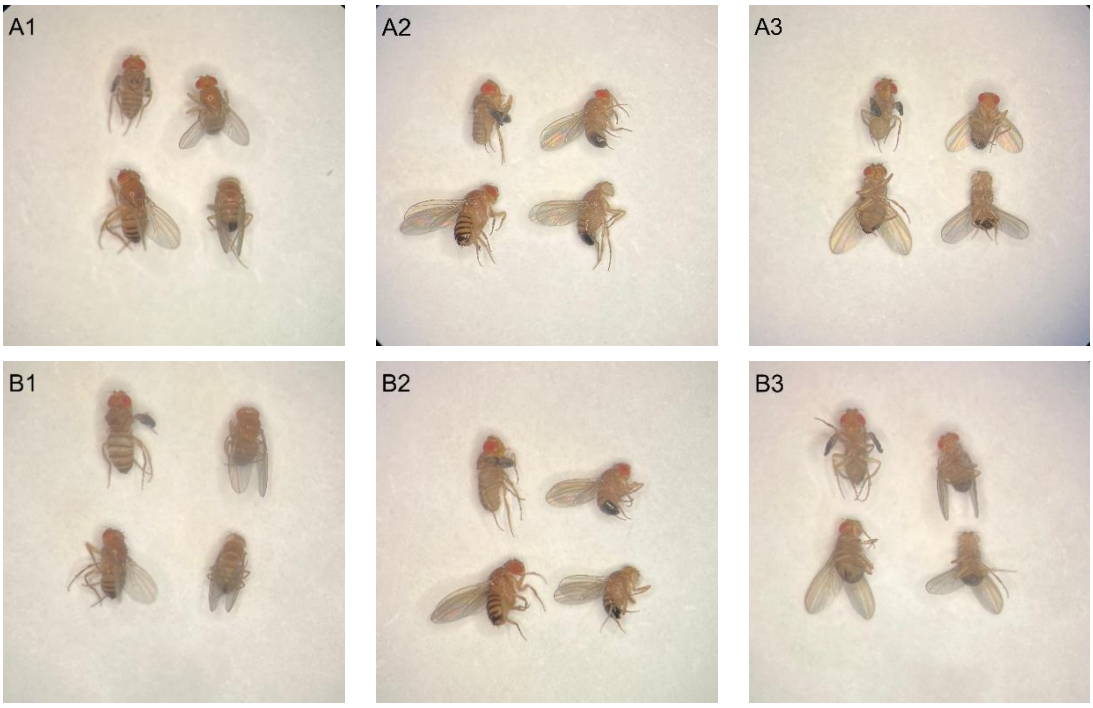

Supplementary figure 6. Phenotypic characteristics of adult flies containing pan-neuronal TRP-channel encoding gene knockdown. A) ELAV-GAL4>Iav-RNAi (upper row) compared to ELAV-GAL4>w1118 (lower row), B) ELAV-GAL4>Nan-RNAi (upper row) compared to ELAV-GAL4>w1118 (lower row).

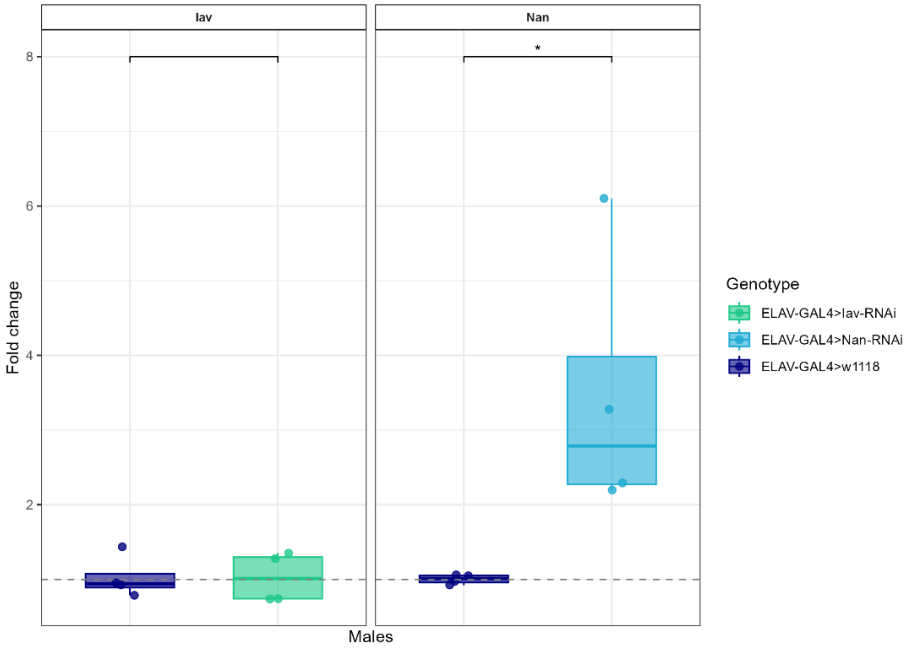

Supplementary figure 7. Relative gene expression following neuron specific knockdown in males. Relative expression levels were quantified by RT-qPCR. Each genotype is represented by four replicates containing ten flies. Statistical significance was assessed by implementing Welch's t-test with unequal variances on the ΔCt values, adjusted with Benjamini-Hochberg multiple testing correction. Significance levels are indicated as adjusted p<0.05 (*), adjusted p<0.01 (**), adjusted p<0.001 (***).

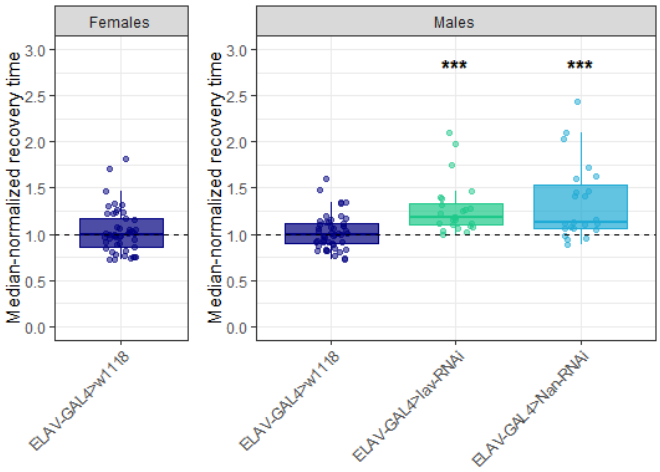

Supplementary figure 8. Median-normalized chill coma recovery of experimental genotypes containing pan neuronal TRP channel knockdown compared to the negative control. Each assay consisted of three replicates containing 8 flies per experimental and control condition. Three hour cold exposure was applied by maintaining the individuals on ice in a 4°C environment. Recovery was manually scored as the time necessary to regain an upright posture. Individuals that displayed movement but did not manage an upright position within the recording duration of 30 minutes, were censored by applying the assay duration as recovery time. Cox proportional hazards model was implemented to perform pairwise comparisons of the experimental genotype to the assay's control survival distributions, accounting for censoring, variability per assay and nesting within replicate. Multiple testing was corrected by applying Benjamini-Hochberg correction. Significance is indicated by adjusted p<0.05 (*), adjusted p<0.01 (**) and adjusted p<0.001 (***).

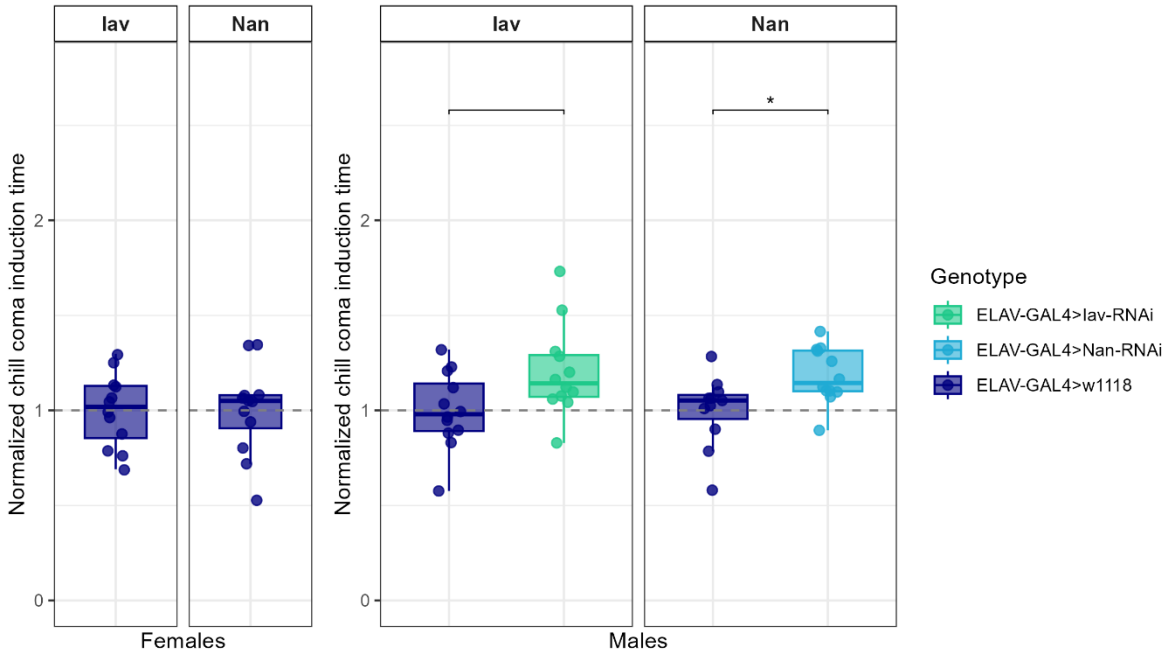

Supplementary figure 9. Normalized per replicate chill coma induction time of individuals containing pan-neuronal TRP-channel encoding gene knockdown. Three replicates containing four female and four male flies of both genotypes were exposed to a precooled Peltier element. Time necessary to induce chill coma was manually scored. Linear mixed model was used to pairwise compare chill coma induction time of both genotypes and multiple testing was corrected using Benjamini-Hochberg method. Statistical significance is indicated as adjusted p<0.05 (*), adjusted p<0.01 (**), adjusted p<0.001 (***). Chill coma induction time was normalized by the mean of the negative control per replicate, thereby normalizing the spread induced by temperature variability between replicates.